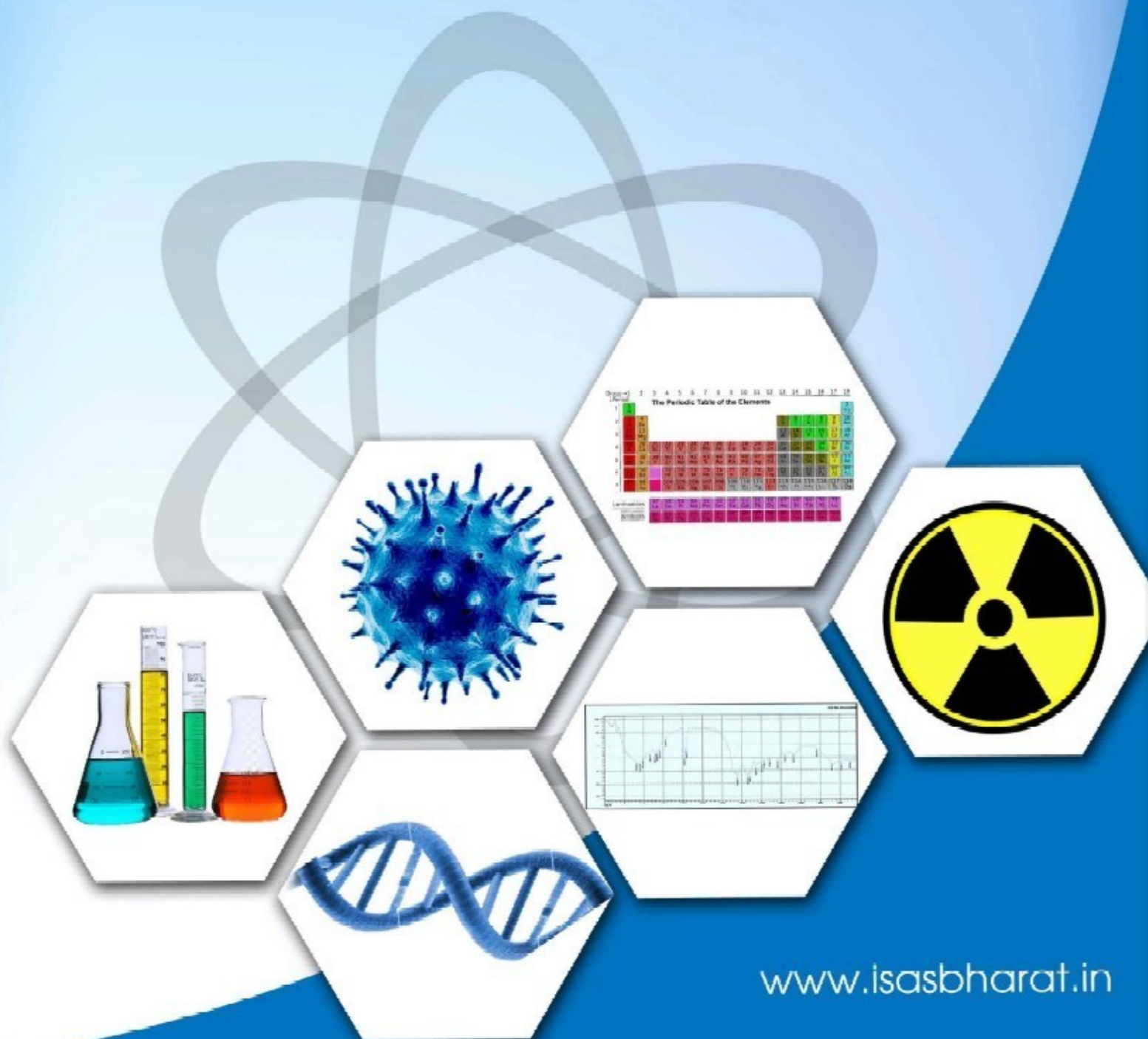




ISSN: 2583-5459
Volume-1 Issue-3
January, 2023

Journal of ISAS

An open access peer reviewed quarterly e-journal by
Indian Society of Analytical Scientists



www.isasbharat.in



ISAS

Journal of ISAS

An open access peer reviewed quarterly e-journal published by Indian Society of Analytical Scientists

Published by: Indian Society of Analytical Scientists (ISAS)

Address: C/O REDS, BARC, Mumbai 400085

Email: isasjournal@isasbharat.in

President ISAS : Dr. P.P.Chandrachoodan

J.ISAS

Editorial Board

Editor in Chief

Dr. Nilima Rajurkar, Pune

Members

Dr. Vijayalaxmi adya, Mumbai

Dr. A.K.Basu, Pune

Dr. Vinay Bhandari, Pune

Dr. Avinash Bharati, Nagpur

Dr. Anu Gopinath, Kochi

Dr. Ravin Jugade, Nagpur

Dr. Padmaja S. Vadodara

Dr. Pradeep Kumar, Mumbai

Dr. Prakash Samnani, Vadodara

Dr. Sridhar T.M , Chennai

Dr. S.K.Yadav, Vadodara

Advisory Board

Chairman

Dr. Raghaw Saran, Nagpur

Members

Dr. V. Sivanandan Achari, Kochi

Dr. V. Balaram, Hyderabad

Dr. J.Manjanna, Belgavi

Dr. V.R.Nair, Kollam

Dr. Amrit Prakash, Mumbai

Dr. S. Sriman Narayanan, Vellur

Dr. Shivaramu Prasanna, Bengaluru

Dr. K.P. Vijayalakshmi, Trivendram

Dr. Mohammed Yusuff K.K., Kochi

Dr. Rajeev Raghawan, Trivandrum

Instruction to Authors

- The Manuscript should be typed in **MS word** (times new roman) with **1.5 spacings** and **font size 12**
- The **title** of the paper should be clear and concise (**font size 14 and bold**), the first letter of each noun and adjective in the title must be in capital letter. It will be followed by names of authors(initials followed by surname) with their affiliation (**font size 12**)
- Corresponding author should be indicated by * with email ID
- The text should be divided into following sections:
 - **Abstract : up to 300 words**
 - **Key words: 5-6**
 - **Introduction**
 - **Experimental**
 - **Results and Discussion**
 - **Conclusions**
 - **Acknowledgement**
- Figures and Tables should be before references with a caption **Figures:** Followed by **Tables:**
- **References**
 - Divisions within the section should be indicated as subheadings
 - The figures and tables should be numbered with Roman numerals and must be mentioned in the text at appropriate places
 - Standard abbreviations for technical terms and journals should be used
 - All constants should be expressed in **SI units**
 - References should be numbered consecutively and should appear in the text as superscript at appropriate places.
 - References should be in following pattern
 - For research paper:**
Authors' initials and surname, Journal abbreviation, Volume, Page, Year.
 - For book:**
Authors' initials and surname, Book name, Publisher, Place, Year.
 - For proceedings:**
Authors' initials and surname Proceedings' of the conference name, place, Page, Month and Year.
- The paper is to be submitted in word file and PDF file to isasjournal@isasbharat.in
- After getting the acceptance of the paper, authors have to submit **signed copyright form and undertaking** before publishing the article



Indian Society of Analytical Scientists



Message from President ISAS

It is very heartening to note the impressive recognition received, from the Users, Researchers, Authors of Publications and Academicians, etc working in the field Analytical Sciences, for the ISAS Journal, which is first of its kind of Indian Journal.

Such an impressive recognition for the ISAS Journal is primarily due to the highly experienced and leading experts who have taken the responsibilities in the Advisory Committee and Editorial Board of the ISAS Journal. The Executive Committee of ISAS consisting of Leading Experts, who effectively served various development sectors for their life, also imparted their vigilant contributions to make the ISAS Journal to maintain good quality standards, attracting good authors of papers, which are well appreciated by the users.

As the current President, ISAS, I am very happy to have lead the ISAS Initiatives to launch the ISAS Journal, as a unique new Indian Initiative and to see that my vision is poised to fructify, meeting the intended high Quality and Relevance.

As I relinquish my very dynamic and fruitful term (2019 to 2023), as President; ISAS and hand over the baton to the next elected incumbent during April, 2023, I am happy that 3 issues of ISAS Journal have been published, with ISSN received, DOI in process and the Journal being poised to receive the UGC recognition soon.

I take this opportunity to wish the Advisory Committee and Editorial Board as well as all the authors of articles and the users of these publications, a great time ahead in terms of value addition and achieving further Excellence and Relevance of the publications that appear in the ISAS Journal to their own R&D work.

I convey my Best Wishes to All elite partners of the Scientific and Technological Community of India, who are striving their best to make India Self Reliant by the Turn of Centenary Year of Indian Independence, 2047.

Till we meet again,

A handwritten signature in blue ink, appearing to read 'Dr. P.P. Chandrachoodan', written in a cursive style.

(Dr P.P.Chandrachoodan)
President,



ISAS

Indian Society of Analytical Scientists



Message

It's matter of great pride that Indian Society of Analytical Scientists is coming out with its 3rd issue on 31st January, 2023 (as scheduled).

The issue contains variety of papers from various fields such as breast cancer cell cure by bufotalin derived from medicinal plant, reduction of industrial pollutants (dyes) utilizing processes like adsorption, cavigation (hybrid of cavitation and coagulation), Pital Bhasma, an alternative of nano medicines, geological sequestration of CO₂ in porous sedimentary medium filled with saline water besides book review by Dr DK Dubey, Director DRDE of the book on analytical techniques for the trace elements in geochemical exploration. Salient feature of the journal is including novel, purposeful papers of high quality; standard maintained by three levels reviews of the articles.

The journal has already been allotted ISSN; doi for each article (including the already published) is under process for world- wide circulation. UGC care needs at least one to two years.

I sincerely wish the journal makes a wide impact in the field of research in allied sciences. Further, It would be pertinent to express our deep gratitude to Dr P.P.Chandrachoodan, President, ISAS for his excellent initiatives in launching ISAS Journal and for all spontaneous support for maintaining excellence and relevance of the journal!

We would miss his guidance during the processing of fourth issue of the journal due to completion of his elected term as president but I am sure his advice would always be there in taking the Journal to distinguished level of quality in maintaining its excellence!.

A handwritten signature in black ink, appearing to read 'R. Saran', with a stylized, cursive script.

Dr. Raghaw Saran
Vice President and Advisor
J.ISAS



Indian Society of Analytical Scientists.



Editorial

It is my pleasure to present the readers third issue of first volume of **“Journal of ISAS”** which is an open access peer reviewed quarterly e-journal with ISSN number: 2583-5459. It is published by Indian Society of Analytical scientists and having free access to all. Our journal is committed to bring high quality research papers which showcase an integrated approach of all branches of science. The present issue is an example of this which focusses on environmental, geological, microbiological, chemical engineering and ayurvedic aspects of research along with a brief review on the book: “Analytical Techniques for Trace Elements in Geochemical Exploration” which can have direct impact on translational research and on scientific community.

I would like to express my sincere gratitude towards Dr. P.P. Chandrachoodan, President ISAS; Dr. Raghaw Saran, Vice president ISAS and Chairman, Advisory board of Journal of ISAS for their constant guidance and support at each stage in bringing out the journal issue. Their inspirational and motivational messages are gratefully acknowledged. I wish to express my special thanks to Editorial board members: Dr. Vijayalaxmi C. Adya and Dr. Vinay Bhandari for their continuous association in this task. Cooperation from Editorial and Advisory board members as well as reviewers is really noteworthy. I congratulate all the contributory authors for sharing their research in the form of their scholarly articles in this issue. My sincere thanks are due to Kailash Gharat, Shivani Kankar and Vaibhav Parse for the technical support.

Nilima Rajurkar

Dr. Nilima Rajurkar
Editor in Chief, Journal of ISAS

..

Journal of ISAS

ISSN : 2583-5459

1(3), Pages 1 to 91, (2023)

(An open access Peer reviewed quarterly e- journal by Indian Society of Analytical Scientists)

Contents

S.No.	Title and Authors	Page no.
1	Research Paper: Pore-scale modelling of CO ₂ sequestration Pradeep Kumar* Email*: pradeepk@barc.gov.in	1-14
2	Research Paper: Isolation and characterization of phytochemical Constituents of cleome rutidosperma leaf methanol extract and its cytotoxicity against MCF-7 Cells Mullai nila k, Karthikeyan J* Email*: karthikeyanj.zoo@presidencycollegechennai.ac.in	15-32
3	Research Paper: Removal of aqueous solution of Methylene blue dye using “ <i>Clitoria ternatea</i> ”: A Novel Adsorbent D. J. Borkar*, P. V. Adhyapak and N. S. Rajurkar Email*: Djborkar778@gmail.com	33-48
4	Research Paper: Conceptualizing Cavigation Methodology by Integrating Cavitation and Coagulation and Application to Dye Wastewater Treatment Krati Sharma, Chethana M., Vinay M. Bhandari*, Laxmi Gayatri Sorokhaibam, Vivek V. Ranade and Deepak J. Killedar Email*: vm.bhandari@ncl.res.in	49-76
5	Research Paper: Synthesis and Characterization of Pital Bhasma Babita Kale* and NilimaRajurkar Email*: babita.kale95@gmail.com	77-90
6	Book Review: “Analytical Techniques for Trace Elements in Geochemical Exploration” by Dr. Raghaw Saran Dr. D.K.Dubey* Email*: dkdubey@rediffmail.com	91

PORE SCALE MODELLING OF CO₂ SEQUESTRATION

Pradeep Kumar

Bhabha Atomic Research Centre, Trombay, Mumbai, India, 40085.

E-mail: pradeepk@barc.gov.in

Received: 30.12.22, Revised: 26.1.23, Accepted: 28.1.23

Abstract

Geological sequestration of CO₂ in porous sedimentary medium filled with saline water requires a clear view of the gas behavior as a function of topology of the hosting pores, linked to capillary phenomena. The sedimentary medium is modeled as a random packing of equal spheres giving rise to 3D network of pore bodies and throats. The injected CO₂ pushes the water from pores of the reservoir. The scenario is simulated by the increase of the curvature of the liquid/CO₂ interface. Eventually a critical state is reached where the liquid is drained from pores. When the liquid counteracts this first drainage step (imbibition), there is a progressive decrease of the interfaces curvature until they merge together, eliminating the CO₂ from pores. This pore-scale investigation of the mechanisms possibly occurring after a gas injection is studied.

Keywords: Drainage, imbibition, surface evolver, capillary pressure, porous media

Introduction

In recent decades, the CO₂ concentration in the atmosphere has rapidly increased¹ with a wondering correlation with global climate changes². As a consequence, increasing efforts have been directed towards finding solutions to mitigate the CO₂ concentration in the atmosphere. One of the most serious solutions is offered by the CO₂ injection directly inside deep geological formations. The formations are potentially capable to store many thousands of gigatonnes of gas, possibly over several thousand years. Meanwhile, large sedimentary basins with easy access (depth around 800 m) are widely distributed worldwide, having tremendous pore volume, capped by impermeable rocks, and containing saline water of no use³. The injected CO₂ invades the porous space leading to non-saturated state and the system converges towards a quasi-equilibrium state, wherein major portion of initial CO₂ is

persisting as disseminated air pockets, part is dissolved inside the contacting solution, and part is mineralized by turning into carbonates.

The CO₂ sequestration in geological formation is the outcome of two key processes: drainage and imbibition. Drainage process occurs during the period of CO₂ injection, the CO₂ bubble disperses inside the pore spaces because the gas-liquid interface advances against the liquid (drainage). Depending on the topology of the pores network, the initially continuous bubble can penetrate the whole network (splitting of bubble sticky CO₂ plume), turning into a series of smaller bubbles, or just slides inside the media depending on the minimization of the interface mean energy (slippery CO₂ plume⁴). In the post injection period, imbibition process initiates. The gas-liquid interfaces recede inside the pore spaces due to the increasing liquid pressure related to the drainage event (imbibition). In the drainage process, different pathways are possible depending on the pore's topology inside the sedimentary reservoir. As a consequence, the drainage and imbibition processes are governed by the capillary pressure at the two fluids which determines the partitioning between liquid and CO₂ saturation in the reservoir, under the final conditions.

We are using below the basic laws of capillarity to understand which processes at the pore scale determine the gas trapping or the out gassing. The interface (meniscus) between the non wetting and wetting phases is curved expressing the capillary pressure between the two contacting phases (Young Laplace equation). The associated surface area and volume of the liquid and gas which share the pore space provide a quantitative estimate of the gas/liquid trapping state of the pores network. These calculations as well as the building of the model pores network is performed through the Surface Evolver software.

Surface Evolver Software

The Surface Evolver software was developed by Brakke⁵ to study the soap film surface shape and minimize its energy according to different constraints, like surface tension, geometry, gravity effects, all parameters related to the stability of one interface under a certain degree of curvature (capillary interface). These characteristics make it a suitable tool to study the effect of these parameters in the CO₂ sequestration strategies, when the injected gas (CO₂) meets the resident aqueous solution (in general, a long-time resident brine). The software requires as inputs the initial surface location, different characteristics of the surface, and the surface dependent energy function. Actually, it operates on surfaces which consist of geometric elements plus auxiliary data such as constraints, boundaries and forces. The basic elements used to represent a surface are vertices (points in Euclidean 3D-space), edges, facets

and bodies. The coordinates of the vertices are the parameters that determine the location of the surface, and are changed according to the minimization procedure. The surface is implemented as union of flat triangles, so that the smoothness of a sphere depends on the number of triangles (Fig. 1). The total surface energy quantity results from the surface tension and other terms like gravitational energy. Then, the software makes the surface to change under these given constraints to obtain the equilibrium configuration (minimum energy). Finally, the shape of interface under equilibrium conditions is displayed and corresponding surface area and volume can be obtained. One of the interesting feature of this software is that the minimization is done without directly applying Young Laplace equation, though it is inherently satisfied. Thus, it can be applied to complex geometries which are difficult to model through a direct use of the Young Laplace relation.

Pore-scale Model of Sedimentary Media

To model the physical processes occurring during the CO₂ sequestration such as drainage/imbibition, an adequate knowledge of the pore space geometry is essential. Natural media have complicated pore space geometries, which are also heterogeneous from place to place. Many models, even sophisticated, are unable to satisfactorily describe the behavior of two immiscible fluids in three-dimensional pore space⁶⁻⁸. To concentrate ourselves on the physical laws without geometrical complexities, we used a model of random packing of equal spheres^{9,10}. The random packing of equal spheres gives rise to a network of pore bodies, the largest pore spaces, connected by throats, the thinnest pore spaces, which coexist permanently and host a continuous liquid or a liquid-gas biphasic mixture (Fig. 1). The pores could be described in terms of tetrahedral sub units, centers of four spheres lying on the vertices of a tetrahedron. The void space inside the tetrahedron corresponds to a pore body while the cross section of each face corresponds to a pore throat. An interface located at the pore throat can accept capillary conditions which makes it to collapse if hosted in the pore body. It becomes obvious that the way the whole reservoir drains or imbibes, meaning that the way each pore empties or fills, will influence the stability of liquid/gas trapped in the pore bodies or pore throats. Our aim is to clearly decipher the main steps and mechanisms in these processes, and renew the basics of the real systems modeling.

This configuration where thin spaces directly coexist with larger spaces is very often called the ink-bottle arrangement by the soil scientists. It makes possible the coexistence of gas and liquid at equilibrium even under pressure, owing to the cohesion of the liquid capillary

bridges which can take place either across the thinnest (high capillary conditions) or across the largest (low capillary conditions) pore spaces. A direct first conclusion is that the throats can host more capillarized liquid than the bodies, while coexisting with gas filled pore body. In other words, we can say that once the pore bodies have been emptied, a re-emptying stage requires a significant change of the local conditions. As a consequence, during a succession of drainage-imbibition events, naturally there is a range of conditions along which a bubble can be trapped in the bodies while the contacting throats are imbibed under varying pressure.

Capillary Pressure

The capillary properties of the pores and throats determine the drainage/imbibition. According to the Young Laplace law, the capillary pressure is the pressure difference (P) across a curved interface between the wetting and the non-wetting phases. It is directly proportional to the surface tension between the two phases, and inversely proportional to the size of the bridge.

$$\Delta P = P_{NW} - P_W = \gamma_{LV} \times \left(\frac{1}{r_1} + \frac{1}{r_2} \right) \text{-----} (1)$$

Where P_{NW} and P_W are the pressures of, respectively, the non-wetting (CO_2) and the wetting (aqueous solution) phases. LV is the surface tension between the two phases. r_1 and r_2 are the main radii of curvature of the meniscus, and for spherical meniscus: $r_1 = r_2$. The two radii are connected to the radius of the hosting pore, through the contact angle made by the meniscus on the solid wall (noted θ), $r_{PORE} = r_{MENISCUS} / \cos(\theta)$, and it is also connected to the curvature of the interface (noted C) by: $C = 1/r_{PORE}$.

The CO_2 is injected in the sedimentary media deeper than 800m, at pressure higher than 10MPa while the temperature ranges over 35-60°C. The critical pressure of CO_2 is 7.39 MPa and the critical temperature is 31.1°C, hence, the CO_2 penetrates the reservoirs as supercritical fluid. Along these P,T conditions, the interfacial tension between CO_2 and brine remains almost constant close to 26 mN/m¹¹ and this value was used in all simulations. Moreover, the wetting phase was assumed to completely wet the solid spheres, i.e. the meniscus sticks to the solid wall with a nil contact angle. That means the solid is hydrophilic enough for the liquid to slip on it without energy cost. In physical chemistry terms, that translates in the following Young Dupré relation:

$$\gamma_{SV} - \gamma_{SL} = \gamma_{LV} \cdot \cos\theta \text{-----} (2)$$

where the subscript defines between which phases the surface tension is considered. When

the liquid-to-vapor surface tension (γ_{LV}) is equal to the difference between the two other surface tension (solid-to-vapor γ_{SV} , and solid-to-liquid γ_{SL}), the contact angle is zero. This is the case of the perfect wetting, characteristic of the surfaces with high γ_{SV} owing to their large cohesion energy (glasses, metals, oxides). On the contrary, the low γ_{SV} solids will have a very high contact angle (organic solids, like Teflon, for instance).

Eventually, the capillary pressure appears entirely governed by the configuration of pore or throat. The smaller the pore, the larger the capillary pressure, and therefore, the most stabilized can be the liquid by the capillary effects. With the presently used ink bottle geometry, it appears that the liquid should persist at the pore throat while the CO₂ should more easily invade the pore body. Our primary objective is to illustrate how such basic heterogeneity controls drastically the evolution and the amount of the gas trapped inside the media, all together with the local (P, T) conditions.

Building Diversely-filled Pores Network

As discussed above, the knowledge of the geometrical distribution of the two immiscible fluids within the pores is of the utmost importance to predict the capillary pressure saturation relationships of the porous media, and therefore, play the primary role in the key processes of drainage, imbibition, and dissolution. First, the exact size of the wall-to-wall distance where a liquid-gas interface takes place also controls the limiting curvature which interface might attain during the varying capillary pressure. Each time the interface curvature exceeds the limit, obeying the Young Laplace relation (equation (1)), the interface collapses and moves to another more favorable place. We assume the Young Laplace equilibrium throughout in our simulation, though it is experimentally known that it can be trespassed¹²⁻¹⁵. Second, spatial characteristic, of consequence in our reasoning, is the surface area of the interface between wetting and non-wetting phase i. e. between the brine solution and the CO₂ phase: it is termed hereafter the bridge area or interface area and is of primary importance while considering the other storage process i.e. gas dissolution in brine solution. On the practical side, the gas or liquid volume present in the pores network are expressed relative to the pore volume itself: this is termed as saturation ratio, a common way to express the liquid/gas partitioning in the usable volume. To do such calculations, and also to evaluate the corresponding capillary pressure, we need to choose a peculiar grain size. In simulation, the spherical grains are considered of diameter of 10 micron, a choice which corresponds to pore diameters around 2

μm . Also, the hydraulic connectivity is assumed to be everywhere, meaning that a change in the pressure conditions make the whole reservoir to react: hydraulic gradient is everywhere active on the transport processes and capillary pressure adjustments.

Liquid Bridge between Two Equal Spheres: Pendular Ring

Let us begin with the simplest situation where a liquid volume is held between two equal spherical grains against the gravity (suspended water) forming a capillary liquid bridge. The bridge is characterized by a constant mean curvature having pendular shape (Fig. 2).

Some part of the spherical grain comes in contact with the wetting phase of the pendular ring. However, in the remaining part of the grain, the liquid spreads over the grain surface in the form of a thin adsorption film. This thin film provides the hydraulic connectivity of the liquid phase throughout the whole packing of spheres. Negligible liquid volume is contained inside the thin film in comparison to the pendular ring. However, in addition to liquid bridge, the film realizes a liquid- CO_2 interface necessarily required for gas dissolution. Hence, the total interface area is taken as the sum of the water thin film area and the ring area, and is expressed (Fig. 3) relative to the area covered by a water monolayer over the two grains. As for the liquid bridge, the two key parameters (Fig. 3) are the curvature of the interface (depending on the capillary pressure, namely the pressure difference across the interface), and the associated volume delimited by the interface, which characterizes the liquid amount wherein any dissolved solutes (like aqueous CO_2 or any weathering products) can settle in. Investigating the pore scale from these two sides, area and volume, allows to get a simultaneous view of the surface/volume ratio, which is directly connected to the trapping/dissolution behaviors.

The amount of liquid held in pendular ring is expressed relative to the liquid volume contained between the two spheres at nil capillary pressure. With increasing capillary pressure, the curvature of the pendular ring goes on increasing, thereby decreasing the liquid amount while the total interface area increases. At this stage, do notice that we normalized the interface area to the area occupied by a monolayer of water (assumed 0.3 nm thick) covering all the solid surfaces. Otherwise, when the value of the normalized interface area comes closer to 1, the water is only present as adsorption films, while a decreasing value points to an increasing amount of water trapped as capillary bridge. The curves (Fig.3 left) can be subdivided into three parts according to the local slope of the characteristic curves. In the first region the slope is very steep indicating that liquid is loosely held and can be carried

away by compensating small capillary traction, while the removal of liquid increases the interface area (Fig.3 right).

In the second region, the local slope gradually varies with capillary pressure: the liquid is more strongly bounded by capillary force, but keeps significant volume trapped as capillary bridges. Yet, the relative total interface area gradually increases with increasing capillary pressure.

In the third region, the slope remains almost constant: the liquid volume is almost zero and the relative interface area close to one. In this domain, the contact between the two fluids is maximal, but the amount inside which one may trap dissolved gas is reduced to one monolayer of water molecules (0.3 nm).

In terms of drainage/imbibition processes, the two-spheres scheme illustrates that it is not possible to dry completely the grain packing, due to the special stability of adsorption films. On complete drainage, the system is left as network of pendular rings trapping a continuous CO₂ bubble. Thus, the liquid remaining in pendular rings contributes towards the residual liquid saturation of the sedimentary systems.

One interesting point, though it is not developed below, is that in the first and the second region, the CO₂ is interacting with water experiencing a certain capillary pressure. And the in gassing effect of the capillarized water at high suction is well-referenced¹⁶⁻²¹.

Liquid Bridge Adhering to Three Spheres: Drainage and Imbibition in Pore Throat

A situation where liquid phase adheres to three spheres allows coming closer to three dimensional pores network. Three sphere configuration corresponds to the faces of a tetrahedral subunit, at the location termed above the pore throat (Fig. 4), opposite to the pore body (center part of the tetrahedron).

The pore throat provides entrance for the liquid-gas interface inside the pore body, so the dimensions of the pore throat determine the capillary retention (imbibition) or the hydraulic movement (drainage) of the interface. Initially, liquid in the form of a continuous phase adhering to three spheres in contact with CO₂ from all sides. The increasing capillary pressure causes the interface to become more curved. On reaching the “critical curvature” the interface splits into three interfaces (Fig. 4). Simulation was carried by successively increasing the capillary pressure expressing the progressive invasion of CO₂ (Fig. 5). At critical curvature, the CO₂ is able to penetrate the central cavity of the throat, which traps therefore a gas bubble in an equilibrium state. Before reaching the corresponding capillary conditions, the liquid phase occupies most of the throat volume, filled after this threshold by

CO₂ ($V_{CO_2} = 0.49$). Do notice that the liquid phase is initially continuous, and the gas bubble is concentrated in the exterior medium, while after the CO₂ invasion, it turns into a biphasic mixture of two immiscible fluids (CO₂ brine) coexisting in the throat spaces.

In drainage, CO₂ invades from one face. At the critical curvature, CO₂ passes through triangular hole, and gets connected to the reservoir. In imbibition, on decreasing capillary pressure, pendular rings start growing and finally merge together spontaneously, eliminating CO₂ from triangular hole so that the CO₂ phase gets disconnected.

After drainage, the (small) liquid volume remains in the pendular rings even with increasing capillary pressure, meaning that the amount of trapped CO₂ negligibly changes (Fig. 6). These pendular rings contribute towards what is called the residual water saturation, namely the water amount always persisting in natural media.

The imbibition process defines the stage where after a drainage period (normally, up to the critical curvature), the capillary pressure starts decreasing, and the liquid-gas interface recedes towards the pore. In a real medium, this stage is afforded when the liquid pressure has sufficiently increased due to the drainage step, to reverse the driving force. At imbibition, the pendular rings start growing up to special capillary conditions at which the rings merge with each other forming a single liquid bridge adhering to the three spheres: the cavity is filled with liquid throwing out the CO₂ from the central portion, and the CO₂ phase now gets discontinuous (Fig. 6). On further decreasing the capillary pressure, the CO₂ amount decreases in a gradual fashion with the gradual decreasing curvature of the liquid gas interface.

The drainage and imbibition processes obviously follow different paths (Fig. 6), and the CO₂ amount trapped at a particular capillary pressure depends on the pathway. During imbibition process, and before attaining the critical curvature, there is a capillary pressure range along which the CO₂ trapped as stable bubbles is drastically larger than that present along the drainage process (Fig. 6; $V_{CO_2} \sim 0.6$).

The Four Spheres Case: Pore Body Drainage and Imbibition

A truly 3-dimensional pore network can be sketched by dealing with the liquid bridge(s) adhering to four spheres tetrahedrally arranged. In this case, each series of three grains displays a pore throat and wedge-shaped contacts (Fig. 7). The CO₂ can enter in the pore body through any the four throats.

Conclusion

In the present work we have carried out pore-scale investigation for CO₂ sequestration in deep saline aquifer media through capillary equilibria integrating the capillarity laws to understand the CO₂-brine interface behavior along the different steps of the post injection period, pressure associated to the drainage process, and its related equilibria towards the gas pressure, these mutual changes controlling the behavior of the global bubble.

The heterogeneity which is well-known to exist in real reservoirs is simply assumed through the equal-size of the constituting spheres, and varying sphere-to-sphere distance. It would be straightforward to introduce a certain degree of varying sphere size, the combination of possibilities becoming infinite of course.

In the present study, we used the “Surface Evolver” software, avoiding the direct implementation of the Young-Laplace law though it is being inherently satisfied. As a consequence, the present strategy and calculations could be extended to complex geometries, as those defined through the packing of grains having varying and complex individual shapes. Study was started with the simplest situation where a liquid volume is held between two equal spherical grains against the gravity (suspended water) forming a capillary liquid bridge of pendular shape characterized by a constant mean curvature. With increasing capillary pressure, the curvature of the pendular ring goes on increasing, thereby decreasing the liquid amount held.

The graph between liquid volume in pores versus capillary pressure can be subdivided into three parts according to slope of the curve. In the first region of very steep slope indicates that liquid is loosely held which can be removed by capillary pressure. The removal of liquid increases the interface area. In the second region is characterized by gradually varying slope indicating more strongly bounded liquid requiring more capillary force, significant volume remains trapped. The relative total interface area gradually increases with increasing capillary pressure. In the third region, the slope remains almost constant, large capillary pressure is needed to remove the liquid volume. In terms of drainage/imbibition processes, the two-sphere scheme illustrates that it is not possible to dry completely the grain packing. On complete drainage, the system is left as network of pendular rings trapping a continuous CO₂ bubble. Thus, the liquid remaining in pendular rings contributes towards the residual liquid saturation of the sedimentary systems.

The pore throat provides entrance for the liquid-gas interface inside the pore body. With the increasing capillary pressure the interface becomes more & more curved and at the “critical curvature” splits into three interfaces causing CO₂ penetration in the central cavity thereby causing CO₂ trapping. The system becomes a biphasic mixture of two immiscible fluids (CO₂-brine) coexisting in the throat spaces. During the imbibition process the capillary pressure starts decreasing, the pendular rings start growing eventually rings merge with each other forming a single liquid bridge adhering to the three spheres. The cavity gets filled with liquid throwing out the CO₂ from the central portion, and the CO₂ phase now gets discontinuous. Simulation of the situation where liquid phase adheres to three spheres. The drainage and imbibition processes follow different paths. The CO₂ amount trapped at a particular capillary pressure is pathway dependent. During imbibition process, before attaining the critical curvature, for certain capillary pressure range during which the CO₂ trapped as stable bubbles is drastically larger than that present during the drainage process.

Figures:

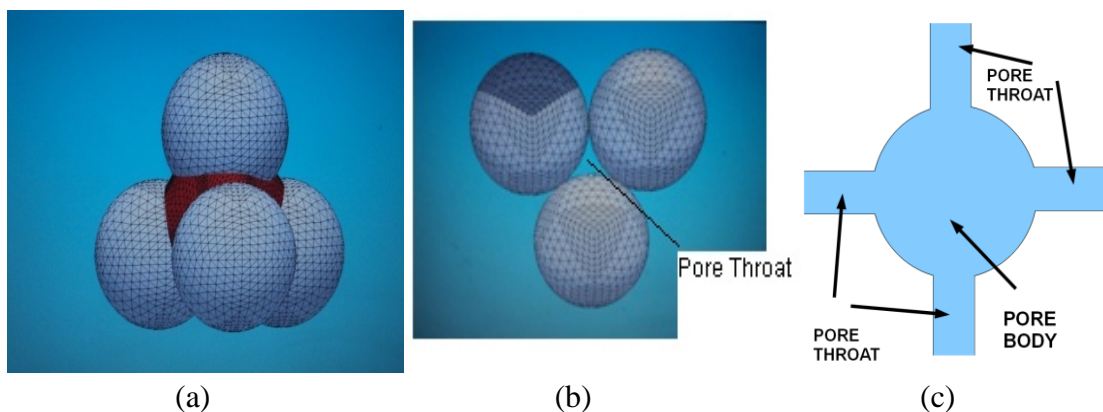


Figure 1. Left, four spheres tetrahedrally arranged, delimiting pore bodies. 'b', pore throat formed by three spheres. 'c', 2D schematic representation of pore body and pore throat.

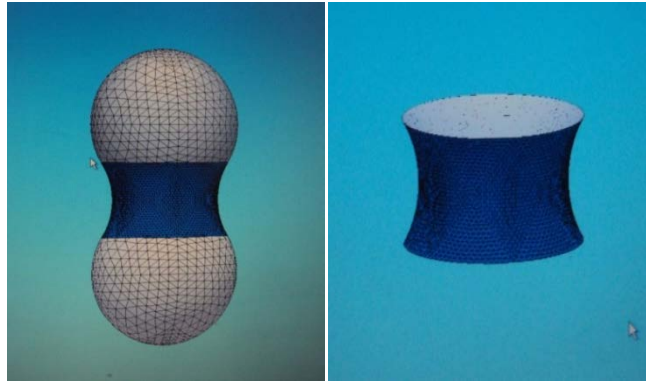


Fig 2. A simulated pendular ring between two equal spheres (left) and the sectional view (right).

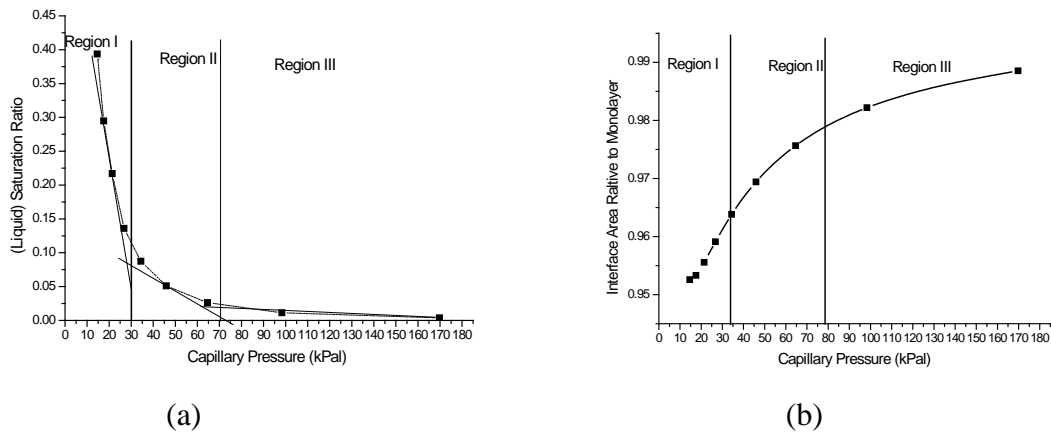


Figure 3. Pendular ring between two spheres. 'a' liquid volume in pores with capillary pressure. 'b' gas-liquid interface area relative to the monolayer area (see text) with capillary pressure.

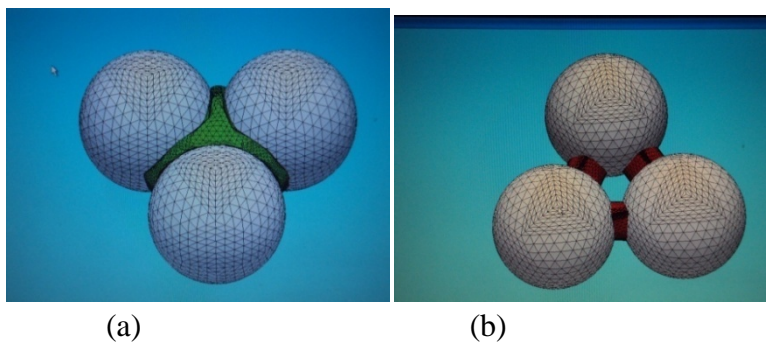


Figure 4. A typical simulated liquid bridge adhering to three equal spheres; before drainage (a) and after drainage (b).

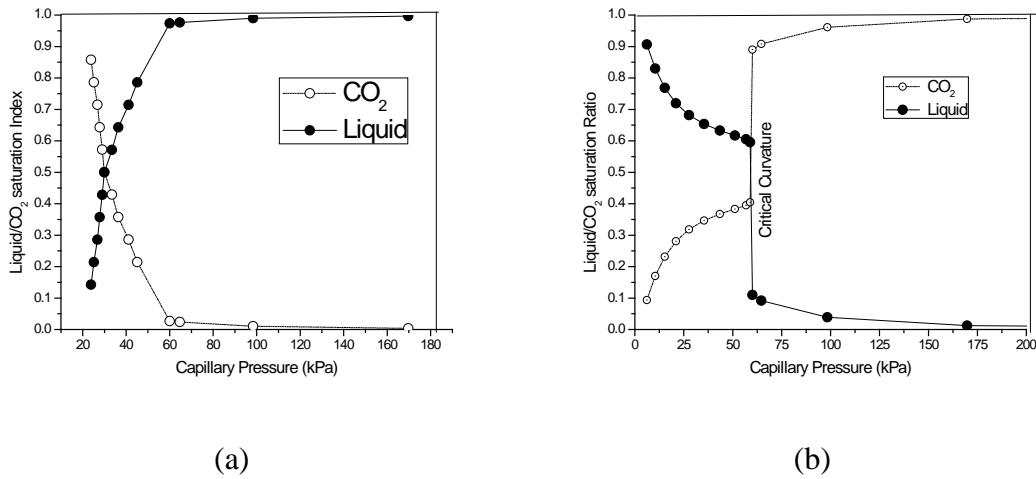


Figure 5. The key processes for pore throat formed by three grains. Drainage(a), Imbibition(b)

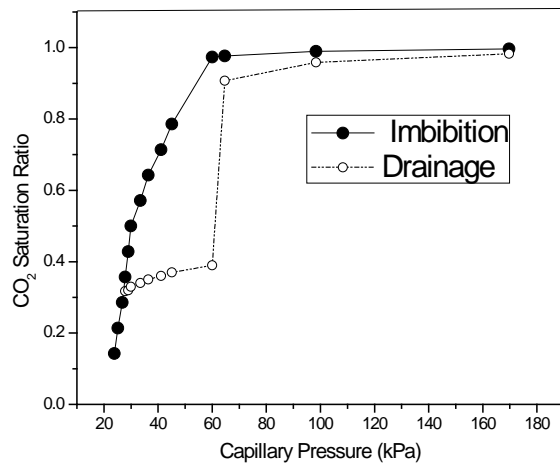


Figure 6. Comparison of volume of CO₂ trapped during drainage and imbibition processes in the pore throat formed by three equal spheres.

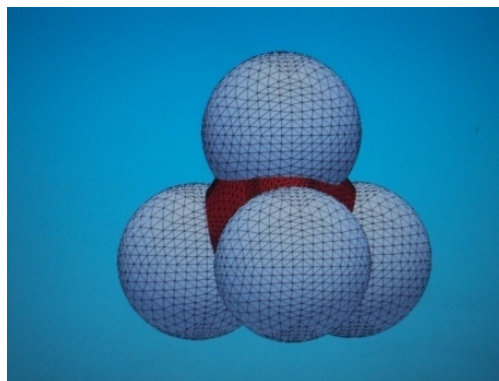


Figure 7. Liquid bridge adhering to four spheres arranged in a tetrahedral configuration.

References

- [1] Oelkers E.H. and Cole D.R. *Elements*: 4, 305. 2008.
- [2] Petit J.R, Jouzel J., Raynaud D., Barkov N.I., Barnola J.M., Basile I., Bender M., Chappellaz J., Davis M., Delaygue G. *Nature*, 399, 429,1999.
- [3] Bachu S. *Environmental Geology* , 44, 277, 2003.
- [4] Doughty C, *Energy Conversion Management* ,48, 1768, 2007.
- [5] Brakke A.K. *Surface evolver manual*. Susquehanna University Selinsgrove, PA 17870. The Surface Evolver software is available from <http://www.susqu.edu/brakke/evolver>. Year 2008
- [6] Van Brakel J. *Powder Technology* , 11, 205, 1975.
- [7] Koplik.J. and Lasseter T.J. *Soc. Petrol.Eng J.* 25(1), 89, 1985.
- [8] Dias M.M., and Prayatakes A.C . *J. Fluid. Mech.*,164,305, 1986.
- [9] Finney J.L. *Proc. R. Soc. London Ser. A. Math. Phys. Sci.*,319, 479, 1970.
- [10] Mason G. *J. Colloid Interf. Sci.*,35(2), 279, 1971.
- [11] Chalbaud C., Robin M., Lombard J.M., Martin F., Egermann P., Bertin H. *Adv. Water Resources*, 32, 98, 2009.
- [12] Shmulovich, K., Mercury L., Thiéry R., Ramboz C., and El Mekki M. *Geochem et Cosmochim. Acta*; 73, 2457, 2009.
- [13] Mekki M., Ramboz C., Perdereau L., Shmulovich K.I., and Mercury L. In *Metastable systems under pressure*. NATO Science for Peace and Security Series A, Chemistry and Biology; 2009: Edited by S.J. Rzoska, A. Drozd-Rzoska et V. Mazur. Springer Verlag, pp. 279-292.
- [14] Bouzid M, Mercury L, Lassin A, Matray J.M. and Azaroual M. *J. Colloid Interf. Sci.*, 355, 494, 2011.
- [15] Bouzid M., Mercury L., Lassin A. and Matray J.M. *J. Colloid Interf. Sci.*;360(2), 768, 2011.
- [16] Mayer R.P. and Stowe R.A. *J. Colloid Interf.Sci.*, 20, 893,1965.
- [17] Mason G. and Marrow R.N. *J. Colloid Interf.Sci.*, 100(2), 519, 1984.
- [18] Mason G. and Marrow R.N. *J. Colloid Interf.Sci.*;1986: 109(1): 46-56.
- [19] Haines W.B. *J. Agri. Soc.*; 20, 97, 1930.
- [20] Mason G. and Mellor W.D. *J. Colloid Interf. Sci.* 176, 214, 1995.

- [21] Suekane T, Thanh N.H., Matsumoto T., Matsuda M., Kiyota M., Ousaka A.
Energy Procedia. 1, 3189, 2009:

**ISOLATION AND CHARACTERIZATION OF PHYTOCHEMICAL
CONSTITUENTS OF CLEOME RUTIDOSPERMA LEAF
METHANOL EXTRACT AND ITS CYTOTOXICITY AGAINST
MCF-7 CELLS**

MULLAI NILA K¹, KARTHIKEYAN J^{2*}

1. Department of Microbiology and Biotechnology, Faculty of Arts and Science, Bharath Institute of Higher Education and Research, Chennai, Tamil Nadu, India
2. PG and Research Department of Zoology, Presidency College, Chennai, Tamil Nadu, India.

E-mail: jaaykay@gmail.com

Received: 22.10.22, Revised: 5.1.23, 13.1.23 Accepted: 16.1.23

ABSTRACT

Natural resources like medicinal plants have been used traditionally to treat or manage various diseases and disorders. Cleome species possess to have major bioactive compounds with clinical significance. The present study was carried out to exploit the *Cleome rutidosperma* for its phytoconstituents and to isolate major bioactive compounds and their efficacy as cytotoxic agent against MCF-7 breast cancer cells. The isolated compound was characterized with GC-MS spectroscopy and the structure was elucidated using spectral data analysis which revealed the presence of a cardiac glycosides derivative that was isolated for the first time from *Cleome rutidosperma* namely Acetic acid 3, 14-dihydroxy-10,13-dimethyl-17-(6-oxo-6H-pyran-3-yl)-hexadecahydro-cyclopenta[α]phenanthren-16-yl ester (Bufotalin). The crude and isolated Bufotalin possess to have potential anticancer activity with an IC₅₀ value of 22.86 μ g/ml and 3.895 μ g/ml respectively, against the breast cancer cell lines. The plant-mediated isolated cardiac glycoside bufotalin will be a potential agent for the control of the proliferation of cancer cells.

Keywords: Bufotalin, GC-MS, FTIR, NMR, MCF-7, *Cleome rutidosperma*.

Introduction

Nature is the best integrative chemist that is of great aid to humankind in many ways. The most abundant healthy natural resources of life are plants¹. Medicinal plants play a crucial role in the discovery of drugs. The origin of modern medicines is highly dependent on traditional medicines². Ayurveda is a restorative framework fundamentally honored in India that has been existent for 5000 years³. The world health organization has estimated that more than 80% of the global population relies on medicinal plants for their primary healthcare⁴. These plants have the natural ability to produce a plant metabolite to balance and survive the harshening environmental conditions and microbial attacks⁵. In recent years, plant species have been scientifically evaluated for their possible medicinal applications. Herbal medicines are a rich source of bioactive compounds that are safe and environmentally friendly⁶.

Plants are the natural reservoirs of bioactive secondary metabolites. Alkaloids, tannins, flavonoids, and phenolics are the most important bioactive constituents present in medicinal plants⁷. The chemical constituents and pharmacological properties of the vast wealth of endangered species were not completely explored. Identification and evaluation of the presence of active principles in these plants is the need of the hour. Every year more than 8 lakh cancer patients were diagnosed in India, while the breast cancer and cervical cancer were found to occur in majority of women across the world⁸. Breast cancer is the most prevalent leading cause of cancer-related death in women⁹. There were about 1,45,000 new cases in India in 2012 and about 70,218 patients died due to breast cancer during this period. It is estimated that the number of cases will increase by 70% in 2035¹⁰. The incidence of breast cancer is higher in urban μ which can be probably due to the change in lifestyle and environmental factors. Traditional medicinal plants are the conventional sources for the separation and isolation of phytoconstituents for the treatment of cancer-related disorders¹¹,¹². Novel therapeutics with potential anticancer activity must be developed to prevent cancer-related deaths, since chemotherapy, and radiation treatments lead to severe side effects. The United States National Cancer Institute has recognized the potential of natural products of plant material as chemo-protective material¹³.

Cleome rutidosperma, commonly known as “Fringed Spider Flower” which belongs to the family Cleomaceae, is a small herb that grows up to 70 cm in height with trifoliate leaves, and small violet-blue flowers. This plant is native to West Africa and has now become naturalized in the tropical and temperate regions of Southeast Asia and other parts of the World¹⁴. The medicinal properties of *C. rutidosperma* has been reported as antimicrobial activity, antioxidant and free radical scavenging activities¹⁵; anti-diabetic effect¹⁶; anti-

hyperglycemic effect¹⁷; antifungal activity¹⁸; and anti-inflammatory effect¹⁹. *Cleome rutidosperma* belonging to the family Cleomaceae comprises 14 genera with two hundred species and most of the species present in the genus were reported to possess bioactive compounds with anticancer potential^{19, 20}. Despite their clinical significance, most of the species belonging to the cleome family were not exploited for their specific chemical constituents. Thus, the earlier studies have established the significant biological activities of *Cleome rutidosperma* on crude preparations. In the present study, an attempt has been made to isolate and elucidate the structure of the isolated compound and to evaluate its efficacy against human cancer cells.

METHODS

Chemicals and media

Chemicals for extraction and column chromatography (analytical grade), methanol was purchased from Hi-Media, Mumbai, India. Silica gel (60-120 mesh) was used for column chromatography and pre-coated silica gel 60 GF254 plates were used for Thin Layer Chromatography (TLC) from Merck Limited, Germany.

Plant material

The whole plant *Cleome rutidosperma* was collected and a voucher specimen was preserved for verification in the Plant Biology and Biotechnology Department, Presidency College, Chennai, Tamil Nadu, India. The disease-free leaves were separated and washed thoroughly with tap water followed by rinsing in double-distilled water and shade dried for fifteen days.

Preparation of extract

Cleome rutidosperma dried powder was used for the hot extraction process with Soxhlet apparatus where methanol is the solvent, the process was continued for eight hours and the collected extracts were concentrated using a vacuum evaporator.

Isolation of bioactive compound Activated silica gel (60-120 mesh) was packed into a glass column (120x30 mm) with n-hexane as solvent was used for the column chromatography²¹. 3grams of methanol extract was loaded on silica gel for the separation of components by the wet slurry method. The column was eluted with the mixtures of hexane and ethyl acetate and finally with 100ml of 100% methanol. The separated fraction was evaluated with TLC using hexane: ethyl acetate: methanol (1.2: 0.5: 0.3).

Spectroscopic analyses of bioactive compound

Gas Chromatography and Mass Spectrogram (GC-MS)

The separated active compound was subjected to gas chromatography-mass spectrometry (GC-MS) analysis which was conducted in JEOL GC mate equipped with Elite- 1 capillary column (30m x 0.25mm) coupled with turbo mass. The column temperature was 110 °C initially held for 2 min, then programmed to 280 °C at a rate of 5 °C/min in the split mode. Helium was used as a carrier gas with a flow rate of 1ml/min. The injector temperature was at 250 °C. The Mass spectrum observed was referred to by the library National Institute of Standards and Technology (NIST).

Fourier Transform Infrared Spectroscopy (FTIR)

50 mg of the column-separated compound was dissolved in 25 ml of deuterated methanol. The sample was dispersed in KBr pellets and loaded in the sample holder of the Perkin Elmer spectrum FT-IR instrument and operated in the range of 450-4000 cm^{-1} . The functional groups were detected from the obtained spectral data.

Nuclear Magnetic Resonance (NMR) Spectroscopy

20mg of the isolated compound was analyzed by NMR (^1H and ^{13}C) by dissolving the compound in 0.5 ml of deuterated methanol and the spectral data was recorded on a Bruker AVANCE III 500 MHz for 6 h at room temperature. 5 mm PABBO-BB probe was used. Methanol-d (Me OD) was used as a solvent. The chemical shifts (δ) were expressed in ppm. The region for ^1H NMR from 0 to 10 ppm and 0 to 200 ppm for ^{13}C NMR was applied for scanning.

IN VITRO ANTICANCER STUDIES

CYTOTOXICITY ASSAY

Cytotoxic efficacy of methanol mediated crude leaf extract of *Cleome rutidosperma* and the derived compound of the extracts were evaluated with 3-(4,5-dimethylthiazol-2-yl)-2,5-diphenyl tetrazolium bromide (MTT) assay. The cells were seeded in 96 well microtiter plates with Dulbecco's Modified Eagle Medium (DMEM) and 10 % Fetal bovine serum (FBS) and incubated till the confluency of 90 to 95% was achieved. After the period of incubation, the wells were loaded with serum-free media and incubated for 60 minutes. Further, the wells were treated with different concentrations of crude methanol extract and the isolated compound Bufotalin and incubated for 24 hours at 37 °C, after the period of incubation of 20 microliters of 5mg/ml (Working solution), MTT was added and further

incubated for 4 hours. At the end of incubation, the medium was removed carefully, and Formazan crystals formed were solubilized using 100 microliters of Dimethyl sulfoxide (DMSO). After 5 minutes the optical density was measured with a microplate reader at 570nm. The growth inhibition (IC₅₀) was determined from the percentage of cell survival which was calculated as per the below equation:

$$\text{Cell Viability (\%)} = \frac{\text{Absorbance of Control}}{\text{Absorbance of Test}} \times 100$$

MCF -7 cells were treated with an isolated compound using 4'-6-Diamidino 2-phenylindole (DAPI) nuclear staining to observe the apoptotic morphology of the cells. The cells were treated with IC₅₀ concentration of Bufotalin for 24 hours and the cells were washed with phosphate buffer saline (PBS) and stained with 5µl of DAPI. The Nuclear morphology was examined under fluorescent microscopy. The apoptotic morphology of the cells was studied by staining the cells with Acridine orange and Ethidium bromide and the cells were observed under fluorescence microscopy.

Statistical analysis

Data were expressed in Mean ± Standard Error (S. E). Statistical analysis was done using a statistical package for social sciences (SPSS) software.

RESULTS

Medicinal plants are the source of bioactive compounds and the qualitative phytochemical findings of the methanol solvent-mediated crude leaf extract of *Cleome rutidosperma* reveal the presence of alkaloids, flavonoids, cardiac glycosides, phenols, steroids, etc., Compounds were isolated from the methanol solvent extract of the plant and the extracts were subjected to column chromatography for the separation of the bioactive compound using n-hexane and ethyl acetate as solvents. Six fractions like fraction A (65:35), fraction B (60:40), fraction C (30:70), fraction D (20:80), fraction E (10:90), and fraction F (5:95) were observed in the eluted column of which fraction F showed prominent antimicrobial activity when compared to other fractions. Further purification of this selected fraction has shown a single spot on TLC (Fig. 1). The GC of the isolated bioactive compound presented in Figures 2 shows the retention time in the column and the detected peaks. The mass spectrometer analysis reveals the presence of a compound 3, 9 á; 14, 15-Diepoxyregn-16-en-20-one, 3, 11 á, 18-triacetoxy- (Fig. 2).

FT-IR spectrum of the purified compound is shown in table 3. It exhibited absorption at 3418, 2053, 1637, 1384, 1323, 1145, 1101 and 621 cm^{-1} . The peak at 3418 cm^{-1} shows the O-H stretch which may be due to the presence of alcohol. The band at 2053 cm^{-1} represents the C=C group. The peak at 1637 cm^{-1} corresponds to C=O stretch, confirming the presence of the unsaturated carbonyl group/ aliphatic group. The bands at 1384 and 1323 cm^{-1} represent the out of plane C-H def -vibration. The peaks at 1145 and 1101 cm^{-1} show C-O stretch which indicates the presence of 3° alcohols and 2° alcohols respectively. In addition, the peak at 621 cm^{-1} indicates a C-H bend which may be due to the presence of an alkene group or methylene rocking.

The column eluted purified compound the yellow crystal, $\text{C}_{26}\text{H}_{36}\text{O}_6$, molecular weight (MW) 444.56. ^1H NMR (500 MHz, MeOD): 0.80 (s, 3H), δ 1.21(t,2H), 1.21 (t,2H), 1.51 (t,1 H), 1.51 (q,2H), 1.61(q,2H), 1.97 (q,1H), 2.05 (m,1H), 2.06 (t,2H), 2.15 (q,2H), 2.23 (d,2H), 2.68 (d, 1H), 4.26 (m,1 H), 4.51 (broad,s) and 5.24 (q, 1H) were considered as tetra cyclic hydrocarbon ring. Pyran ring were observed at 2.35 (s, 3H), 5.69 (d, 1H), 7.53 (s, 1H) and 7.62 (d, 1H) as acetyl group (Fig.3).

^{13}C NMR was performed to observe the presence of bufotalin and the characteristic proton signal were observed at (125 MHz, MeOD): δ 9.88 (C-19), 9.90 (C-18), 22.32 (C-2''), 22.35 (C-11), 24.62 (C-7), 29.30 (C-6), 47.09 (C-2), 47.26 (C-1), 47.43 (C-12), 47.50 (C-15), 47.55 (C-4), 47.57 (C-10), 47.73 (C-5), 47.73 (C-8), 47.74 (C-13), 47.77 (C-9), 47.77(C-17), 47.90 (C-16), 47.94 (C-3), 48.11 (C-14), 102.24 (C-5¹), 105.55 (C-2¹), 110.24 (C-3¹), 110.42 (C-4¹), 171.63 (6 (C=O)) (Table 2 and Fig.4).

The structure of the isolated compound was elucidated using ^1H NMR and ^{13}C NMR and the molecular formula was found to be $\text{C}_{26}\text{H}_{36}\text{O}$. The m/z value of the isolated compound, according to MS data was 429.18 ($\text{M}^+ - \text{CH}_3$), 401.06 ($\text{M}^+ - \text{COCH}_3$), 355.10 ($\text{M}^+ - \text{COCH}_3 - \text{CO}_2 - \text{H}_2$), 281.07 ($\text{M}^+ - \text{C}_7\text{H}_{15}\text{O}_4$), 221.11 ($\text{C}_{15}\text{H}_{24}\text{O}^+$) 182.76 ($\text{C}_{12}\text{H}_{22}\text{O}^+$), 147.05 ($\text{C}_{10}\text{H}_{11}\text{O}^+$), 73.05 ($\text{C}_4\text{H}_9\text{O}^+$). Based on ^1H and ^{13}C NMR, this compound contains 19 Tetracyclic Hydrocarbon rings, five pyran rings, and two acetyl groups which were named Bufotalin (Acetic acid 3, 14-dihydroxy-10, 13-dimethyl-17-(6-oxo-6H-pyran-3-yl)-hexadecahydro-cyclopenta[α] phenanthren-16-ylester) (fig.5).

Cytotoxic activity of methanol crude extract and isolated compound Bufotalin

Methanol extract of *Cleome rutidosperma* was tested against MCF-7 breast carcinoma cell line with varying concentrations of 25 $\mu\text{g/ml}$, 50 $\mu\text{g/ml}$, 75 $\mu\text{g/ml}$, 100 $\mu\text{g/ml}$, and 125 $\mu\text{g/ml}$.

the methanol extract exhibits significant activity against the breast cancer cell line with an IC_{50} value at 22.86 μ g/ml after 48hrs (Table3). The Cytotoxicity of the isolated compound was evaluated against MCF-7 breast cancer cell lines using an MTT assay and the cells were treated with different doses of isolated compound bufotalin ranging from 0.0044 μ M/L to 0.0179 μ M/L. The results reveal the potential of the Bufotalin against the breast cancer cell lines with an IC_{50} value of 2.68 μ g/ml. Further, the apoptosis in the anticancer activity of Bufotalin was observed using DAPI and Acridine orange and Ethidium bromide staining to observe the nuclear and cell morphology. The DAPI results reveal that the impact of Bufotalin over the MCF cells results in the chromatin condensation resulting in the bright blue colour of the apoptotic cell nuclei and the live cells were light blue. The apoptotic cell percentage increases with increasing concentration and confirms the anticancer efficacy of the Bufotalin isolated from the crude methanol leaf extract of *Cleome rutidosperma*.

The data presented in Table 4 represents the cell viability assay using the MTT assay to check the efficacy of the isolated compound Bufotalin from the methanol leaf extract of *Cleome rutidosperma* against MCF-7 breast carcinoma cell line with the concentration ranging from 2 μ g/ml, 4 μ g/ml, 6 μ g/ml, 8 μ g/ml and 10 μ g/ml. The cell lines were maintained in the structural environment, and the cytotoxic activity was observed at 24hrs and 48hrs after the exposure as that of crude extracts. The potential compound Bufotalin shows a potential anticancer efficacy against the MCF-7 cell line with an IC_{50} value of 12.84 after 24hrs and 3.895 μ g/ml after 48hrs.

The enlargement of cells with membrane blebbing was apparent in the cells. The morphological observation (Figure 6b and d) reveals the structural alterations in the shape of the cells, apoptotic cells with vacuolation are evidenced and the cells were detached from the monolayer culture suggesting cell death.

DISCUSSION

Plants produce a diverse range of bioactive molecules making them a rich source of different types of medicines. The natural extracts of plants are an important source for the identification of new biologically active compounds with possible applications in the pharmaceutical field. Phytotherapy embraces the isolation from herbs, of compounds with unique chemical structures, which are pharmacologically active²². The bioactive compounds were characterized using chromatographic methods and crude methanol leaf extract of *C.*

rutidosperma was purified by silica gel column chromatography. Six fractions were collected from the column of which fraction F shows prominent antimicrobial activity. To identify the nature and structure of the compound, it was further subjected to FTIR, ¹H NMR, and ¹³C NMR. ¹H NMR and ¹³C NMR and observations reveal the presence of the carbonyl group, alcohols, and aliphatic groups.

NMR spectral analysis of the isolated compound confirms the structural configuration and the compound materials have been identified as Bufotalin. Bufotalin represents the class of compounds that belongs to cardiac glycosides. The presence of bufadienolides was recorded from plant and animal sources²³. The bufadienolides were characterized by six membrane lactone rings with 2 double bonds attached in 17 beta position at the positive Hexa hydro cyclo Penta phenanthrene skeleton.

In Chinese medicine, bufadienolides were commonly used to treat various disorders, especially in cancer patients in China²⁴. Bufotalin exhibits many pharmacological and biological activities in addition to antitumor and cardiogenic activity²⁵. Anti-cancer agents induce apoptosis to arrest the tumor cell proliferation and progression²⁶. Bufalin is shown to induce cell differentiation and apoptosis were interlinked and regulated by distinct protein kinase C isoenzyme²⁷. Cardiac glycosides like bufotalin act as potent inhibitors over cancer cell growth²⁸. Cardiac glycosides inhibit cancer cell proliferation even in minimal concentrations²⁹. Bufotalin was used in traditional Chinese medicine to inhibit the growth of the proliferation of human hepatocarcinoma cells Hep-G2³⁰. Bufotalin is a potential candidate for the treatment of pancreatic cancer when administered along with gemcitabine a standard anticancer drug³¹.

Two alkaloids aspara doxonine and para doxenoline were isolated from the chloroform fraction of methanol extract of *C.paradoxa*³². A steroid derivative 17-(4-hydroxy-1, 5-dimethylhexyl)-2, 3, 7-(acetyloxy) gona-1, 3, 5(10)-trien-15-ol was isolated and identified from the phenolic extract of *C.arabica* and named as Clive-92^{33,34}. Ten compounds were identified by 35 Jordheim *et al.* (2009) from the flowers of *C.hassleriana*. Palmitic acid, Cleomaldeic acid, glucocapparin, glucocleomin were isolated and identified from *C.viscosa*^{36,37}. In the present investigation a cardiac glycosides derivative was primarily isolated from *Cleome rutidosperma* namely Acetic acid3,14-dihydroxy-10,13-dimethyl-17-(6-oxo-6H-pyran-3-yl)-hexadecahydro-cyclopenta[α]phenanthren-16-yl ester.

Alkaloids, polyphenols phenylpropanoids, and terpenoids were said to possess anticancer properties.^{38,39} NCI- United States of America has set the limit for the activity for crude extracts with the IC₅₀ value i.e., 50% of inhibition of proliferation with less than 30µg/ml after the exposure to 72 hrs. of exposure⁴⁰. The crude extract with the IC₅₀ value of less than 20µg/ml is highly cytotoxic in nature⁴¹. The results observed in the present study show the potent cytotoxic effect on MCF-7cells with methanol and aqueous extract of *Cleome rutidosperma*. The IC₅₀value was 108.260µg/ml concerning 24hrs and 22.86µg/ml after 48hrs of exposure. The IC₅₀ value was much lower than the recommendation of NCI, the USA for the characterization of a pure compound as the anti-carcinogenic agent.

The anti-cancer sensitivity of *E. guineermisis* is due to the presence of flavonoids⁴², phytocompounds alkaloids, and flavonoids of *Onobis hirta* are responsible for the superior anti-cancer activity against cancer cells⁴³. Polyphenols and flavonoids are known to have antioxidant and anticancer activity⁴⁴. As the prevalence of cancer cases is on the rise, it is necessary to screen and search the naturally available bioactive compounds with the potential to act against the cancer cells. Many compounds have been analyzed for their anticancer potential. Out of 974 small molecules screened from 1981 to 2006, 12% are designed from natural products inhibitor of the target of interest, and inhibition of active sites of the endogenous substrates such as ATP⁴⁵.

Bufadienolides are an important group of polyhydroxy C-24 steroids and their glycosides. Bufadienolides were derived both from animal and plant sources. The plant families Crassulaceae and Hyacinthaceae are abundant sources of bufadienolides, a type of cardiac glycoside traditionally used for the treatment of cardiac dysfunction and show some toxic effects⁴⁶. The structural modifications of these compounds may make them a productive area of research and to design of a new lead compound. The compound that has the potential to kill the cancer cells with a specific concentration while not affecting the non-malignant cells was therapeutically useful. The cardiovascular side effect of these compounds pronounced restriction in the application of Bufotalin for the treatment of cancer in the form of chemotherapeutic drugs.

In the present study, it is evident that the nontoxic compound bufotalin was isolated from the methanol leaf extract of *Cleome rutidosperma*. Many researchers are in the search of novel compounds with specific anticancer potential. The ethnomedicine importance of bufotalin intended to study the cytotoxic efficacy of the plant-mediated compound isolated from

Cleome against the MCF-7 cell line. The result presented in the table reveals the cytotoxic effects of bufotalin on breast cancer cell lines. With the IC_{50} value 12.840 μ g/ml after 24hrs and 3.893 μ g/ml with reference to 48hrs, the results suggest the cytotoxicity of bufotalin on cancer cell lines.

The cytotoxic effect of bufotalin based on the time and dosage has been reported against Hep 3b, HT-29, and MCF-7 cells⁴⁷. It is evident from the results that bufotalin has time-dependent activity concerning MCF-7 cell lines, further the anticancer potential of bufotalin on a nude mouse model suggesting that the bufotalin inhibits the cancer growth by the activation of p53 signaling⁴⁸. The growth inhibitors activities of the drugs utilized to treat cancer cells were achieved by the induction of apoptosis⁴⁹. The present study reveals a dose-dependent increase in the percentage of apoptosis which amounts to 69.65% proved to 10 μ g/ml concentration when compared to control.

Bufadienolides were considered a potent cytotoxic agent against different cancer cells⁵⁰. Chemically modified bufadienolides can kill the malignant cells without damaging the normal non-malignant cells⁵¹. Biotransformation is a process by which the nature of the substances was altered by the secreting metabolites; structural diversity plays a major role in the mechanism of action against the Cancer cells. The biotransformation of the structural configuration of the cardiac glycoside compound bufadienolides isolated from *Cleome rutidosperma* possesses to have cytotoxic activity against the breast cancer cells. The compound bufotalin isolated from the *Cleome rutidosperma* methanol mediated extract was bio-transformed by the metabolites of the plant. The structural elucidation reveals the bio-transformed compound with potential cytotoxic activity. The isolated compound obtained was studied against the MCF-7 breast cancer cells for their cytotoxic nature. Bufotalin isolated from the leaf extracts shows potential cytotoxic activity against tested cells with an IC_{50} value of 0.0039 μ mol/ml, it is essential to evaluate the potential of the compound in vivo.

CONCLUSION

The leaf methanol extract of *Cleome rutidosperma* and the isolated compound Bufotalin has potential cytotoxic activity against MCF-7 breast cancer cells. The activity of the isolated compound is much higher when compared with the crude extract of the tested plant. The inhibition of cancer cell proliferation and loss of cell viability is varying with the time and dose dependent manner with crude and isolated compound. Further studies may throw light

on the clinical application of plant derived bufotalin and the mechanism behind the biological action against the cancer cells.

Figures:



Figure: 1 TLC profiling of isolated compound from methanol leaf extract of *Cleome rutidosperma*

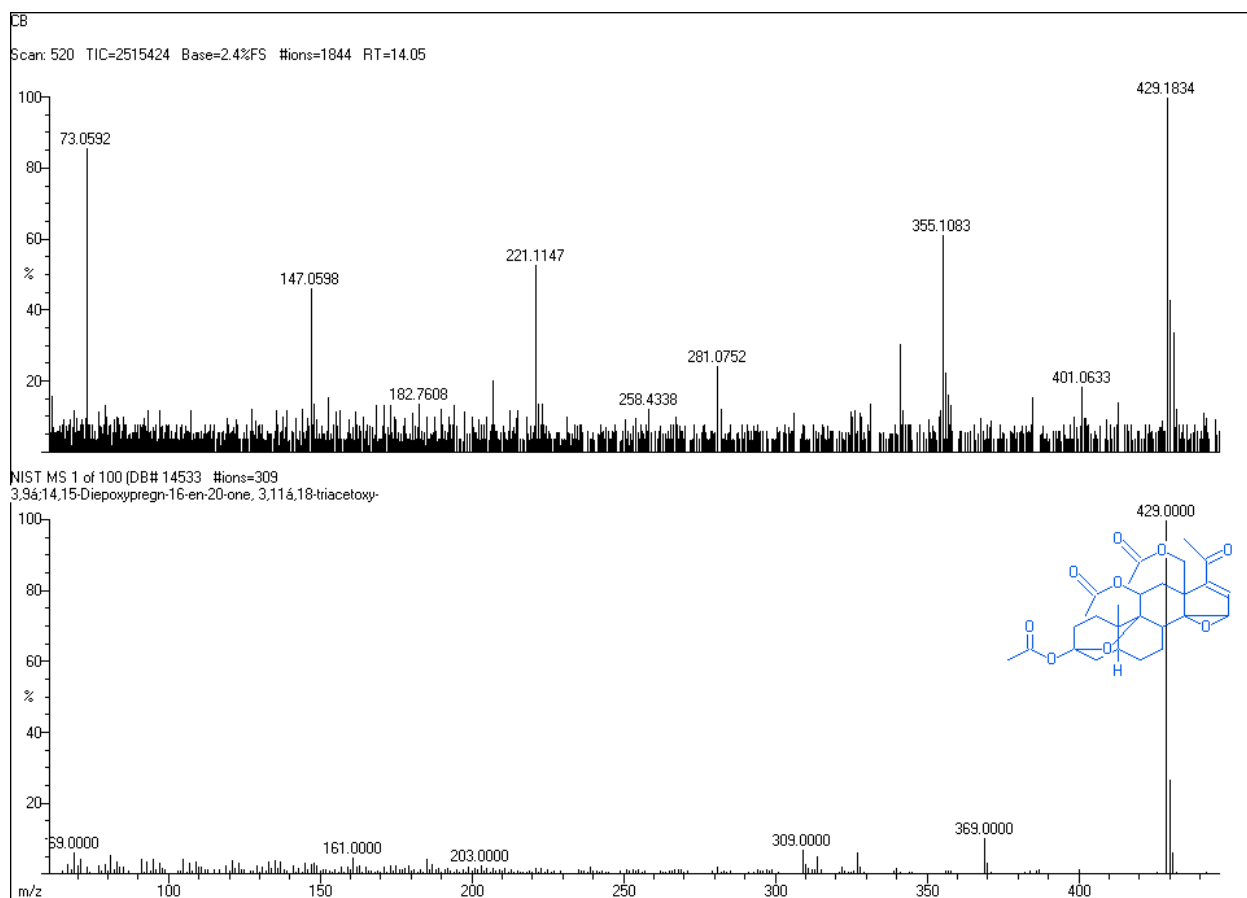


Figure: 2 Mass spectrogram of compound isolated from methanol leaf extract of *Cleome rutidosperma*

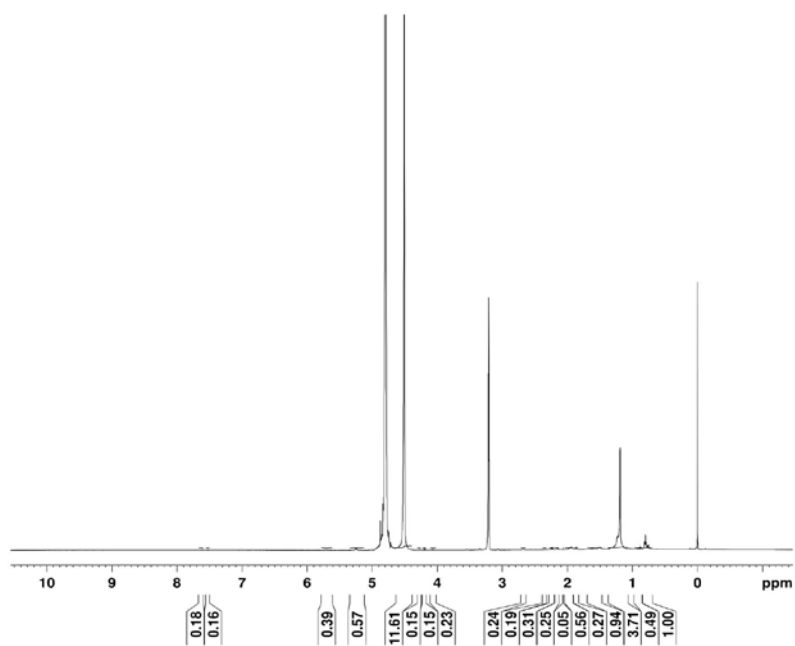


Fig. 3: ^1H NMR spectrum at 500 MHz in MeOD

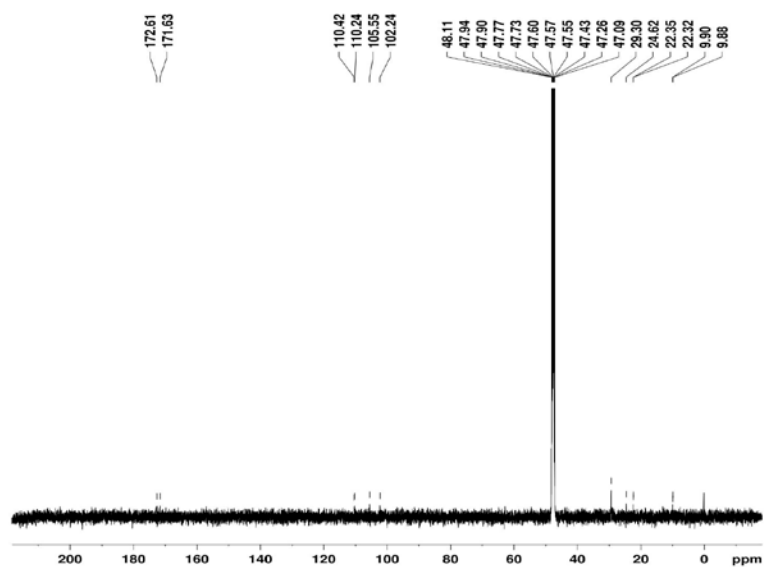


Fig. 4: ^{13}C NMR spectrum at 125 MHz in MeOD

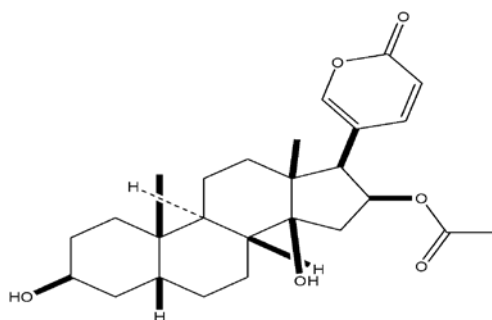
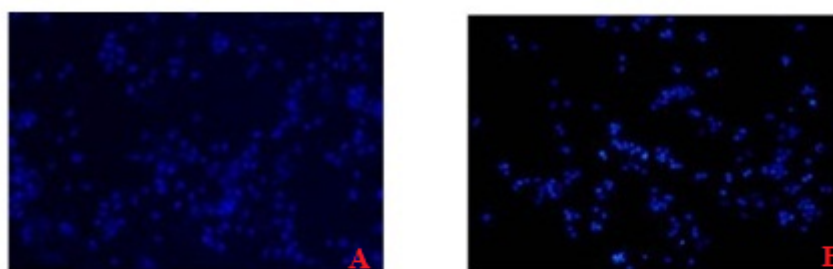
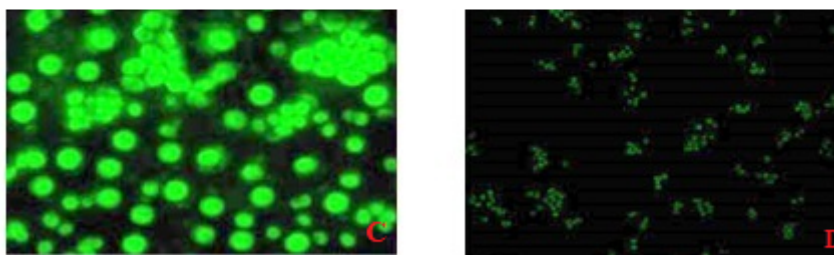


Fig. 5: Chemical structure of compound



Nuclear staining Using DAPI of breast cancer celllines (MCF-7) (a) untreated, (b) MCF-7 cells treated with Bufotalin isolated from *Cleome rutidosperma* methanol leaf extract



Staining with Acridine orange of Human Breast Cancer cells MCF-7 (c) Untreated (d) MCF-7 cells treated with Bufotalin isolated from *Cleome rutidosperma* methanol leaf extract

Figure 6: Invitro studies on the cytotoxic activity of Bufotalin isolated from the *Cleome rutidosperma* leaf extract.

Tables:

Table 1: FT-IR spectrum data of isolated compound

Functional group	Type of vibration	Region (cm ⁻¹)
O-H	O-H str	3418
C=C	C=C str	2053
C=O	α, β-Unsaturated carbonyl group (Six membered) / aliphatic C=O str	1637
C-H	C-H def	1384
C-H	C-H def	1323
C-O / C-O-H	C-O str / C-O str (3° alcohol)	1145
C=C-O-C / C-O-H	C-O str / C-O str (2° alcohol)	1101
C-H bend	Mono substituted alkene / Methylene rocking	621

Table 2: ¹H- and ¹³C- NMR data of Bufadienolide

Bufadienolide (Bufotalin)					
Position No.	¹ H NMR (ppm)	¹³ CNMR (ppm)	Position No.	¹ H NMR (ppm)	¹³ CNMR (ppm)
Tetracyclic Hydrocarbon ring			Tetracyclic Hydrocarbon ring		
1	1.21 (t, 2H)	47.26	16	5.24 (q, 1H)	47.90
2	2.15 (q, 2H)	47.09	17	2.68 (d, 1H)	47.77
3	4.26 (m, 1H)	47.94	18	0.80 (s, 3H)	9.90
4	2.06 (t, 2H)	47.55	19	0.80 (s, 3H)	9.88
5	2.05 (m, 1H)	47.73	3- & 14-(OH)	4.51(broad, s)	---
6	1.61 (q, 2H)	29.30	Pyran ring		
7	1.61 (q, 2H)	24.62	1	---	---
8	1.97 (q, 1H)	47.73	2	7.53 (s, 1H)	105.55
9	1.51 (t, 1H)	47.77	3	---	110.24
10	---	47.57	4	7.62 (d, 1H)	110.42
11	1.51 (q, 2H)	22.35	5	5.69 (d, 1H)	102.24
12	1.21 (t, 2H)	47.43	6(C=O)	---	171.63
13	---	47.74	Acetyl group		
14	---	48.11	1(C=O)	---	172.61
15	2.23 (d, 2H)	47.60	2	2.35 (s, 3H)	22.32

ppm-parts per million, ¹H-one proton, ¹³C-carbon thirteen

Table 3: Cytotoxicity effects of isolated compound of *Cleome rutidosperma* against MCF-7 breast cancer cell line by MTT assay

Concentration ($\mu\text{g/ml}$)	24hrs treatment		48hrs treatment	
	Cell Viability (%)	Cell Death (%)	Cell Viability (%)	Cell Death (%)
2	87.29 \pm 0.883	12.71	59.57 \pm 1.595	40.43
4	84.31 \pm 1.365	15.69	49.47 \pm 1.139	50.53
6	77.80 \pm 0.831	22.20	40.65 \pm 1.826	59.35
8	68.15 \pm 1.403	31.85	33.42 \pm 1.758	66.58
10	61.06 \pm 1.318	38.94	30.35 \pm 1.125	69.65
Control	100 \pm 0.00	0.00	100 \pm 0.00	0.00
IC₅₀	12.840		3.895	

Table 4: Cytotoxicity effects of methanol leaf extract of *Cleome rutidosperma* against MCF-7 breast cancer cell line by MTT assay

Concentration ($\mu\text{g/ml}$)	24hrs treatment		48hrs treatment	
	Cell Viability (%)	Cell Death (%)	Cell Viability (%)	Cell Death (%)
25	65.98 \pm 0.510	34.02	52.32 \pm 0.708	54.68
50	62.30 \pm 0.380	37.70	46.46 \pm 0.653	59.54
75	57.54 \pm 0.490	42.46	40.28 \pm 0.596	63.72
100	52.02 \pm 0.580	47.98	33.97 \pm 0.848	66.03
125	45.91 \pm 0.470	54.09	28.37 \pm 0.284	71.63
Control	100 \pm 0.00	0.00	100 \pm 0.00	0.00
IC₅₀	108.260		22.860	

ABBREVIATIONS

- FTIR:** Fourier Transform Infrared Spectroscopy
GC-MS: Gas Chromatography-Mass Spectrometry
NMR: Nuclear Magnetic Resonance
TLC: Thin Layer Chromatography
MTT: 3-(4,5-dimethylthiazol-2-yl)-2,5-diphenyl tetrazolium bromide
DMEM: Dulbecco's modified Eagle medium
FBS: Fetal bovine serum

DMSO:	Dimethyl sulfoxide
NIST:	National Institute of Standards and Technology
DAPI:	4-6-Diamidino 2-phenylindole
PBS:	Phosphate Buffer Saline
SPSS:	Statistical Package for Social Sciences

REFERENCES

1. W. Russell, G. Duthie, *Proc Nutr Soc.*, 70, 389, 2011.
2. R. Abu-Dahab, F. Afifi, *Sci. Pharm.*, 75, 121, 2007.
3. Ajazuddin, S. Saraf, *Pharmacogn Rev.*, 6, 154, 2012.
4. NR. Farnsworth, DD. Soejarto, *Econ. Bot.* 39, 231, 1985.
5. PA. Egwaikhide, SO. Okeniyi, CE. Gimba, *J. Med. Plants. Res.* 3, 1088, 2009.
6. M. Pradeepa, V. Kalidas, N. Geetha, *Int. J. App. Pharm.* 8, 7, 2016.
7. A. Kumar, R. Ilavarasan, T. Jayachandran, M. Decaraman, P. Aravindhan, *Pakistan J Nutri.* 8, 83, 2009.
8. K. Kaarthigeyan, *Indian J. Med. Paediatr. Oncol.* 33, 7, 2012.
9. N. Azamjah, Y. Soltan-Zadeh, F. Zayeri, *Asian Pac. J. Cancer Prev.* 20, 2015, 2019.
10. J. Ferlay, et al., *Int. J. Cancer.* 136, 359, 2015.
11. O. Awodele, AA. Adeyomoye, DF. Awodele, V. Kwashi, IO. Awodele, DC. Dolapo, *J. Cancer Edu.* 26, 497, 2011.
12. AA. Shahat, AY. Ibrahim, MS. Alsaid, *Indian J. Tradit. Know.* 14, 28, 2015.
13. NP. Gullett, et al., *Seminars in Oncology.* Elsevier. 258, 2010.
14. AA. Mitchell, BM. Waterhouse, 2nd Ed. *Misc. Pub. No.6/98*, 1998.
15. A. Bose, S. Mondal, JK. Gupta, T. Ghosh, D. Debbhuti, S. Si, *Oriental Pharm. Exp. Med.* 8, 135, 2008.
16. IO. Okoro, IA. Umar, SE. Atawodi, KM. Anigo, *Int. J. Pharm. Sci. Res.* 5, 2490, 2014.
17. O. Okoro, IA. Umar, SE. Atawodi, KM. Anigo, *Int. J. Pharm. Pharm. Sci.* 7, 289, 2015.
18. A. Knunta, SK. Mohanty, *Res. J. Pharm. Tech.* 4, 1103, 2011.
19. A. Annadurai, JS. Ahmed, *Adv. Appl. Sci. Res.* 5, 122, 2014.
20. H. Singh, A. Mishra, AK. Mishra, *Biomed. Pharmacother.* 101, 37, 2018.
21. MH. Laurence, JM. Christopher, 2nd ed. *Blackwell Publication* 180, 1989.
22. R. Londonkar, JV. Hanchinalmath, *Int. J. Cur. Pharm. Res.* 6, 28, 2014.
23. L. Novonty, HA. Ghuloom, NA. Al-Hasawi, *Res. J. Pharm. Biol. Chem. Sci.* 10, 1147, 2019.

24. JB. Puschett, E. Agunanne, MN. Uddin, *Am. J. Kidney Dis.* 56, 259, 2010.
25. RJ. Clifford, JH. Kaplan, *PLoS ONE* 8, e84306, 2013.
26. PL. Kuo, CY. Chen, YL. Hsu, *Cancer Res.* 67, 7406, 2007.
27. M. Kurosawa, Y. Tani, S. Nishimura, S. Numazawa, T. Yoshida, *Am. J. Cell Physiol.* 200, C459, 2001.
28. CM. Xie, XT. Lin, D. Wu, Ye. Tan, CHK. Cheng, J. Zhang, *Oncotarget.* 9, 13783, 2018.
29. JM. Calderon- Montano, EB. Moron, M. Lopaz-La, *Oncogene* 33, 2947, 2014.
30. DM. Zhang, et al., *Eur. J. Pharmacol.* 692, 19, 2012.
31. Y. Chen, Q. Guo, B. Zhang, M. Kang, Q. Xie, Y. Wu, *Oncology Lett* 4, 792, 2012.
32. R. Azza, Abdel-Monem, *Natural Product Research*, 26, 3, 2012.
33. Ravindra G. Mali, *Pharmaceutical Biology*, 48, 105, 2010.
34. S. Tandon, A. Chatterjee, SK. Chattopadhyay, R. Kaur, AK. Gupta, *Industrial Crops Products* 31, 335, 2010.
35. M. Jordheim, M. Andersen, C. Nozzolillo, VT. Amiguet, *J. Phytochem*, 70, 740, 2009.
36. VT. Aparadh, BA. Karadge, *Pharmacognosy Journal* 2, 324, 2010.
37. R. Jente, J. Jakupovic, GA. Olatunji, *Phytochem.* 29, 666, 1991.
38. Spiridon E. Kintzios, *Crit. Rev. Plant Sci.* 25, 2, 2006.
39. HJ. Park, MJ. Kim, E. Ha, JH. Chung, *Phytomedicine*, 15, 147, 2008.
40. ESS. Abdel-Hameed, SA. Bazaid, MM. Shohayeb, MM. El-Sayed, EA. El-Wakil, *Euro. J. Med. Plants.* 2, 93, 2012.
41. W. Mahavorasirikul, V. Viyanant, W. Chaijaroenkul, A. Itharat, KN. Bangchang, *BMC Complement Altern Med* 10, 55, 2010.
42. S. Vijayarathna, S. Sasidharan, *Asian Pac. J. Trop. Biomed.* 2, 826, 2012.
43. WH. Talib, AM. Mahasneh, *Sci. Pharm.* 78, 33, 2010.
44. W. Ren, Z. Qiao, L. Wang Zhu, L. Zhang, *Med. Res. Rev.* 23, 519, 2003.
45. DJ. Newman, GM. Cragg, *J. Nat. Prod.* 83, 770, 2020.
46. A. Kamboj, A. Rathour, K. Mandeep, *Int. J. Pharm. Pharm. Sci.* 5, 20, 2013.
47. CL. Su, TY. Lin, CN. Lin, SJ. Won, *J. Agri. Food Chem.* 57, 55, 2009.
48. S. Lin, et al., *Oncol. Lett.* 15, 1566, 2018.
49. HM. Wang, et al., *Cancer Sci.* 101, 2612, 2010.
50. GA. Cunha-Filho, et al., *Toxicon* 56, 339, 2010.
51. D. Daniel, C. Susal, B. Kopp, G. Opelz, P. Terness, *Int. Immunopharmacol.* 3, 1791, 2003.

“Removal of aqueous solution of Methylene blue dye using “*Clitoria ternatea*”: A Novel Adsorbent”

D. J. Borkar^{1*}, P. V. Adhyapak² and N. S. Rajurkar³

1*. Anantrao Thopte College, Bhor, Pune 412206, INDIA

2. Centre for Materials for Electronics Technology (C-MET), Pune 411008, INDIA

3. Department of Chemistry, Savitribai Phule Pune University, Pune 411007, INDIA

*Email: dhananjayborkar@atcbhor.com, djborkar778@gmail.com

Received: 15.1.23, Revised: 23.1.23, Accepted: 28.1.23

ABSTRACT

Textile, paper, plastic and paint industries discharge large amount of waste water containing dyes. Dyes are stable to light, non-biodegradable and difficult to degenerate hence they should be removed before discharging the effluents into the environment to diminish health damage and demolition of the environment. The existing work establishes the use of acid treated *Clitoria ternatea* leaves powder (ATCTLP) for the removal of methylene blue (M.B.) dye from its aqueous solution. For this purpose, batch adsorption process was used. The study revealed that maximum removal of the M.B. dye (5 mg L^{-1}), was found to be 90.86 % at pH 7, contact time 60 min, adsorbent dose 0.02 g and particle size $105 \mu\text{m}$. The adsorbent was characterized using FESEM, EDX, FTIR, X-RD techniques before and after adsorption which clearly indicates effective adsorption of dye on it. The studied adsorbent is cost effective and can be applied for effluent treatment from dye industry.

Key word: Methylene blue, *Clitoria ternatea*, Adsorption, Dye removal

1. Introduction

A Huge quantity of waste water containing dyes is produced by textile industries. About 60,000 tons of dyes are discharged in to the environment, 80% of which are azo dyes¹. Trace quantity of dyes also affects plant and animal life². The dyes are carcinogenic and genotoxic³. Chemical precipitation, solvent extraction, flocculation, coagulation, membrane filtration, chemical oxidation, ion-exchange, reverse osmosis and adsorption are some methods used for waste water treatment. However, most of these methods are neither environmentally friendly nor economically feasible. Amongst all these methods, more effective and superior technique is Adsorption⁴; in terms of efficiency and cost effectiveness. It is a sludge free clean operation with maximum removal of dye even from very dilute solutions. Several investigators have reported variety of agricultural waste as adsorbents; in view point of their good adsorption capacity such as almond gum⁵, rice biomass⁶, neem sawdust⁷, rice husk⁸, and

wheat shell⁹. Removal of different dyes using various adsorbents was reported from our laboratory¹⁰⁻¹². Natural low-cost adsorbents are one of the best applicants for the removal of dye from wastewater. Natural adsorbents were basically composed lignocellulose material such as lignin cellulose and hemicellulose^{13, 14}, which improve adsorption capacity. In the present work, *Clitoria ternatea* Leaves (local name: Gokarn) were used as an adsorbent after chemical treatment.

2. Experimental

2.1. Materials

Fresh leaves of *Clitoria ternatea* were collected from home garden. The Methylene Blue ($\lambda_{\text{max}}= 661\text{nm}$) dye used in this study was obtained from Fisher Scientific (Qualigens fine chemicals).

2.2. Preparation of adsorbent

The garden-fresh leaves of *Clitoria ternatea* were thoroughly washed with water, dried under sunlight and soaked with 1:1 ortho-phosphoric acid for 24 hours and were then filtered through Whatman filter paper no. 42. The soaked leaves were boiled and washed with distilled water until free from organic components. It was then dried in an oven and sieved through mesh (size 105- 710 μm) to get uniform particle size. It was stored in air tight glass container until further use.

2.3. Preparation of dye solution:

A stock solution was prepared and diluted further as per the requirements. For absorbance measurement a UV-Visible double beam spectrophotometer (Shimadzu) was used. The concentration of dye was determined, before (C_o) and after (C_e) batch adsorption process, at 661nm.

2.4. Batch Adsorption process

Batch Adsorption process was used to study the maximum removal of dyes under optimized conditions. Various parameters viz. pH, contact time, adsorbent dose, particle size, concentration and temperature were optimized to obtain maximum removal of dye. Each adsorption experiment was carried out with 25 mL dye solution in 100 mL round bottom flask.

2.5. Characterization of adsorbent

The various physico-chemical techniques were used to characterize (before and after adsorption) chemically treated *Clitoria ternatea* adsorbent. FTIR spectrophotometer (Shimadzu 8400) was used to study IR spectrum (wave length 4000-400 cm^{-1}) of adsorbent,

using KBr disk for reference. Field Emission Scanning Electron Microscopy (FET Nova nanoSEM-450) was used to study surface morphology of adsorbent. Presence of different elements was determined with the help of energy dispersive X-ray spectrum (Brouker SLASH-6130) detector

3. Experimental procedure

3.1. Adsorption of Dye:

25 ml of desired concentration of MB was stirred for different time intervals by adding the desired quantity of adsorbent. pH of the solution was adjusted by means of 0.1N HCl and 0.1N NaOH. The solution was stirred using magnetic stirrer at constant speed (1100 rpm) for various time interval. After centrifugation (3000 rpm) for 10 minutes, supernatant solution was filtered through Whatman filter paper No. 42 and filtrate was analyzed with UV-Visible spectrophotometer. The following equation was used to calculate extent of dye removal

$$\% \text{ dye removal} = \frac{C_o - C_e}{C_o} \times 100 \quad \text{----- (1)}$$

Where, C_o = Initial concentration of dye solution (mg L^{-1}),

C_e = Concentration of dye solution (mg L^{-1}) after adsorption.

At a time only one parameter was varied keeping others constant.

3.2. Recovery of Dye: Dye was recovered at optimum condition of adsorption by using 25 ml of water, 0.1N NaCl, 0.1 N NaOH and 0.1 N HCl solutions and contact time 40 min.

Recovery of dye was determined by measuring the absorbance with UV- Visible spectrophotometer and following equation

% recovery of dye was calculated using the equation given below,

$$\% \text{ Recovery} = \left(\frac{c_d}{c_a} \right) \times 100 \quad \text{----- (2)}$$

Where: C_d is amount of dye desorbed (mg L^{-1}) and C_a is amount of dye adsorbed (mg L^{-1}).

4. RESULTS AND DISCUSSION:

The effect of various parameters on removal of dye is discussed below

4.1. Effect of pH:- Fig.1 shows % removal of dye as a function of pH

As can be seen from above Fig. the extent of adsorption of dye increases with increase in pH and remains almost constant after pH 7 indicating maximum removal at this pH. Similar results are also reported by Rajurkar et.al.¹², At lower pH adsorption of MB was lower due to H^+ ions competing with the MB cationic group at absorption site which decreases the dye adsorption. H. Dargo et. al.¹⁵ and Reddy et. al.¹⁶.

4.2. Effect of contact time:- The % removal of dye as a function of contact time is presented in Fig.2

Fig.2, indicates a rapid increase in % removal up to 60 min. and then a gradual decrease in it. Similar results were reported by Rajurkar et. al,¹². Around 82.4 % of MB was removed within 60 min, due to strong attractive forces between the adsorbate and adsorbent¹⁷. Initially, adsorption increases with increase in contact time. At optimum contact time, surface area of adsorbent, gets completely adsorbed by dye. At this point, adsorbed and desorbed dyes are in equilibrium with an adsorbent. After optimum contact time, further no adsorption takes place.

4.3. Effect of adsorbent dosage: - Fig.3 presents effect of adsorbent dose on dye removal.

An examination of Fig.3 shows that after certain amount of dose, % removal decreases and the optimum dose is 0.02 g.

Adsorbent dose plays important role in the removal of dye. Initially adsorption sites are not saturated and are available for adsorption. After equilibrium, with increasing adsorbent dose, the amount of adsorbent adsorbed per unit mass of adsorbate decreases due to saturation of adsorption sites due to aggregation of adsorbate and decreases the total surface area of adsorbent. Thus, in turn, increases diffusion path length which decreases percentage removal^{18, 19}. The equilibrium state was found to be at 0.02 g adsorbent dose.

4.4. Effect of particle size on adsorbent: -

Fig.4 depicts effect of adsorbent particle size on the removal of dye.

It is seen from Fig.4, that % removal of dye decreases with increasing particle size, the maximum dye removal being at 105 μ m particle size of adsorbent. It is attributed to decrease in surface area and less availability of adsorption sites for adsorption with particle size increase¹³.

4.5. Effect of concentration on adsorbent: - Effect of initial concentration on % removal is shown in Fig.5

The experiments were carried out using various initial concentrations of adsorbate (MB dye). The study of Fig.5 indicates that, removal of adsorbate decreased from 90.86% to 79.5% (30 mg L⁻¹). Adsorption is more predominant at 5 mg L⁻¹, due to strong driving forces of concentration gradient. Similar results are reported by earlier researchers^{20, 21}.

4.6. Effect of Temperature on adsorbent: -Effect of temperature (298 °K to 318 °K), on % removal is shown in Fig.6

To study the effect of temperature on the adsorption of MB on adsorbent, adsorption experiments are carried out over temperature range 25°C to 45°C. An examination of Fig.6, reveals that the amount of dye adsorbed decreases with increase in temperature as the

solubility of MB increases at high temperature. Optimum adsorption temperature was observed at 25°C. (93.83% removal)

5. Application of the developed method to actual industrial sample:

The developed method was applied for removal of MB dye from textile industrial effluent. For this purpose, sample was collected from Akkalkot M. I. D. C. area, Solapur district, before and after Effluent Treatment Process (ETP).

Sample collected from textile industry before effluent treatment procedure for MB was found to have MB concentration 5.2 mg L⁻¹ while after ETP it was 1 mg L⁻¹ indicating 80.55% removal.

Removal of MB from collected sample before ETP was carried out by using developed method under optimized conditions which showed 93.15% removal.

Thus, our developed method is found to be more effective than that used in the industry.

6) Adsorption Isotherms studies: -To study the adsorption isotherms, optimized conditions were used in adsorption experiments.

6.1. Freundlich isotherm: The linearized form of equation is given by following equation,

$$\log q_e = \log K_f + 1/n \log C_e \text{ -----(3)}$$

Where:- q_e = Amount of MB adsorbed at equilibrium,

C_e = equilibrium concentration of MB in solution,

K_f & n = Constant indicates the adsorption capacity and intensity of adsorption respectively.

The graph $\log q_e$ verses $\log C_e$ is shown in Fig.7. The adsorption of dye obeys Freundlich adsorption isotherm ($K_f = 12.11$). The K_f value which is a measure of the amount of dye absorbed per unit weight of adsorbent, indicates favorable adsorption process²². The 'n' is the adsorption intensity ($1/n = 0.81$) found in the range of $1 < 1/n < 10$. The values of $R^2 = 0.991$, $K_f = 12.11$, $1/n = 0.81$ are shown in Table 1

6.2. Langmuir Isotherm: Langmuir equation is given below,

$$1/q_e = 1/ab \times 1/C_e + 1/b \text{ ----- (4)}$$

Where:- q_e = Amount of dye adsorbed at equilibrium,

C_e = Equilibrium dye concentration,

a = Langmuir constant (K_L),

b = The maximum adsorption capacity, q_m (mg/g)

As can be seen from Graph of $1/q_e$ verses $1/C_e$, $R^2=1$ and hence adsorption of MB on studied adsorbent does follow Langmuir isotherm.

6.3. Temkin isotherm: Temkin isotherm is expressed by the following equation

$$q_e = B \ln A + B \ln C_e \quad \text{-----(5)}$$

Where: $B = RT/b$,

A and B are the Temkin isotherm constants, b is the constant related to heat of adsorption,

R is the gas constant (8.314 J/mol k),

T is the absolute temperature (K),

q_e is the amount of dye adsorbed at equilibrium (g/g),

C_e is the equilibrium concentration of the dye (g L^{-1}).

Linear graph ($R^2 = 0.913$) indicates the adsorption process obeys Temkin isotherm. The values of $A = 3.23$ and $B = 12.42$ are shown in Table 1

6.4. Dubinin-Radushkevich (D-R) isotherm: D-R model decides whether adsorption process is either physical or chemical adsorption process²³. D-R isotherm equation is as follows:

$$\ln q_e = \ln Q_{DR} - K\varepsilon^2 \quad \text{-----(6)}$$

Where q_e = the amount of dye adsorbed (g/g), Q_{DR} is the maximum adsorption capacity of dye (g/g), K is the Dubinin-Radushkevich constant (kJ^2/mole) and ε is Polanyi potential given by the equation

$$\varepsilon = RT \ln (1 + 1/C_e) \quad \text{----- (7)}$$

Where R is the gas constant in J/mol K. T is the temperature in kelvin and C_e is equilibrium concentration of dye solution (g L^{-1}).

A graph of $\ln q_e$ versus ε (Fig.10) gives a straight line ($R^2 = 0.895$) with a slope of K (0.21) and an intercept (3.3) of Q_{DR} , Biosorption mean free energy E(kJ/mol) is calculated from D-R constant K and is calculated by following equation

$$E = 1/\sqrt{-2k} \quad \text{----- (8)}$$

Where: E is the biosorption mean free energy (kJ/mol) and K is the D-R constant.

The transfer of one mole of solute from solution to the surface of adsorbent is due to the biosorption mean free energy (E) which describes the adsorption performance of the system.

Value of $E < 8$ indicates physical adsorption and $E > 8$ indicates chemical adsorption process²⁰. The value of the mean free energy of MB dye was calculated (1.55 kJ/mol) and indicates physical adsorption process.

Study of Table 1 reveals that adsorption of MB on the *ATCTLP* obeys Freundlich ($n < 1$), Temkin and Dubinin-Radushkevich (D-R) isotherm ($E < 8$).

7. Adsorption Kinetic studies: Adsorption mechanism and adsorption characteristics of adsorption were studied by using various kinetic models.

Adsorption kinetic of MB onto the adsorbent is express by following equation,

$$\log(q_e - q_t) = \log q_e - K_1 / (2.303)t \quad \text{-----(9)}$$

Where:- q_e and q_t are amount of dye adsorbed (mg g^{-1}) on adsorbent at equilibrium at time t respectively, K_1 is rate constant of pseudo –first order adsorption (min^{-1}).

A plot of $\log(q_e - q_t)$ verses time ($R^2 = 0.23$) was used to determine pseudo-first order rate constant ($k_1 = 4.9 \times 10^{-6} \text{ min}^{-1}$, $q_e = -6\text{g/g}$) which indicates that it does not follow pseudo-first order kinetics ($R \neq 1$).

Adsorption capacity on the solid phase is determined by Lagergren pseudo-second order equation. It is given by following expression as²⁴,

$$t/q_t = 1/(K_2 q_e^2) + t/q_e \quad \text{-----(10)}$$

Where, K_2 is rate constant of second order adsorption ($\text{g mg}^{-1} \text{ min}^{-1}$).

Second order rate constant is determined from Fig.11. The value of rate constant $K_2 = 0.23$, $q_e = 5.88$ and $R^2 = 1$ shows good linearity of plot and better fit to Lagergren pseudo –second order kinetic model.

7.1. Intraparticle diffusion model:

Diffusion of the adsorbate from the outer surface into the pores of the adsorbent was studied on examination of plot q_t verses $t^{1/2}$ (fig.12), The slope ($k_{id} = 0.03$) and the intercept value (5.53) indicate that the line does not pass through origin which indicates, there are some other factors affecting the adsorption. The sorption process has a tendency to be followed by two phases. The two phases in this plot suggest that the sorption process proceeds by surface sorption and intraparticle diffusion. The intraparticle diffusion equation is given by

$$q_t = k_{id} t^{0.5} + C \quad \text{-----(11)}$$

Where: k_{id} = Particle diffusion rate constant in $\text{mg/g/min}^{0.5}$; and C is intercept.

A plot of q_t verses $t^{0.5}$ gives values of k_{id} (slope) and C (intercept) from the equation.

The value of k_{id} and C is found to be 0.03 and 5.53 respectively.

7.2. Thermodynamic studies:

Thermodynamic parameters such as change in free energy (ΔG°) kJ/mol, enthalpy (ΔH°) kJ/mol, and entropy (ΔS°) kJ/mol K, were calculated by using following equations.

$$\Delta G^\circ = \Delta H^\circ - T \Delta S^\circ \quad \text{----- (12)}$$

$$\Delta G^\circ = -R T \ln K \quad \text{----- (13)}$$

$$K = \frac{q_e}{C_e} \quad \text{----- (14)}$$

$$\ln K = \frac{\Delta S^\circ}{R} - \frac{\Delta H^\circ}{RT} \quad \text{----- (15)}$$

Where: K is equilibrium constant, R is gas constant, T is temperature in K.

ΔG° is calculated from equation (12) while ΔH° and ΔS° values were obtained from the slope and intercept of plot $\ln K$ versus $1/T$, the negative value of ΔG° indicates the adsorption is spontaneous and thermodynamically favorable for adsorption of MB. The negative value of ΔH° indicates physisorption and endothermic nature of adsorption. The negative value of ΔS° indicates change in surface morphology and increase in randomness at liquid solid interface²⁰.

A plot of $\ln K$ versus $1/T$ is shown in Fig. 13

The thermodynamic parameters obtained from above plots are recorded in following Table.2 Above data reveals that, the ΔG° values are negative representing the spontaneous nature and thermodynamically favorable adsorption for MB²⁰. The negative value of ΔH° shows exothermic process²⁴. The negative value of ΔS° designates decreased disorder at liquid solid interface²⁵.

The distribution coefficient K values for adsorption process of MB on *ATCTLP* at different temperatures were calculated and it is reflected in following table

Table 3 reveals that, maximum adsorption was observed at temperature 298 °K due to maximum distribution coefficient value (20.52).

8. Recovery of Dye:

Recovery of dye was carried out by using various eluents (25 ml); water, 0.1N NaCl, 0.1 N NaOH and 0.1 N HCl solutions. The results are shown in Figure 14.

An examination of Fig. 14 shows that, HCl was found to be most efficient solvent for recovery of adsorbed dye. It was further used to recover a dye (5 mg L⁻¹) from loaded adsorbent at optimized conditions using various volumes of HCl (0.1N). A study of Fig.15 shows that, 50.22 % MB dye was recovered using 25 ml of 0.1N HCl. The result shows that the adsorbed dye can be effectively recovered. Thus, bio adsorbent can be regenerated and reused for further removal.

9. Characterization studies

9.1. FTIR Studies:

FTIR spectrum of virgin adsorbent (a) shows a peak at 3410 cm⁻¹ which indicates the presence of H-bonded –OH stretching vibration in phenolic compound present in cellulose of adsorbents. In spectrum (b), Strong broad band at 3437 cm⁻¹ due to -OH stretching vibration. There are two inflections observed in Fig. (a) and (b). in figure (a) band at about 2851-2916

due to medium -CH stretching and In figure (b), the absorption bands at 2853 and 2918 cm^{-1} can be assigned to symmetric and asymmetric vibrations of the C-H_3 bonds in the dimethylene groups of MB molecules²⁶. An examination of Fig.16 shows considerable change in the peak intensity indicating adsorption of MB on the adsorbent

9.2. FESEM Studies: The morphological characteristics of adsorbent were studied with FESEM and corresponding micrograph is shown in Fig.17.

An observation of Fig. 17a shows, SEM micrograph of virgin adsorbent possess irregular plate like long narrow shallow depression and highly porous rough surface structure indicates better opportunity for adsorption. The appearance of a dark molecular cloud over the superficial layer of the dye loaded adsorbent (Fig.17b) confirms the adsorption of dye on to the surface of adsorbent. There are no empty porous spaces left on the surface of adsorbent because 90.86 % dye adsorb on to the surface of adsorbent.

9.3. EDX studies: The EDX spectrum of *ATCTLP* and MB loaded *ATCTLP* is shown in the Fig. 18a & 18b respectively

Energy dispersive spectrum of adsorbent (18a) shows the elements Ca, C and O. While Energy dispersive spectrum of adsorbent loaded with MB (18 b), confirms presence of 'N' in the dye.

CONCLUSIONS:

The present study shows the effectiveness of *ATCTLP* in the removal of methylene blue dye from aqueous solutions. The maximum dye removal (90.86 %) of MB (5 mg L^{-1}) was observed at pH 7, contact time 60 min, adsorbent dose of 0.020 g, particle size of $105\text{ }\mu\text{m}$. The adsorption isotherm study indicates that, adsorption of MB on *ATCTLP* is physical adsorption process. It follows Freundlich, Dubinin-Radushkevich and Temkin isotherms. The adsorption kinetic study shows adsorption of MB follows pseudo-second order kinetics and Intraparticle diffusion model. Thermodynamic studies revealed that adsorption is spontaneous and endothermic process. *ATCTLP* is efficient adsorbent for removal of MB dye. The adsorbed dye can be effectively recovered using 0.1 N HCl solutions as an eluent.

ACKNOWLEDGMENT:

One of the authors, Dr. D. J. Borkar, is thankful to UGC, Savitribai Phule Pune University Pune, C-MET Pune, President and Principal of Anantrao Thopte College, Bhor. This research did not receive any specific grant from funding agencies in the public, commercial or not-for profit sectors.

Figures:

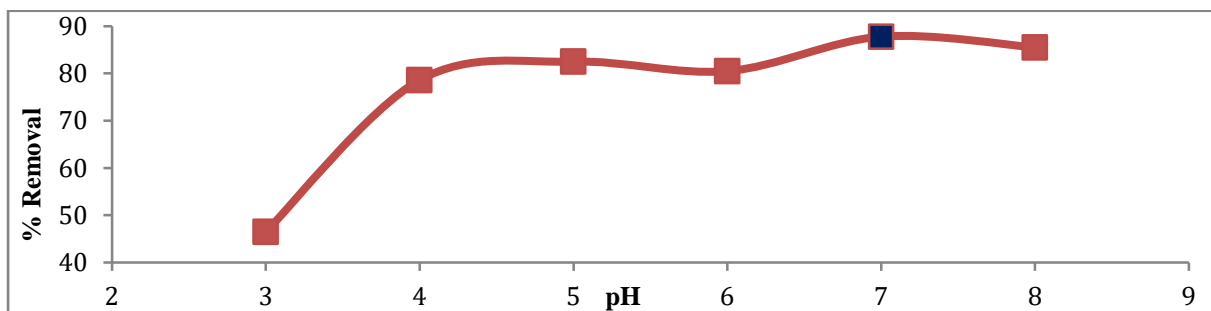


Fig.1.Effect of pH on removal of MB
[Contact time: 30 min, Adsorb. dose:10mg, Particle size: 420 μ m, Concentration: 5mg L⁻¹]

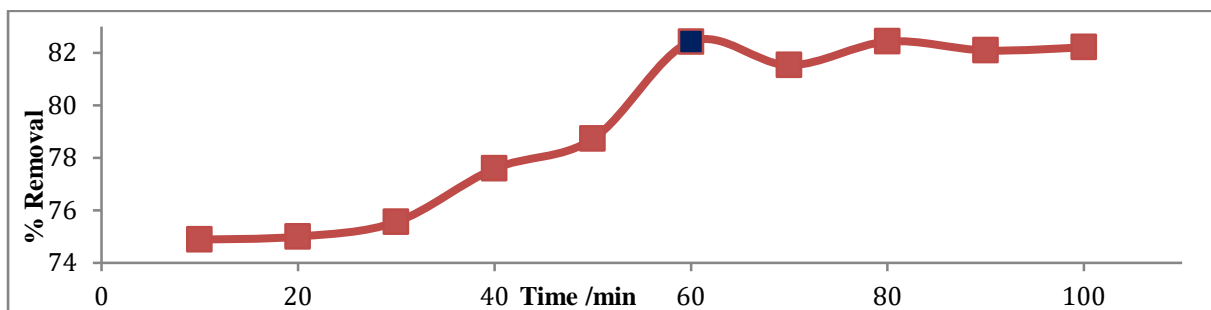


Fig.2. Effect of contact time on removal of MB
[pH: 7, Adsorbent dose: 10 mg, Particle size: 420 μ m, Concentration :5 mg L⁻¹]

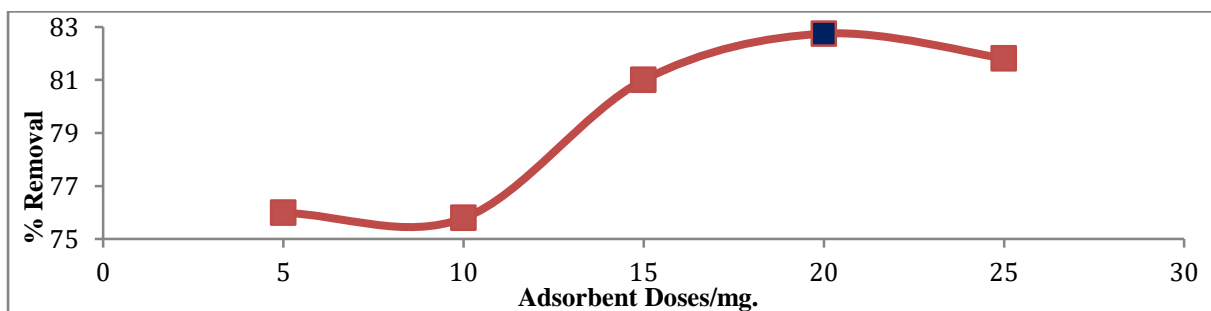


Fig.3. Effect of adsorbent doses on removal of MB
[pH: 7, Contact time: 60 min, Particle size: 420 μ m, Concentration:5 mg L⁻¹.]

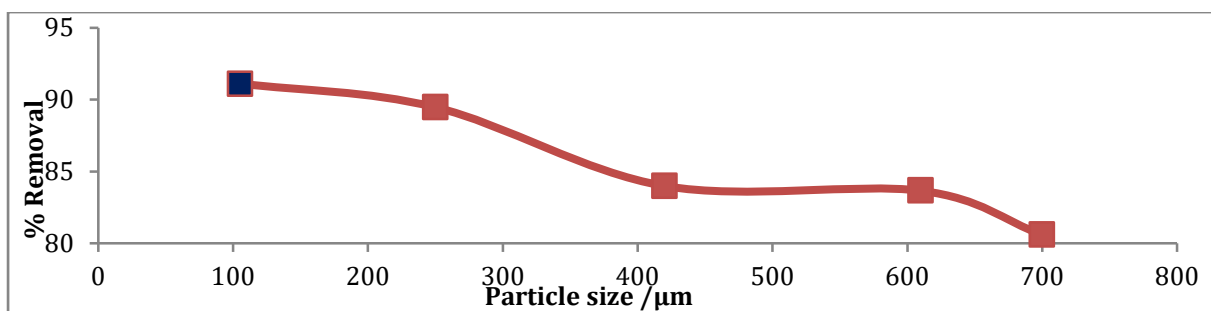


Fig.4. Effect of particle size of adsorbent on removal of MB
[pH: 7, Contact time: 60 min, Concentration: 5mg L⁻¹. Adsorbent dose: 20mg]

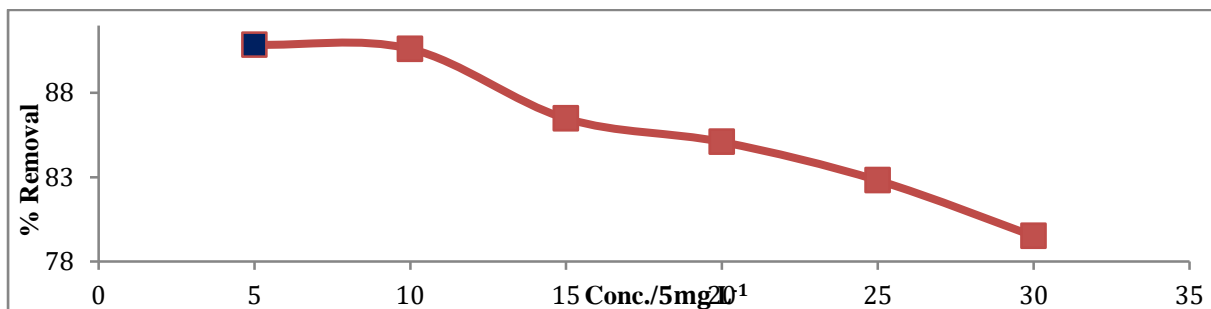


Fig.5. Effect of concentration, on removal of MB
[pH: 7, Contact time: 60 min, Adsorb. dose:20mg, Particle size: 105 μ m.]

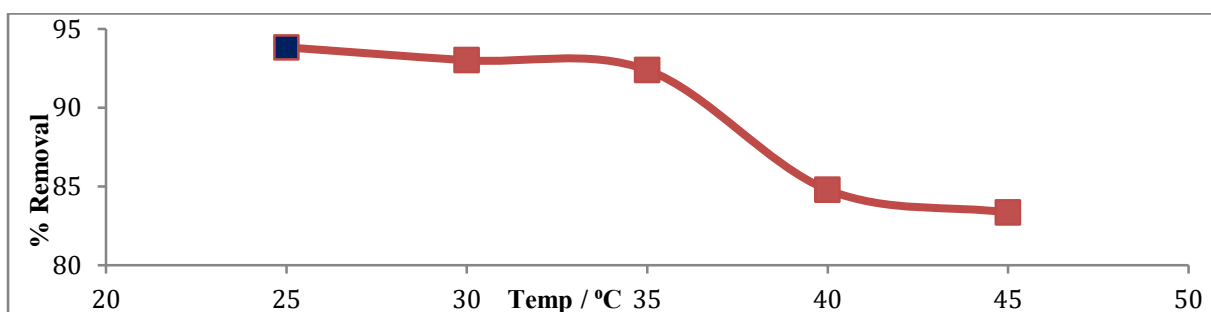


Fig.6. Effect of temperature on % removal of MB
[pH:7, Cont. time: 60 min, Adsorb. dose: 20 mg, Particle size: 105 μ m, Conc: 5 mg L⁻¹.]

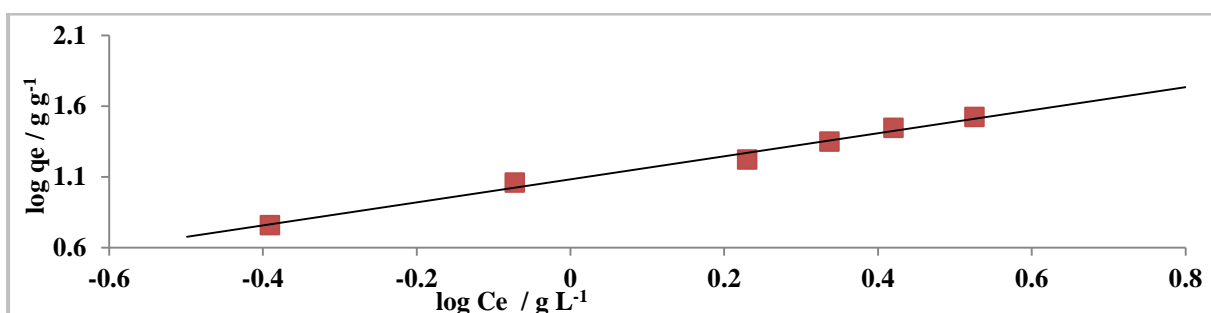


Fig.7. Freundlich isotherm plot for adsorption of MB on ATCTLP under optimized condition.

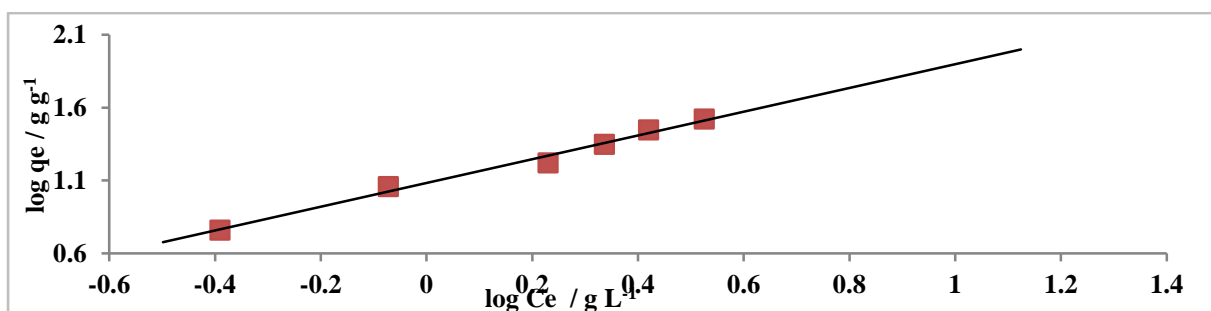


Fig.8. Langmuir isotherm plot for adsorption of MB on ATCTLP under optimized condition.

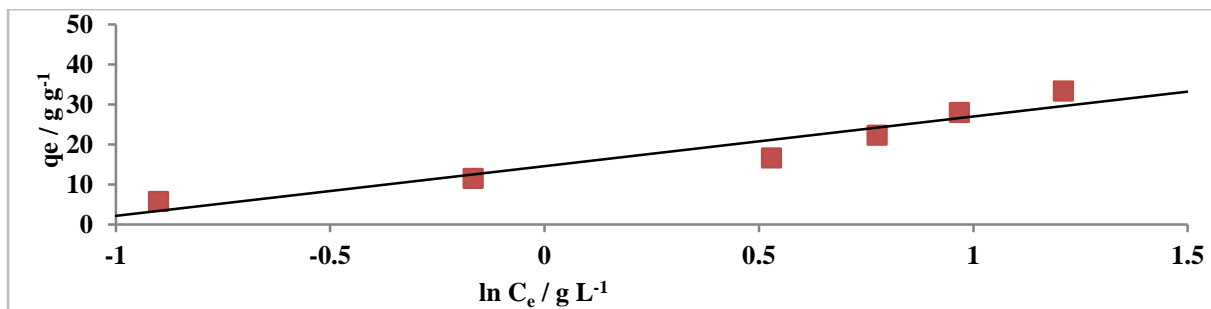


Fig.9. Temkin isotherm plot for adsorption of MB dye on ATCTLP under optimized condition.

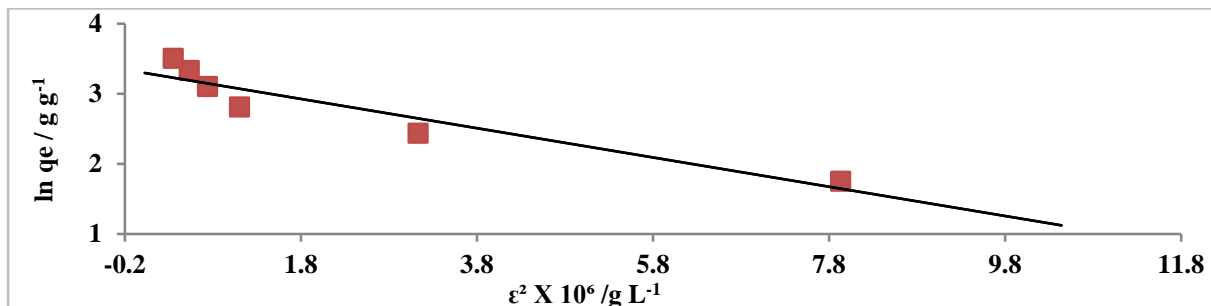


Fig.10. D-R Isotherm plot for adsorption of MB dye on ATCTLP under optimized condition.

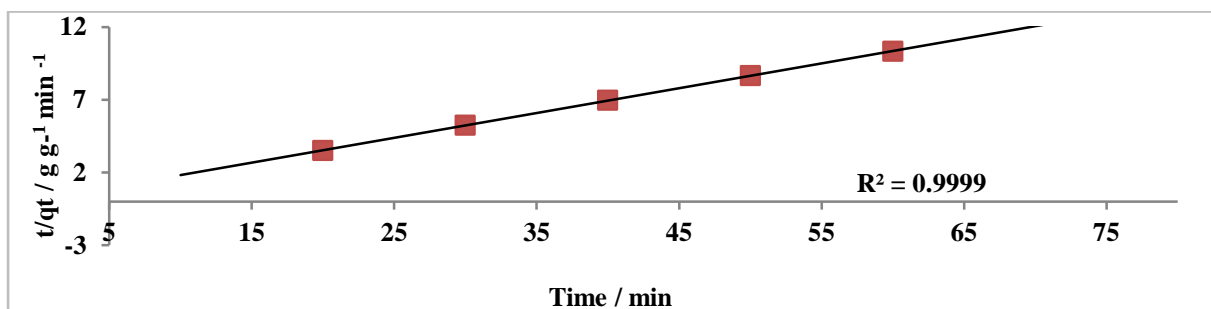


Fig.11. Pseudo -second order plot for adsorption of MB dye on ATCTLP under optimized condition.

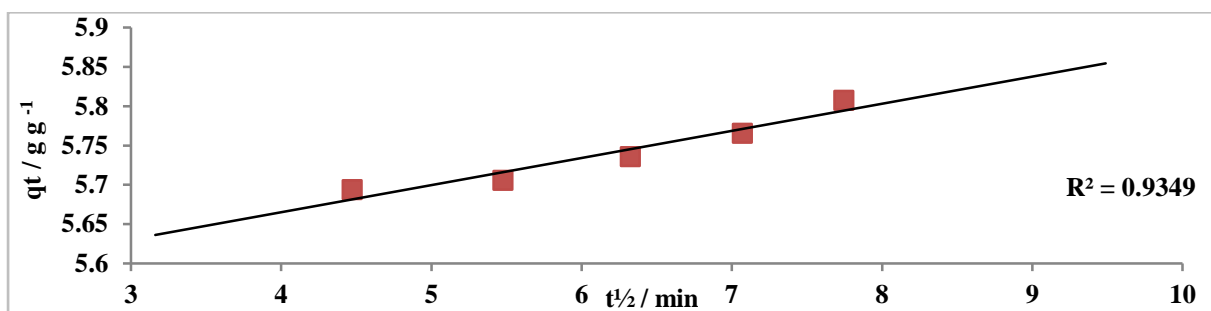


Fig.12. Intraparticle diffusion plot for adsorption of MB dye on ATCTLP under optimized condition.

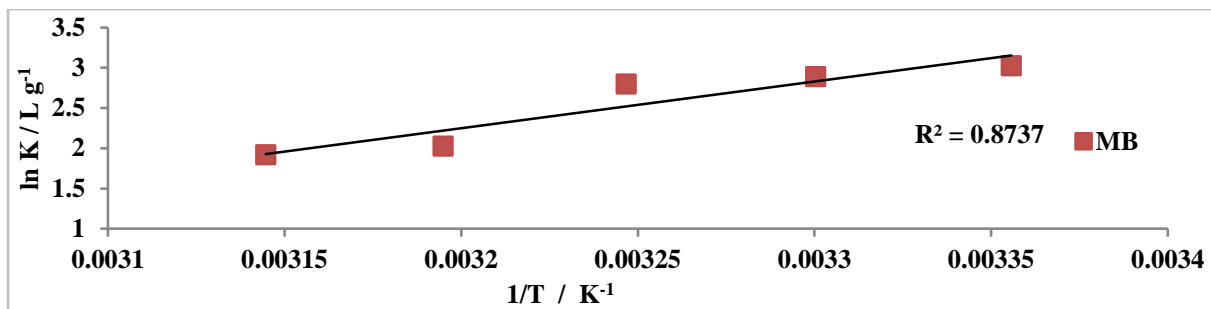


Fig.13. Plot of ln K verses 1 /T for adsorption of MB dye on ATCTLP under optimized condition.

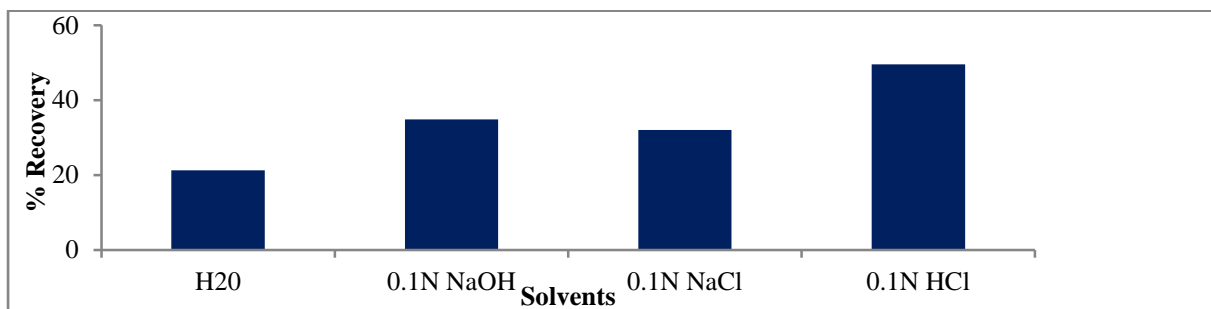


Fig.14. % Recovery of dye from dye loaded adsorbent using different eluents.

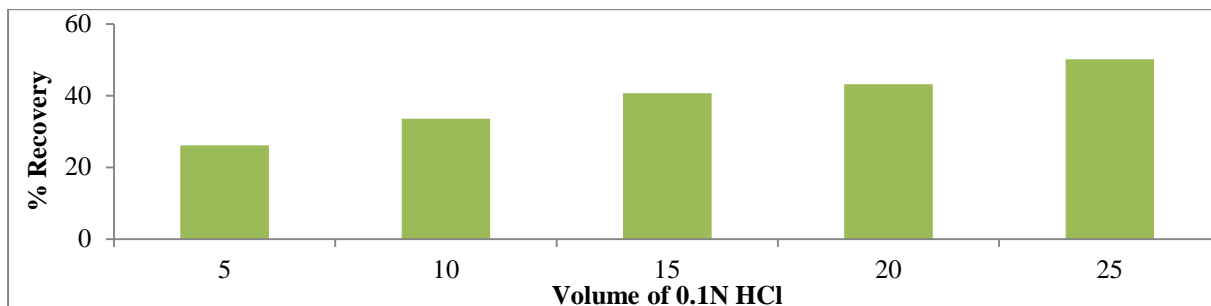


Fig.15. % Recovery of MB dye from dye loaded on adsorbent using 0.1 N HCl.

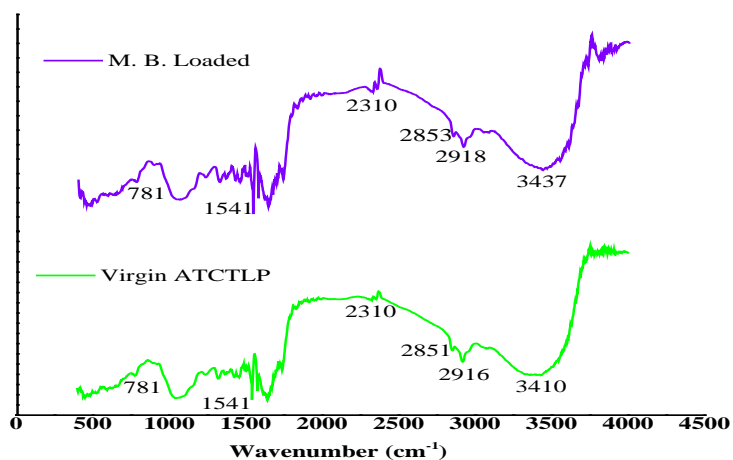


Fig. 16. FTIR Spectrum of ATCTLP (a) and MB loaded ATCTLP (b).

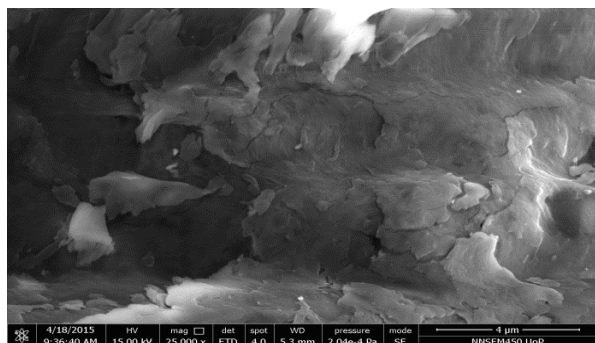


Fig.17a, SEM micrograph of Virgin ATCTLP

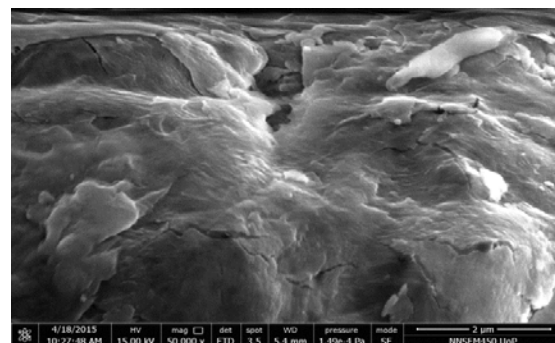


Fig.17b, ATCTLP loaded with MB.

Virgin adsorbent

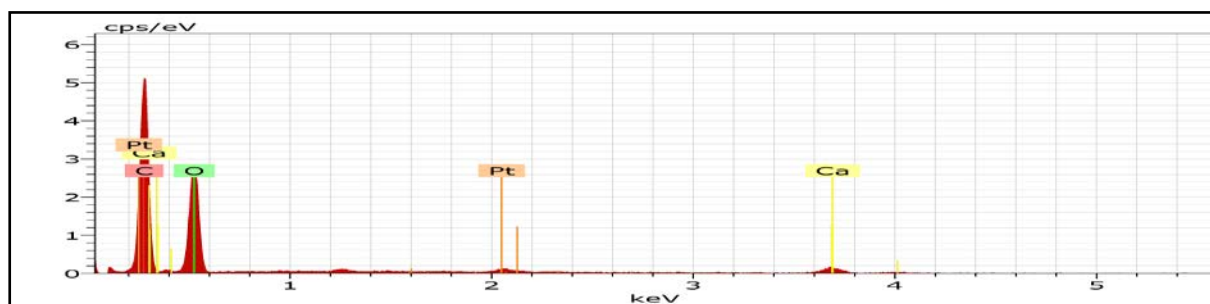


Fig. 18a, EDS of ATCTLP

M.B. loaded adsorbent

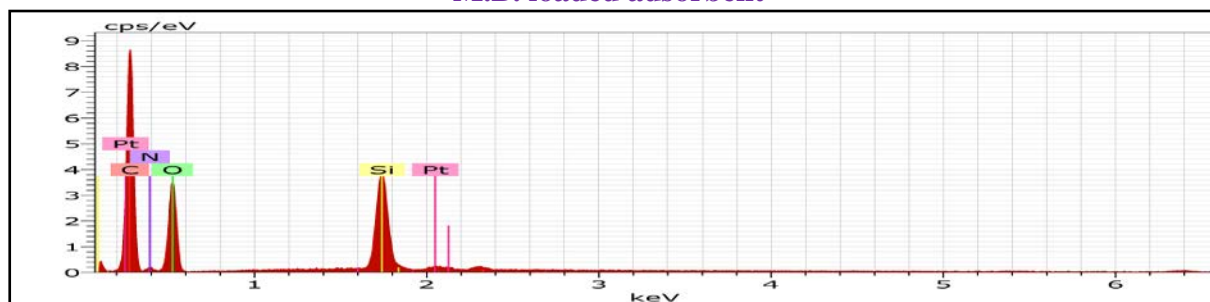


Fig. 18b, EDS of ATCTLP loaded with MB

Tables:

Table: 1. Isotherm constants for absorption of MB dye on *ATCTLP* adsorbents.

Adsorption Isotherm	Constants	Values
Freundlich Isotherm	R^2	0.989
	K_f	12.11
	$1/n$	0.81
Langmuir Isotherm	R^2	1
	A	0.19
	B	78.92
Temkin Isotherm	R^2	0.912
	A	3.23
	B	12.42
D-R Isotherm	R^2	0.895
	Q_{DR} (g/g)	27.19
	K (kJ/mol)	0.21
	E (kJ/mol)	1.55

Table:2. Thermodynamic parameter for MB sorption by *ATCTLP* adsorbents.

Sr. No.	Temp. (°K)	ΔG° (kJ/mol)	ΔH° (kJ/mol)	ΔS° (kJ/mol k)
1.	298	-7.81	-48.17	-0.12
2.	303	-7.13		
3.	308	-6.46		
4.	313	-5.78		
5.	318	-5.10		

Table:3. Variation of K with temperature for adsorption on MB dye on *ATCTLP* adsorbents.

Temp. (°K)	298	303	308	313	318
$K / L \text{ mg}^{-1}$	20.52	17.96	16.40	7.58	6.81

REFERENCES:

1. Quiang Liu, IOP vof. Ser.: Earth Environ. Sci. 514, 052001, 2020
2. R. Jain, S. Sikarwar, Int. J. Environ. Pollut., 27, 158, 2006.
3. Amr A. Essawy, A. El-Hag Ali, M. S. A. Abdel-Mottaleb, J. Hazard. Mater., 157 (2-3), 209.2008.
4. Robinson, T., McMullan, G., Marchant, R. and Nigam, P., Bioresource Technology, 77, 247, 2001.
5. F. Bouaziz, M. Koubaa, F. Kallel, F. Chaari, D. Driss, R. E. Ghorbel, S. E. Chaabouni,

- Industrial crops and products, 74, 903, 2015.
6. MSU Rehman, I. kim, J. Han, Carbohydr, Poylm.; 90(3), 1314, 2012.
 7. S. D. Khattri, M. K. Singh, J. Hazard. Mater., 167, 1089, 2009.
 8. O. Abdelwahab et al., J. Aquat res; 31, 1, 2005.
 9. Y. Bulut and H. Aydin, Desalination, 194, 259, (2006).
 10. Borkar D. J., Rajurkar N. S. and Adhyapak P. V., J. of Applicable Chemistry 5 (5), 1064, 2016. (10)
 11. M. R. Pawar J. ISAS 1 (1), 97, 2022
 12. N. S. Rajurkar, M. R. Pawar, Env. Obsever. 13, 215, 2013.
 13. N. S. Rajurkar and N. S. Walvekar, J. Applicable. Chem, 3(6), 2602 2014.
 14. N. S. Rajurkar and Asha Desai, Journal of Applicable Chemistry, 4 (5), 1446, 2015.
 15. L. Oliveira, N. Cordeiro, A. J. D. Silvestre, I. C. Torres and D. Evtuguin, Industrial Crop Prod, 26, 163, 2007.
 16. Hayelom Dargo, Nigus Gabbiye, and Adhena Ayalew, International Journal of Innovation and Scientific Research, 9 , 317, 2014.
 17. B. Srinivasa Reddy, V. Krishna Veni and K. Ravindhranath, Journal of Chemical and Pharmaceutical Research, 4(11), 4682, 2012.
 18. M. M. Abd El-Latif, A. M. Ibrahim, M.F.E1-Kady, J. American Sci. 6, (6), 267, 2010.
 19. S. Saiful Azhar, A. Ghaniey Liew, D. Suhardy, K. Farizul Hafiz and MD. Irfan Hatim, American J. Appl. Sci., 2(11), 1499, 2005.
 20. H. Runping et al., J. of Hazardous Materials. 141, 156, 2007.
 21. N. S. Rajurkar and D. R. Mahajan, J. Applicable.Chem, 4(4),1206, 2015.
 22. G. Kavitha, V. Venkateswaran, Journal of Applied Chemistry, 10 (9), 68, 2017.
 23. P. Velmurugan, V. Rathinakumar, G. Dhinakaran, Int. J. of Environ. Sci, 1(7), 1492, 2011.
 24. Narayan saibaba K. V. and King P., International Journal of Research in Engineering and Technology, 1(3), 17, 2013.
 25. Nitin Sharma, Tanveer Alam, Arshi Rastogi, Hina Tarannum and Gita Sain., J. Applicable. Chem, 4, (3), 871, 2015.

Conceptualizing Cavitation Methodology by Integrating Cavitation and Coagulation and Application to Dye Wastewater Treatment

Krati Sharma^{1,4}, Chethana M¹, Vinay M. Bhandari^{1*}, Laxmi Gayatri Sorokhaibam², Vivek V. Ranade^{1,5} and Deepak J. Killedar³

1. Chemical Engineering and Process Development Division
CSIR-National Chemical Laboratory, Pune, India
2. Visvesvaraya National Institute of Technology, Nagpur, India
3. Civil Engineering and Applied Mechanics Department
Shri G.S. Institute of Technology and Science, Indore, India

*Email: vm.bhandari@ncl.res.in

Received: 17.1.23, Revised: 28.1.23, Accepted: 29.1.23

Abstract

The present work provides a proof of concept for a new hybrid process, cavitation, by combining cavitation and coagulation and its application to dye wastewater treatment. Both acoustic and hydrodynamic cavitations were evaluated. Removal of a commonly used dyes such as Congo red was investigated by cavitation in the concentration range of 50 to 500 ppm. A broad spectrum of coagulants including two inorganic coagulants; poly aluminium chloride, iron (III) chloride, and natural biocoagulants derived from *Moringa oleifera*, *Cicer arietinum* and *Acanthocereus tetragonus* were employed to substantiate the concept of cavitation. A vortex diode device employing vortex flow for cavitation, was used for the hydrodynamic cavitation (HC) -based cavitation. Cavitation in the form of acoustic cavitation + coagulation, showed significant improvement over individual processes; acoustic cavitation alone was largely ineffective for dye removal. Increase over conventional coagulation to the extent of 24% and 48% was observed for the two inorganic coagulants-Iron (III) chloride and PAC SAB 18, while for *Moringa oleifera*, *Acanthocereus tetragonus*, and *Cicer arietinum* the increase was 27%, 33%, and 29% respectively. The pH has a large impact on the cavitation process, similar to coagulation and the coagulant dose could be reduced by more than half by adjusting pH to 3. Auramine O dye removal was effective using hydrodynamic cavitation compared to coagulation. The developed cavitation process, especially using biocoagulants, could be an effective alternative to the conventional chemical coagulation in the form of a green process in dye wastewater treatment.

Keywords: *Biocoagulant, Dye removal, Effluent treatment, Pollution, Process integration,*

1. Introduction

The industry sectors such as textile industry, dye industry, or industries using dyes for different applications produce large volumes of wastewater that need to be treated appropriately to remove both biodegradable and non-biodegradable dyes prior to the discharge. The effluent is colored with complex characteristics of high chemical oxygen demand, dissolved and suspended impurities, heavy metals, etc¹. The nature of dyes varies greatly in terms of properties such as molecular weight, complex structures; but most importantly, in terms of biodegradability. In recent years, use of refractory dyes, that are non-biodegradable, has increased significantly² posing serious limitations to not only discharge of waters but also to the conventional biological treatment processes³. The refractory pollutants can have undesirable effects even at very low concentrations, can pose health hazards apart from impacting the photosynthetic activity of flora and also the other aquatic life adversely⁴.

Many conventional techniques for dye wastewater treatment that are not only well researched, but are also in commercial practice include both physical and chemical processes such as coagulation/flocculation, membrane filtration, adsorption, chemical oxidation, ion exchange, apart from biological processes^{5,6}. The biological treatment processes are largely ineffective for removing colour from the wastewaters⁷. In recent years, due to a large number of refractory dyes that are difficult to degrade, many of these conventional methods have severe limitations in effectively treating the wastewater or incur higher costs apart from generating secondary waste⁸.

To overcome the limitations of conventional techniques, many advanced processes need to be applied at higher costs e.g. electro-coagulation, advanced oxidation processes of the type electro-oxidation, newer materials of the type of chemically modified adsorbents or nanocomposites, etc. Process integration of the type of ultrasound-assisted adsorption has also been reported to enhance dye removal⁹. In view of the pollution control norms which are getting stricter with time, there is a major challenge in not just treating these wastewaters effectively, but also techno-economically to achieve degradation of complex and recalcitrant pollutants. The present work is an attempt to devise and develop one hybrid process by effectively combining the conventional coagulation process with newer cavitation process.

In recent years, the use of acoustic and hydrodynamic cavitation for the treatment of industrial wastewaters has been shown to be effective and some newer forms of cavitating devices have been reported^{5,10,11}. The cavitation process has a major advantage in terms of ease of operation, scalability, low cost of operation, and most importantly, no secondary waste generation since the organic pollutants largely get mineralized into water and carbon dioxide¹²⁻¹⁵. The cavitation process, an advanced oxidation process, involves generation, growth and collapse of the cavities through physical means. The collapse of the cavity or bubble is termed as implosion, opposite to explosion, and generates extreme conditions of temperature (~5000- 10000K) and pressure (~1000- 5000 atm) at the localized point of implosion. As a consequence, water splits and generates hydroxyl radicals which subsequently oxidize the organic pollutants. From industrial wastewater treatment point of view, only acoustic and hydrodynamic cavitation are most promising¹⁶. In the case of acoustic cavitation, cavities get generated by inducing ultrasound waves in the liquid medium (> 16 kHz), while in hydrodynamic cavitation, it is achieved by devising conditions of sudden pressure drop using constriction (cavitating devices) in the flowing fluid. Although significant work has been reported in the area of sonochemical reactors and its application in wastewater treatment, its implementation for actual industrial practice is still negligible due to the reasons of high cost of treatment and operational difficulties, especially in power dissipation. The impact of cavitation processes can be dramatically increased by combining it with other oxidation process employing catalysts or additives¹⁷.

The conventional effluent treatment invariably employs coagulation processes for reducing part load of pollutants from the effluents. Coagulation, in itself, is rarely a complete process and therefore requires subsequent treatment methods such as adsorption, oxidation to meet the desired pollution control norms. There are a number of coagulants commercially available in both inorganic and organic class ranging from low cost alum, ferric chloride to more expensive polymeric coagulants and organic coagulants. The effectiveness of the coagulation process can be significantly improved by the appropriate physical or chemical combination of one or more different coagulants to increase the floc size, improved settling, reduced sludge generation and to reduce the cost. Further improvements in this process can also be obtained by using natural bio-coagulants or their formulations¹⁸.

Biocoagulants are emerging as a safe and economic option over chemical coagulants. *Moringa oleifera* is a naturally occurring tree found in India, South Saharan Africa and South-America.¹⁹ *Acanthocereus tetragonus* (also called barbed wire cactus, sword pear, dildo cactus, night blooming cereus, triangle cactus) belongs to Cactaceae family. *Cicer arietinum* commonly known as chickpea belongs to Fabaceae family and subfamily Faboideae. All three of them are reported as coagulants in water/wastewater treatment¹⁸.

Though, extensive investigations on cavitation and coagulation have been reported for removal of different pollutants, hybrid technology using in-situ coupling of cavitation with coagulation is not reported so far. The present study is an attempt to provide proof of concept for a new cavitation process in this regard that investigates combination of acoustic and hydrodynamic cavitation with coagulation for dye removal. Removal of one commonly used model dye, Congo red- an acidic dye, was investigated in detail. Use of inorganic coagulants, PAC SAB 18 and iron (III) chloride was compared to evaluate the effect of the new process. Three different natural biocoagulants namely, *Acanthocereus tetragonus*, *Moringa oleifera* and *Cicer arietinum* were also evaluated in this regard. Further, dye removal was compared with hydrodynamic cavitation by using the concept of cavitation, for a cavitating device employing vortex flow- vortex diode. The present study is the first of its kind exploring and developing a suitable combination of cavitation and coagulation in the form of cavitation; acoustic cavitation+coagulation and hydrodynamic cavitation+coagulation.

2. Materials and Methods

2.1 Materials

Congo red is an anionic di-azo dye with molecular formula $C_{32}H_{22}N_6Na_2O_6S_2$. This is benzidine based dye with two azo groups and has an aromatic structure. Auramine O is a cationic dye containing amino and imino groups with molecular formula $C_{17}H_{22}ClN_3$. It is also combined with hydrochloric acid. This is a basic dye classified under Diarylmethane class. Orange G is an anionic azo dye with molecular formula $C_{16}H_{10}N_2Na_2O_7S_2$. Congo red (CR), auramine O (AO), and orange G (OG) dyes were purchased from Loba Chemie. The physiochemical properties of the dyes are given in **Table 1**. Chemical coagulants PAC SAB 18, polyDADMAC, Iron (III) chloride hexahydrate, and Iron (III) Chloride were procured from Sigma Aldrich. All the chemicals and reagents used in this study were of analytical

grade. All the solutions were prepared using distilled water. The pH of the solution was adjusted using 0.1 M HCl and 0.1 M NaOH. The plant pads of biocoagulant, *Acanthocereus tetragonus* were collected from campus of National Chemical Laboratory (NCL), Pune, India. *Moringa oleifera* and *Cicer arietinum* biocoagulants were purchased from local market of Pune, India.

2.2 Preparation of bio-coagulants

Moringa oleifera seeds were de-shelled, and dried at ambient temperatures ($40 \pm 5^{\circ}$ C) for one day before milling. The whole kernels were milled into a fine powder using a food blender. *Moringa oleifera* seed solution was made by dissolving 5 g of powder with 100 ml of distilled water and solution was stirred for 30 min to extract the active coagulant part and the extracted solution was used for the treatment of the synthetic dye wastewater. The detailed method has been reported in our previous work.¹⁸

Acanthocereus tetragonus pads were collected and washed thoroughly with tap water, and manually chopped into small pieces after removing the spines. The external skin as well as the inner off-white portion of the cactus pieces were ground with a food processor and extracted with water in equal weight by volume ratio. It was then filtered to remove the fibrous part. Fresh extracts were prepared for each batch run.

Cicer arietinum seeds were collected, and ground to make it into powdered form. The powder was used as coagulant and stored under refrigeration.

2.3 Experimental

The dye solutions of concentrations 50 mg/L, 100 mg/L, and 500 mg/L were prepared by using distilled water. The coagulation experiments were performed using jar test apparatus (Stuart SW6, UK) consisting six paddles and six beakers. The effect of concentration, coagulant dose was studied by using a rapid mixing at 200 rpm for 2 min followed by slow mixing at 40 rpm for 20Min.. A settling time of 30 minute was provided after which the supernatant was collected and filtered before each analysis. The acoustic cavitation and cavigulation (acoustic cavitation+coagulation) experiments were performed using UCB-100 Sonicator at 40 kHz and 250 W power for 15 minute. Hydrodynamic cavitation and

cavitation (hydrodynamic cavitation+coagulation) were performed with hydrodynamic cavitation pilot plant designed at CSIR-NCL, Pune. The details of pilot plant and experimental are well discussed in our earlier work^{11,20-22}. The setup consists of holding tank of 50 litre capacity and a multistage centrifugal pump of rating 2.2 kW. The pressure drop was adjusted using the control valve connected to the bypass line. Flow rate transmitter, pressure transmitter, and thermocouple are provided for the measurement of the flow rate, pressure, and temperature of the solution respectively. The temperature of the solution was kept constant using the coolant which is circulated in coils in the holding tank. The samples for the analysis were collected at predetermined time intervals.

Cavitation experiments were performed adopting three different schemes as given below, while running the respective cavitation process:

Acoustic cavitation (Sonication)+ Coagulation

Scheme 1: Addition of coagulant with 2 min rapid mixing in jar test apparatus followed by 15 min of Cavitation.

Scheme 2: Addition of coagulant (no mixing provided separately) followed by 15 min of Cavitation.

Scheme 3: First 10 min only cavitation followed by addition of coagulant (no mixing provided after addition) and next 5 min Cavitation.

Hydrodynamic Cavitation using vortex diode + Coagulation

Scheme 1: Addition of coagulant with 15 min mixing in Cavitation setup through bypass at low flow rate, followed by 2 h of Cavitation.

Scheme 2: Addition of coagulant (no mixing provided separately) followed by 2 h of Cavitation.

Scheme 3: First 1 h Hydrodynamic Cavitation followed by addition of coagulant (15 min mixing provided after addition through bypass at low flow rate), followed by 1 h Cavitation.

2.4 Dye removal studies

The sample solution was filtered after each cavigation and coagulation experiment using Whatman. 41 filter paper. The dye concentration was calculated on the basis of the absorbance values obtained using spectrophotometer (spectroquant pharo-100) at λ_{\max} value of 498 nm, 475nm and 433 nm for CR, OG and AO dyes respectively. The percentage dye removal was evaluated taking difference in initial and final dye concentration using the formula:

$$\text{Percentage dye removal} = \frac{C_o - C_e}{C_o} \times 100$$

Where, C_o is initial dye concentration (mg/L) and C_e is Final dye concentration (mg/L)

3. Results and discussion

3.1 Coagulation

3.1.1 Effect of coagulant dose

Coagulant dosage is one of the most important parameters affecting the efficiency of coagulation. A coagulant dose lesser than the required may lead to insufficient floc formation while over-dosing of coagulants leads to the re-stabilization of the colloidal particles. This also determines the techno-economic viability of the process. The dye removal efficiency of various coagulants viz. inorganic coagulants; PAC (Polyaluminium chloride) SAB 18, iron (III) chloride hexahydrate and organic coagulant; polyDADMAC and effect of varying their coagulant doses for 50, 100 and 500 ppm of auramine O, Orange G, and Congo red dye is shown in **Figs. 1 to 3**.

It can be seen from **Fig. 1** that, the dye removal was in the range 23 to 30% for 30 ppm of coagulant dose of PAC SAB 18, iron (III) chloride hexahydrate and polyDADMAC respectively for 50 ppm of initial dye concentration of auramine O dye, which started decreasing with further increase of coagulant dose. There was a decrease or no significant increase in removal for all the three coagulants for increased doses. This behavior may be attributed to the re-stabilization or re-dispersion of charge particles of dye. This observation is in agreement with the results reported by Zonoozi et al.²³. For 500 ppm of dye, not more

than 20% of dye removal could be achieved with any of the three coagulants, even at coagulant doses as high as 1000 ppm.. Similar dye removal efficiency of various coagulants used in the study has been observed for all three concentrations of auramine O dye.

Fig. 2 provides data for the Orange G dye removal. A gradual increase in dye removal with an increase in coagulant dose was observed using all the three coagulants for all the dye concentrations except in the case of polyDADMAC for 50 ppm initial dye concentration, where removal efficiency slightly decreased from 42.8% to 34.8% after 75 ppm of coagulant dose. For lower concentrations of dye, higher removal efficiency using iron (III) chloride hexahydrate was observed in comparison to PAC SAB 18 while for 500 ppm initial concentration only 11.43% dye removal was observed even at a high dose of ICH (1000 ppm) whereas up to 51.53% dye removal was achieved using PAC SAB 18 (1000 ppm) coagulant. The higher removal efficiency of polyDADMAC at lower doses may be due to the fact that these high molecular weight organic coagulants generally follow charge neutralization along with bridging mechanism with polymers, resulting in dense and easily settleable flocs even at lower doses ²⁴.

The results of Congo red dye are presented in **Fig. 3**. With an increase in coagulant dose, a sudden increase in dye removal using PAC SAB 18 coagulant was observed, whereas a gradual increase in removal efficiency was observed in the case of ICH. The sudden increase in dye removal in the case of PAC SAB 18 may be due to over saturation of formation of amorphous hydroxide precipitate which promote the enmeshment of colloidal particles in a sweep floc enhancing the overall removal even at lower doses as it is reported that sweep flocculation mechanism is one of the predominant mechanism with metal coagulants²⁴. The dye removal was found to be more than 95% at 20 ppm, 30 ppm and 200 ppm dose of PAC SAB 18 and 45 ppm, 60 ppm and 200 ppm dose of ICH for 50, 100 and 500 ppm of initial dye concentration respectively.

In spite of being an organic polymer, the requirement of comparatively higher doses of polyDADMAC than the other two coagulants to achieve the maximum removal was surprising. According to Razali et al.²⁵ addition of polyDADMAC destabilize the particles resulting in change in zeta potential value, and create microflocs. Up to 96% of dye removal was observed at 80 and 150 ppm of coagulant dose for 50 and 100 ppm of initial dye

concentration respectively. Even at polyDADMAC dose of as high as 500 ppm, only 55.46% dye removal was observed for 500 ppm of initial dye concentration.

3.1.2. Selection of coagulant

The results of **Figs. 1 to 3**, indicate that performance of coagulants depends on the nature of dyes, coagulant dose and also the initial dye concentration. Almost similar removal efficiency was achieved using all three coagulants for removal of auramine O dye irrespective of initial dye concentration and coagulant doses. Whereas polyDADMAC was observed to be most suitable for the removal of orange G dye at all the initial dye concentrations, PAC SAB 18 displayed high removal efficiency at higher dye concentration. In the case of Congo red dye, PAC SAB 18 and ICH were found to be highly efficient even at lower coagulant dose, on the other hand higher coagulant doses of polyDADMAC were required to achieve maximum removal, which was very less at higher initial dye concentration of Congo red dye (500 ppm) even at higher coagulant doses. Comparatively lower coagulant doses were sufficient for high removal of Congo red dye than required in the case of other two dyes for all the dye concentrations.

3.1.3. Effect of nature of dye

The removal of auramine O dye was lowest among the three dyes. Orange G was also found to be difficult to remove, though polyDADMAC showed up to 55% dye removal for the orange G dye. Congo red was observed to be an easily removable dye for which very high removal with all three coagulants was observed.

The dye removal behaviour is expected to depend on molecular weight, structure of dye, solubility, and the nature of dyes. It is also a well-recognized fact that dyes having longer molecular chains or larger molecular weights are more favorable for removal by coagulation^{26,27}. Many dyes with low molecular weight and cationic dyes may not get effectively removed using coagulation²⁶. Among the dyes taken for the study, auramine O is the only cationic dye having the lowest molecular weight i.e. 303.83 g/mol and orange G is highly soluble among three, having a solubility of 80 mg/ml in water. The characteristics of auramine O and orange G dyes contribute to low removal of these dyes using coagulation. Among the three dyes, Congo red has high molecular weight of 696.66 g/mol and has a di-

azo long chain structure which indicates its easy removal. Kim et al.²⁸ also related the low removal of dye as a function of the solubility of dye.

3.2. Cavitation

3.2.1. Effect of initial dye concentration

Cavitation was studied (Acoustic and Hydrodynamic) for the removal of Congo red, auramine O, and orange G dyes. The effect of initial dye concentration (50, to 500 ppm) on the removal efficiency was investigated for all three dyes. For the HC, operating time was 2 h and the experiments were conducted at 0.5 and 2 bar pressure drop conditions. **Fig. 4** shows the extent of degradation of auramine O and Congo red dye. The dye removal in auramine O dye increased with an increase in initial dye concentration from 50 to 100 ppm for both the pressure drop conditions, while the degradation decreased with a further increase in initial dye concentration (100 to 500 ppm). In Congo red, the maximum dye removal was achieved at 50 ppm. The decrease in dye removal at higher dye concentration values may be due to a lack of availability of OH^\bullet radicals responsible for oxidation of pollutant²⁹. Saharan et al.³⁰ found an increase in the degradation of orange G dye (30-150 μM) with an increase in initial dye concentration using circular venturi, slit venturi, and orifice plate while Pradhan and Gogate³¹ have observed lower degradation of pollutant at higher concentrations.

3.2.2. Effect of pressure drop

The pressure drop was varied from 0.5 to 2 bar. The effect of pressure drop is shown in **Fig. 4**. High pressure drop condition was favourable for the removal of both Congo red and auramine O dyes at all the initial dye concentrations. A dye removal of up to 45%, 73%, and 12% in the case of auramine O and 23%, 11%, and 10% in the case of Congo red was observed at 2 bar pressure drop for 50, 100 and 500 ppm of initial dye concentration respectively in 2 h. Saharan et al.¹⁴ reported the effect of inlet pressure (3-7 bar) for the decolourization of acid red 88 dye and it was found that the rate of degradation increases up to 5 bar inlet pressure and then decreased. Gogate and Pandit³² also discussed the importance of the optimum inlet pressure conditions at which maximum cavitation intensity can be achieved emphasizing the importance of the quantum of total collapse pressure generated as a result of the collapse of single cavity and the total number of cavities being generated in the

solution. However, degradation of orange G dye was very low, less than 5% irrespective of the initial dye concentration and pressure drop conditions.

Saharan et al.³⁰ reported degradation of orange G dye using orifice, slit venturi and circular venturi as cavitating devices and found that hydrophilicity or hydrophobicity of dye molecule is important in degradation. It relates to the state of pollutant molecule in the solution i.e. molecular or ionic state. If the pollutant is in molecular state, it can easily enter the region of gas water interface of cavities due to hydrophobic nature and thus more readily subjected to OH[•] radical attack and also to the thermal decomposition³³. Thus the overall decomposition is attributed to the pyrolysis and free radical attack occurred at both cavity and water interface and bulk liquid medium. While hydrophilicity relate to the ionic orientation of dye molecule to remain in the bulk solution and hence, less prone by OH[•] radical attack. It was also reported that orange G molecules are in ionic (hydrophilic) form in basic pH range and very low decomposition was observed for orange G at pH range of 7.3-9 which is similar to ~8.5 pH of this study. It has been also reported that only 10% of the OH[•] radicals generated can enter the bulk medium¹⁴. Among the dyes, orange G has high solubility in water and also found to be most difficult to degrade whereas auramine O dye was observed to be easily degradable.

3.3. Cavigation

Three different schemes in cavigation have been developed to study the process. The schemes are formed in such a way that the individual effect of each coagulation and cavitation is explored and also the combined effect of the two processes, in a specified manner. It is to be noted that the rates of degradation of pollutants by cavitation and rates of removal of pollutants by coagulation could be widely different and the schemes are expected to highlight information in this regard that is not available in the literature. The combination in both the forms of cavitation (Hydrodynamic and acoustic) with coagulation was studied.

Scheme 1:

This scheme aims to evaluate the removal of pollutants by coagulation separately followed by the combined effect of coagulation and cavitation. The time for coagulation is provided separately in this scheme as mixing was done initially after which the solution is subjected to cavigation. The comparison of the results of this scheme of cavigation, with results of coagulation and cavitation separately, will help in understanding the enhancement if any due

to cavitation as no separate time for only cavitation has been provided in this scheme. The importance of providing extra coagulant mixing time is also highlighted.

Scheme 2:

The scheme-2 evaluates simultaneous processing effect of coagulation and cavitation. This scheme will help in understanding the competition of rates of coagulation and cavitation, as no extra time for cavitation or coagulation is provided and both processes are performed simultaneously, immediately after the addition of coagulant. The results would reveal dominance of the rate of any one process over the other.

Scheme 3:

Scheme-3 evaluates the removal of pollutants first through cavitation and then combined effect with coagulation. In this scheme, cavitation is done initially after which coagulant is added. The results obtained with this scheme will help in understanding the importance of providing separate time for only cavitation to investigate breakdown of pollutant species/ altering nature and composition of effluent stream in the process when performed separately.

In general,

- a) Cavitation or coagulation may take part in the overall process either completely or partially.
- b) Any one of the processes may be assisting the other or
- c) There may be dominance or interference of any one of the processes completely over the other which will result in affecting the overall efficiency of cavigation.

3.3.1. Acoustic cavitation+coagulation

This study was carried out by taking Congo red (50 and 100 ppm) as the model pollutant. The efficiency of cavigation process with two chemical coagulants; PAC SAB 18 and Iron (III) chloride and three biocoagulants; *Moringa oleifera*, *Acanthocereus tetragonus*, and *Cicer arietinum* was investigated.

For comparison, the individual processes were performed separately. The extent of dye removal (Congo red 50 and 100 ppm) using only acoustic cavitation for natural pH, pH 3 and pH 5 was negligible.

Effect of Schemes adopted

It was observed that the schemes adopted in cavitation played a significant role in the understanding of the process. The major experimental findings are summarized in **Table 2**. From **Figs. 5** and **6** the comparative results for coagulation and cavitation can be observed at natural pH for PAC SAB 18 and iron (III) chloride as chemical coagulants for the removal of 50 and 100 ppm of initial concentration of Congo red dye. High removal of 74% and 85% with scheme 2 and scheme 3 (15 ppm coagulant dose) of cavitation respectively over 37% of coagulation using PAC SAB 18 was observed for 50 ppm of Congo red dye. Similarly, improvement in dye removal efficiency with scheme 3 of cavitation using PAC SAB 18 (20 ppm dose) was attained over coagulation for 100 ppm of Congo red dye. Also in the case of iron (III) chloride (20 ppm dose), a higher dye removal of 46% was achieved with scheme 3 of cavitation in comparison to only 22% with coagulation for 100 ppm of dye.

Figs. 7 to **9** show the comparative results using biocoagulants with natural pH condition of the dye solution. An improvement in dye removal using cavitation over coagulation was in the range of almost 25% with schemes 2 and 3 (330 ppm coagulant dose) in the case of *Moringa oleifera*, 30% with scheme 3 (300 ppm coagulant dose) and almost 20% with scheme 1 and scheme 3 (860 ppm coagulant dose) in the case of *Acanthocereus tetragonus*, 29% with scheme 3 (400 ppm coagulant dose) in the case of *Cicer arietinum* for 50 ppm initial dye concentration. Also, for 100 ppm initial dye concentration, with schemes 1, 2 and 3 of cavitation (300 ppm coagulant dose), very high removal over coagulation was observed using *Acanthocereus tetragonus*.

The formation of very large and dense flocs in scheme 2 and scheme 3 were observed in comparison to coagulation and scheme 1, which also reveal better efficiency with these two schemes. It should also be noted that, at all the points where scheme 1 was showing better removal efficiency, scheme 2 and scheme 3 were more efficient than scheme 1. Scheme 3 was observed to be more efficient than scheme 2 in all the cases. As no dye removal was observed with only cavitation, it can be concluded that, it may have assisted the overall cavitation process to improve its efficiency.

In scheme 2 and scheme 3, cavitation may have assisted the overall process by changing the form of organic pollutant totally or partially as a result of which further addition of coagulant may enhance efficiency in these schemes of cavitation. In scheme 3, a considerable time for cavitation (initial 10 min) to act upon the dye has been provided which likely improves efficiency of scheme 3 over scheme 2. Providing separate mixing of coagulant initially may not help as no time for cavitation was allowed to assist the process separately in scheme 1.

Effect of pH

A pH range of 3 to 5 and *Moringa oleifera* as a bio-coagulant/ PAC SAB 18 as a chemical coagulant were selected for the pH study. The results are depicted in **Figs. 10 to 11**. For the same coagulant dose, a higher extent of removal was obtained in acidic condition of pH 3, while almost the same removal has been observed at natural pH and pH 5 (except higher removal in the case of 20 ppm dose of PAC SAB 18 for removal of 100 ppm of Congo red dye at pH 5) using both the coagulants in cavitation (three schemes) and coagulation. A decrease of pH leads to dye protonation thereby reduction of charge density and induce self-aggregation of dye molecules and as a result, less coagulant is required for destabilization³². Some studies, however reported that, pH does not affect the removal efficiency of biocoagulants³⁴ though, Patel and Vashi³⁵, reported increase in the removal of Congo red at a lower pH value with *Moringa oleifera* as a coagulant due to the change in the surface charge of the coagulant along with the stabilization of the suspension.

In the case of PAC SAB 18 (10 ppm dose), 41%, 58% and 43% dye removal with schemes 1, 2 and 3 were observed compared to only 20% dye removal with coagulation at pH 5 for 50 ppm initial concentration of Congo red dye. At pH 5, an improvement of ~17% in removal efficiency with cavitation (scheme 2) over coagulation was obtained using *Moringa oleifera* (800 ppm coagulant dose) for 100 ppm initial concentration of Congo red dye. In the case of highly acidic pH conditions i.e. pH 3, the removal efficiency of cavitation (scheme 2 and scheme 3) using PAC SAB 18, was very less in comparison to coagulation at 2.5 and 5 ppm coagulant dose for removal of 50 and 100 ppm of initial dye concentration respectively. Also in acidic conditions (pH 3) only 41% dye removal was observed using cavitation (scheme 2) which was up to 60% using coagulation for a 50 ppm initial concentration of Congo red dye. It is possible that in cavitation, the high-frequency sound waves may

destroy partly the flocs formed. The instability of the flocs in acidic conditions has been reported in earlier studies²⁶.

Effect of selection of coagulant

The efficiency of cavitation was observed to be dependent on the nature of coagulant. A lowering in efficiency with cavitation in comparison to coagulation has been identified only in case- *Moringa oleifera* and iron (III) chloride as coagulants. **Fig. 12** shows the change in pH of the dye solution with increase in dose of all the coagulants used in the study which shows acidic nature of *Moringa oleifera* and iron (III) chloride. At low pH conditions, flocs are more fragile and may get dissolved in the solution due to high frequency sound waves, hence affecting the overall efficiency in cavitation. In general, PAC SAB 18 as chemical coagulant and *Acanthocereus tetragonus* as biocoagulant were found to be most efficient coagulants in cavitation.

3.3.2 Hydrodynamic cavitation+coagulation

The experiments were performed selecting auramine O and Congo red dyes with initial dye concentration of 100 ppm and 500 ppm respectively. PAC SAB 18 was selected as coagulant (coagulant doses of 25 ppm in the case of auramine O dye and 100 ppm in the case of Congo red dye). A pressure drop of 2 bar in cavitation and cavitation was used. **Fig. 13** shows the comparative results of hydrodynamic cavitation, coagulation and cavitation (hydrodynamic cavitation+coagulation) adopting three schemes for both the dyes. It has been observed that, in the case of auramine O dye, the removal using cavitation was considerably higher than only coagulation but lesser than cavitation. In comparison to 73% of dye removal observed in cavitation, only ~ 50% dye removal was observed with all the schemes. In the case of Congo red dye, removal observed was 19% with scheme 1, and 26% with scheme 2 and 3 of cavitation compared to 23% with coagulation, which was higher than that in cavitation alone. As discussed in the case of acoustic cavitation+coagulation, formation of flocs in cavitation has been observed and found to play a significant role in improving efficiency in cavitation, but in this case no such flocs were observed. Flocs formation at the intermediate stage of the process may occur, but may not withstand conditions of stress due to the motion of the fluid at high flow rate leading to the breakage of these flocs or floc formation may not

take place in the HC process leading to lower efficiency of cavitation in form of HC+coagulation. More investigations are however required in this regard.

4. Conclusions

The present study clearly highlights the benefits of developing new hybrid technologies for dye wastewater treatment as cavitation in form of acoustic cavitation+coagulation was observed to be very efficient for dye removal for Congo red dye wastewater when compared to the efficiency of coagulation and acoustic cavitation individually.

1. A separate time for cavitation assists the whole cavitation process to improve its efficiency in the case of acoustic cavitation+coagulation for the removal of Congo red dye (Scheme-3).
2. Highly acidic condition in cavitation at some points was not favorable and acidic coagulants were also effective at high doses.
3. Low coagulant doses were required in acidic conditions for attaining the same removal efficiency of Congo red dye in coagulation and cavitation (AC+coagulation).
4. PAC SAB 18 amongst the chemical coagulants and *Acanthocereus tetragonus* amongst biocoagulants were found to be the most efficient
5. Study of cavitation in form of coagulation+HC for removal of auramine O and congo red dyes accentuate the need for modifications for better removal efficiency.
6. Auramine O dye was found to be the most easily degradable using hydrodynamic cavitation compared to coagulation, while Congo red was easy to remove using coagulation but not with HC; Orange G was found to be most difficult to remove using either of the processes.

Overall it has been found that the molecular weight, structure and solubility of dye, nature of coagulants are the important parameters. It can be concluded a combination of two or more treatment processes is required to meet the desired level of removal.

Figures:

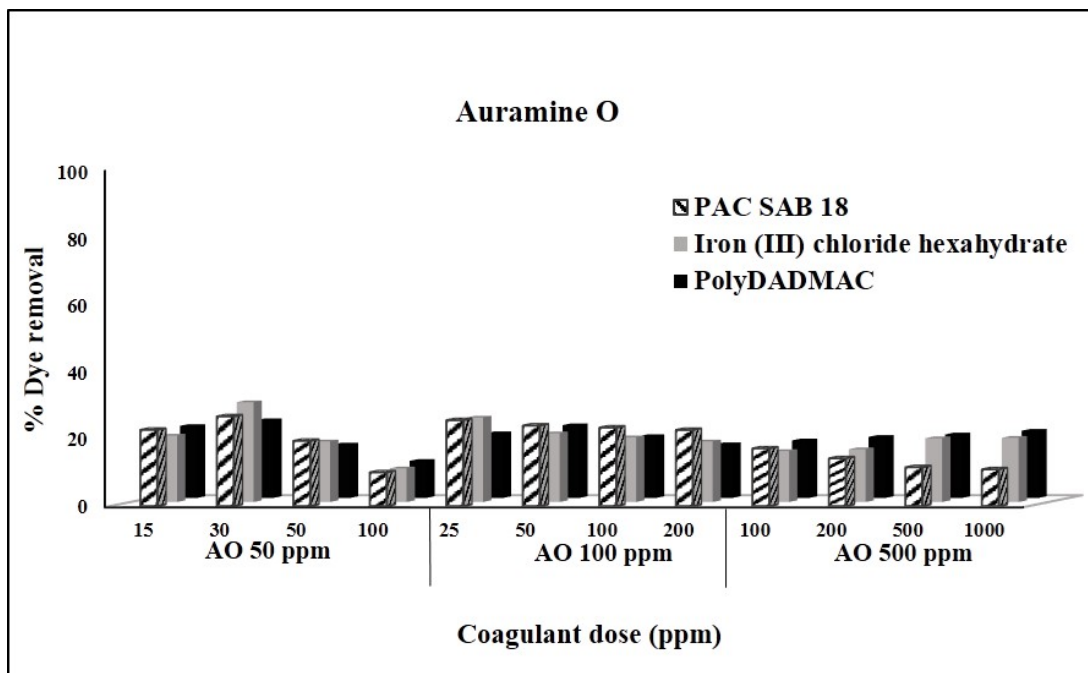


Fig. 1. Effect of coagulant doses on dye removal for auramine O dye

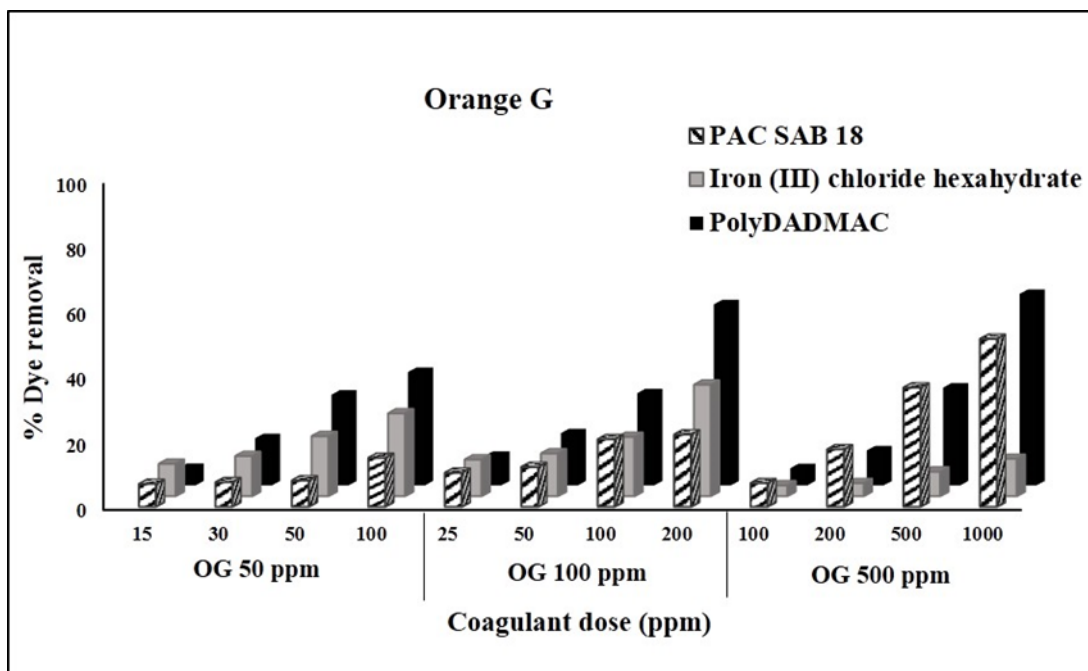


Fig.2. Effect of coagulant doses on dye removal for orange G dye

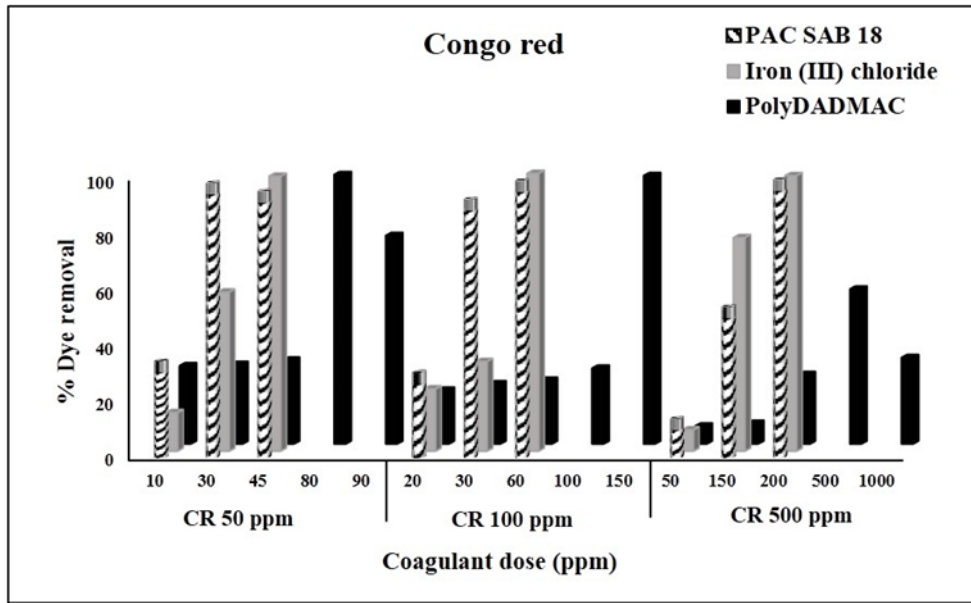


Fig. 3. Effect of coagulant doses on dye removal for Congo red dye

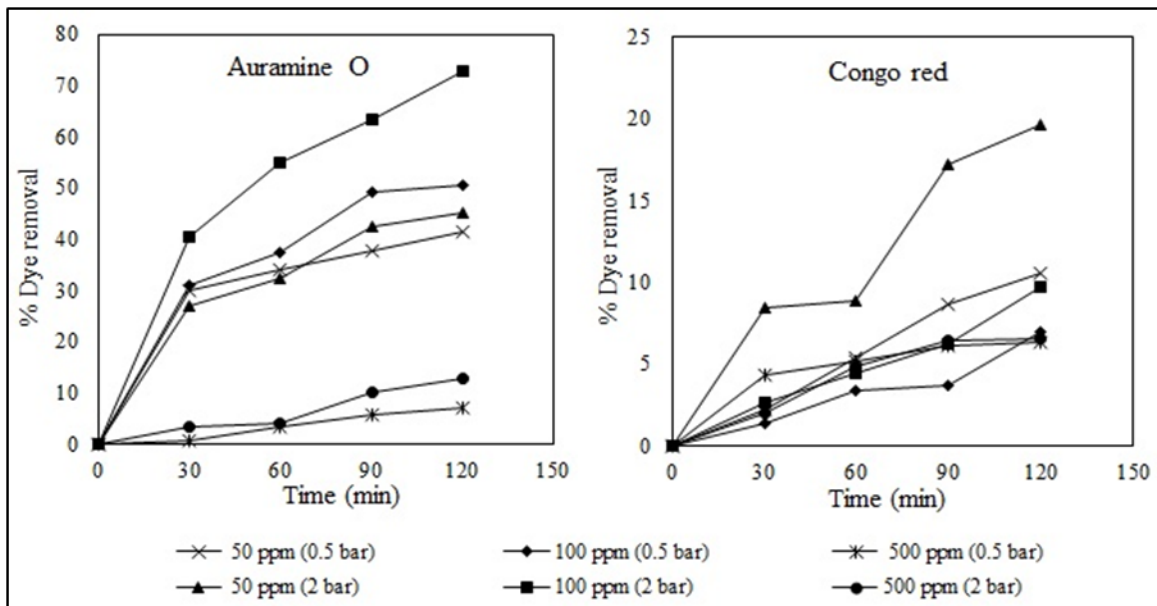


Fig. 4. Effect of initial dye concentration and pressure drop

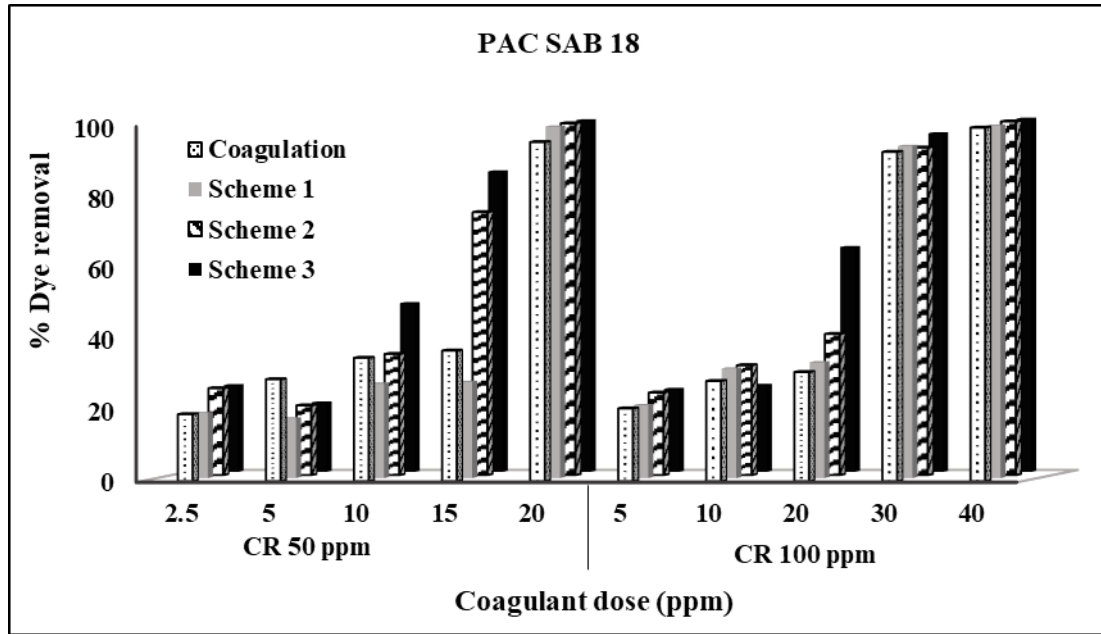


Fig. 5. Comparative results of cavigation (three schemes) and coagulation using PAC SAB 18 as coagulant

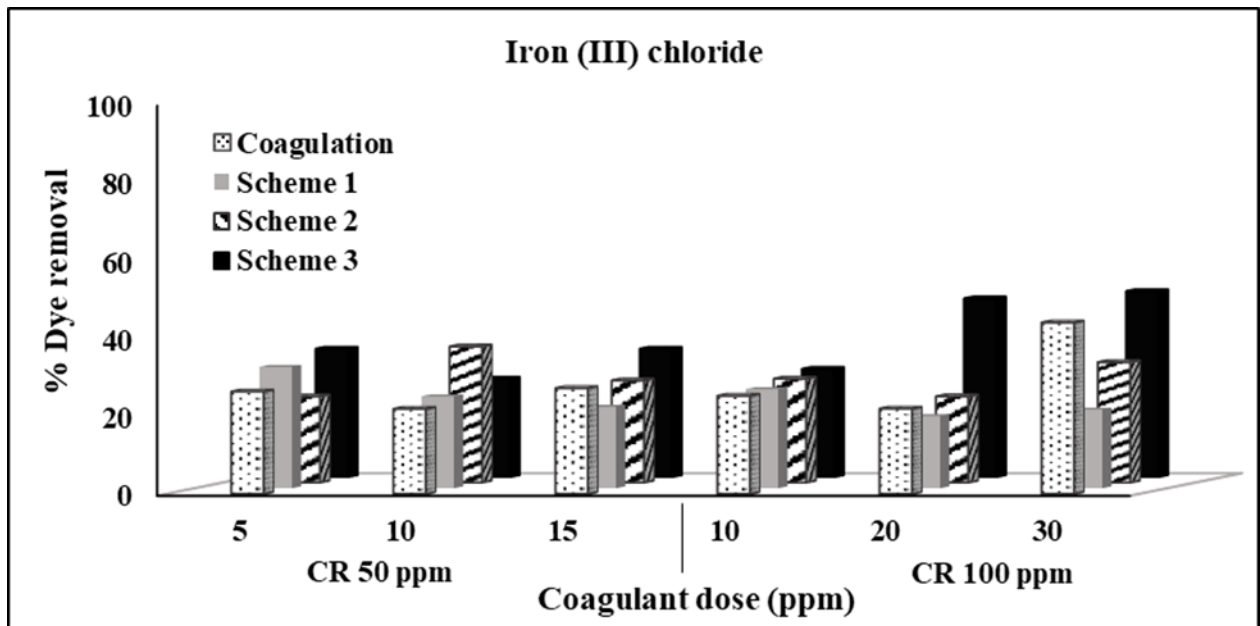


Fig. 6. Comparative results of cavigation (three schemes) and coagulation using Iron (III) chloride as coagulant

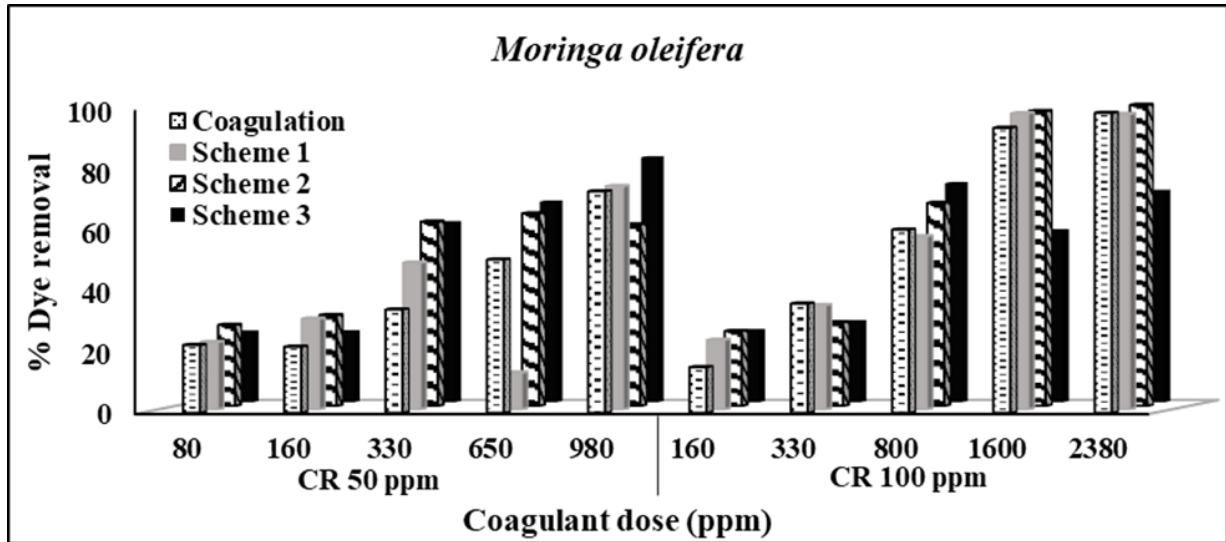


Fig. 7. Comparative results of cavigulation (three schemes) and coagulation using *Moringa oleifera* as coagulant

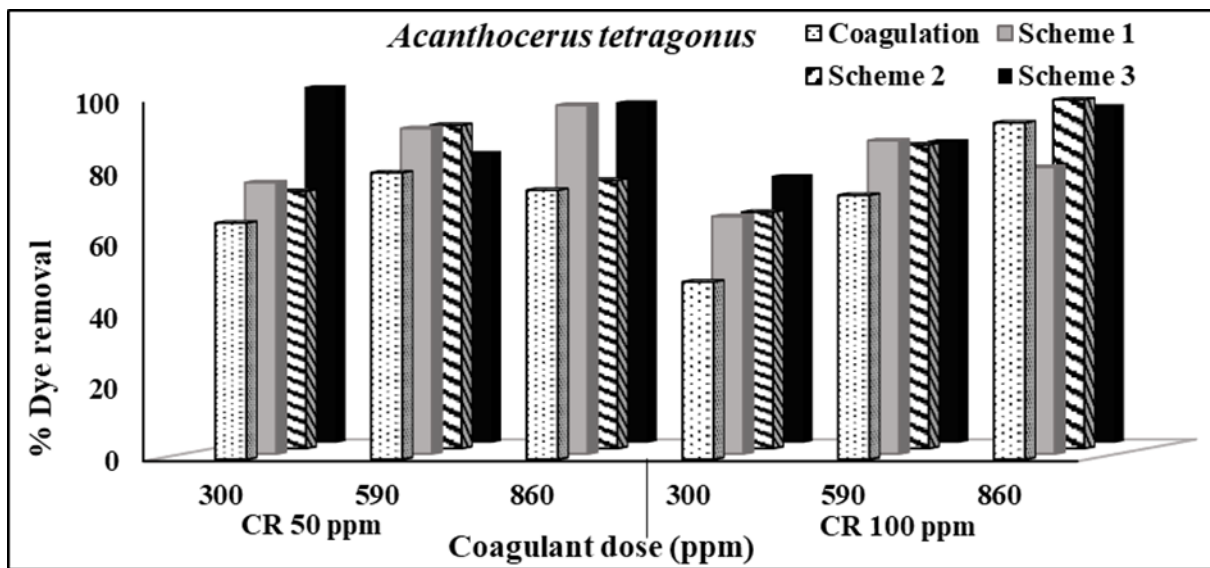


Fig. 8. Comparative results of cavigulation (three schemes) and coagulation using *Acanthocerus tetragonus* as coagulant

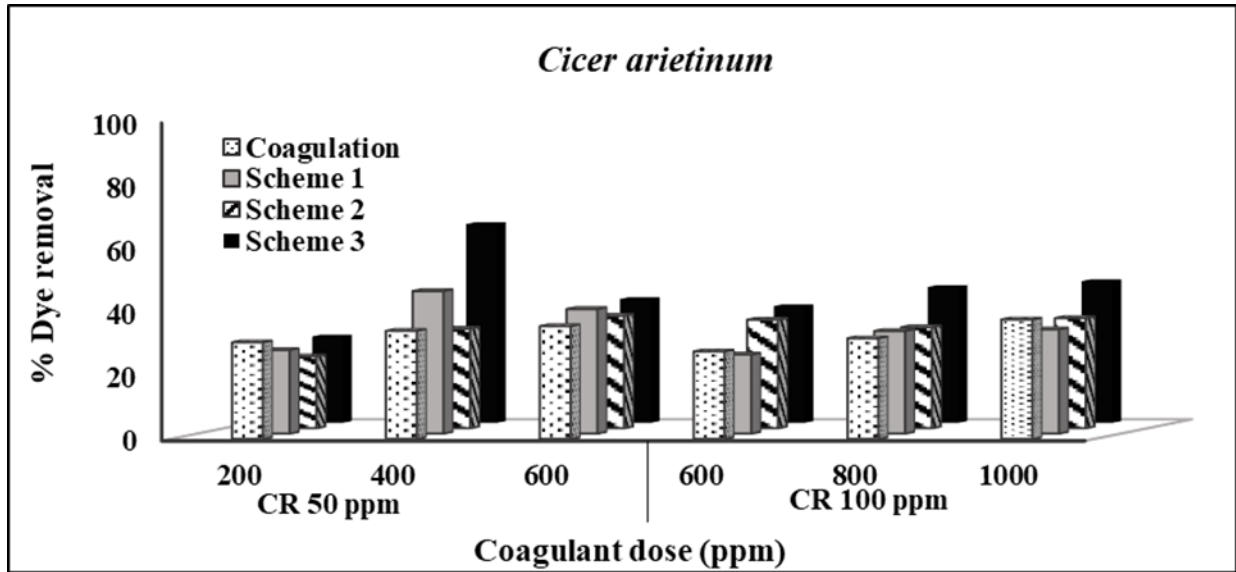


Fig. 9. Comparative results of cavigation (three schemes) and coagulation using *Cicer arietinum* as coagulant

^aAdjusted pH, ^bNatural pH

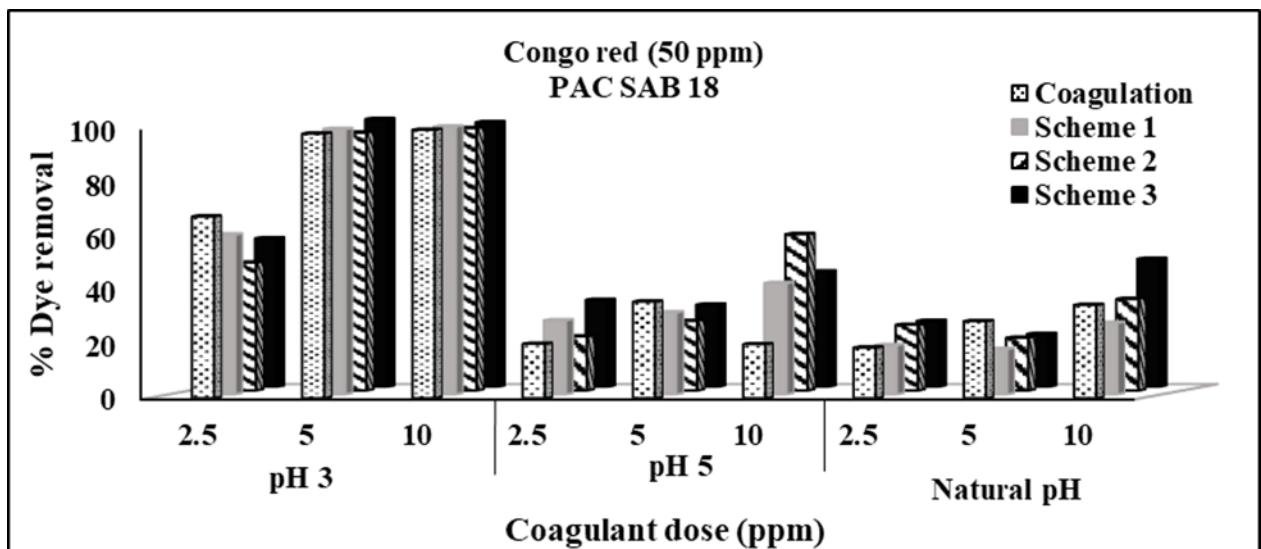


Fig. 10A. Effect of varying pH on efficiency of coagulation and cavigation (three schemes) using PAC SAB 18 as coagulant

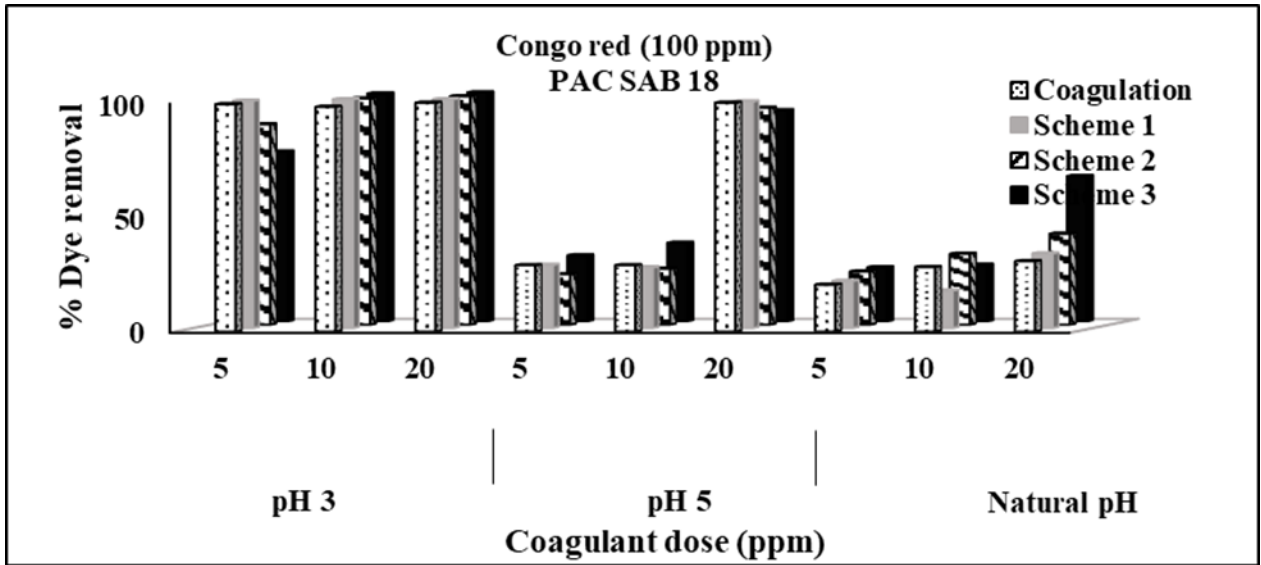


Fig. 10B. Effect of varying pH on efficiency of coagulation and cavigation (three schemes) using PAC SAB 18 as coagulant

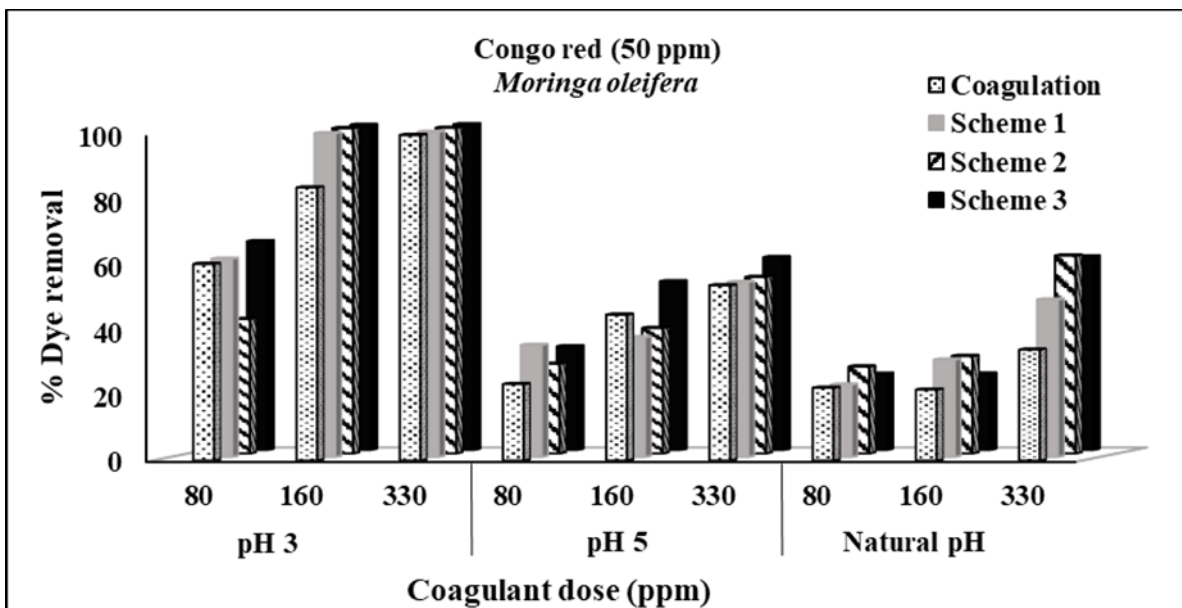


Fig. 11A. Effect of varying pH on efficiency of coagulation and cavigation (three schemes) using Moringa oleiferaas coagulant

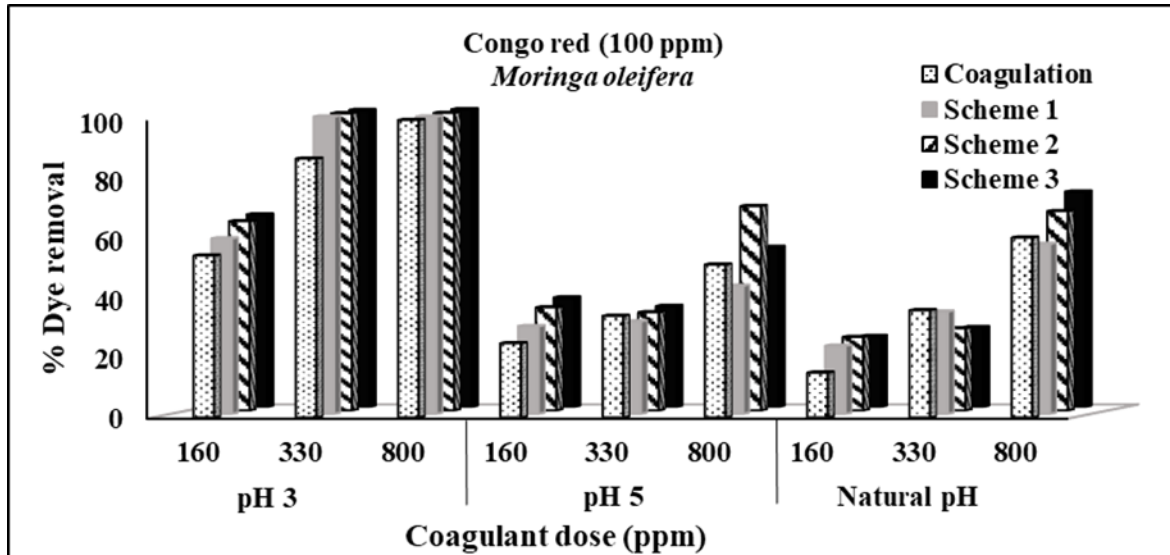


Fig. 11B. Effect of varying pH on efficiency of coagulation and cavigation (three schemes) using *Moringa oleifera* as coagulant

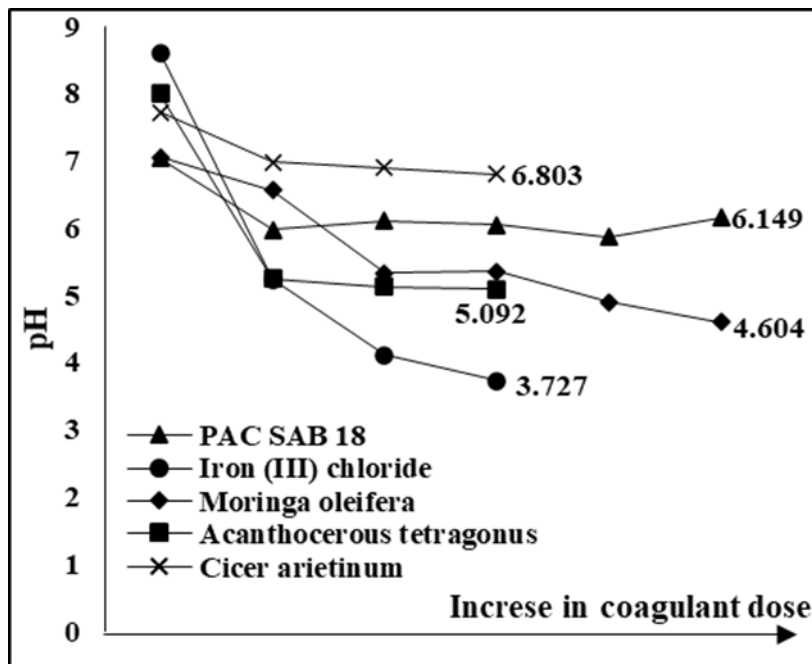


Fig. 12. Effect of increase in coagulant dose on pH

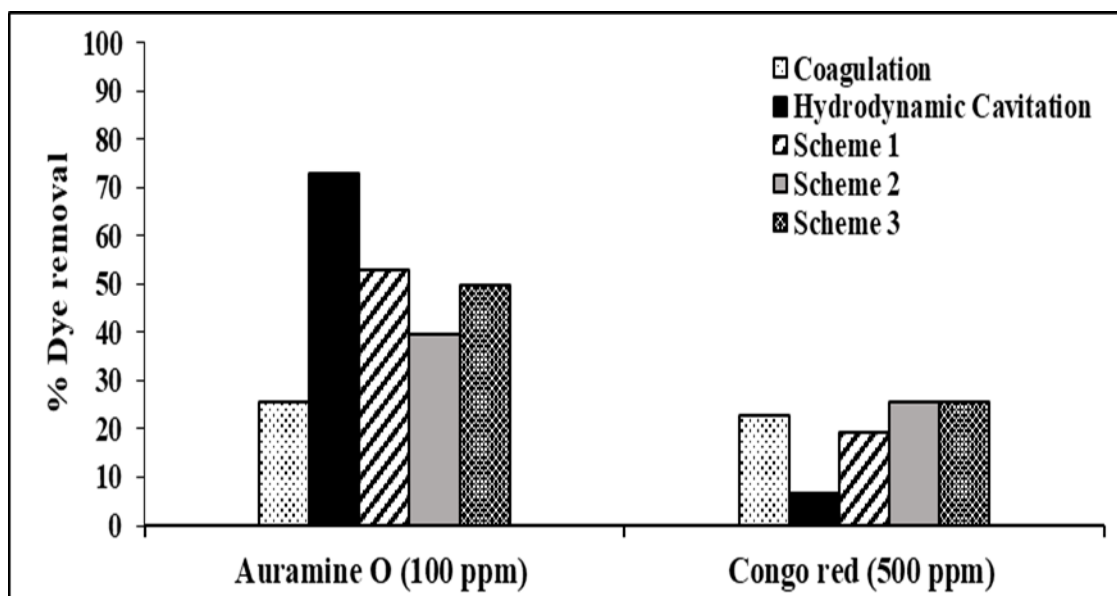


Fig. 13. Comparative results of cavitation (three schemes), cavitation and coagulation using PAC SAB 18 as coagulant

Tables:

Table 1. Physicochemical properties of dyes

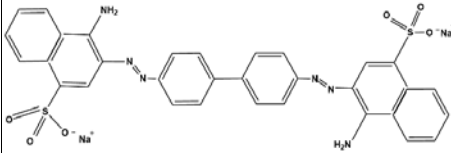
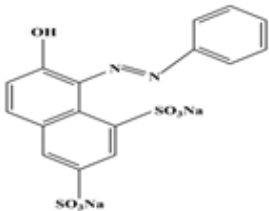
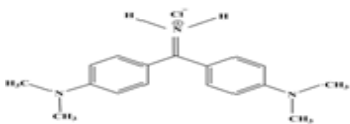
S. No.	Name of dye	Molecular Structure	Molecular Weight (g/mol)	Solubility in water (mg/ml)	Appearance
1.	Congo red	 The structure shows a central biphenyl core. Each phenyl ring of the biphenyl is connected via an azo (-N=N-) group to a naphthalene ring. Each naphthalene ring has an amino group (-NH ₂) and a sodium sulfonate group (-SO ₃ Na) attached to it.	696.65	10	Solid powder
2.	Orange G	 The structure shows a naphthalene ring system. It has a hydroxyl group (-OH) at position 1, a sodium sulfonate group (-SO ₃ Na) at position 4, and another sodium sulfonate group (-SO ₃ Na) at position 5. An azo group (-N=N-) is attached at position 6, which is further connected to a phenyl ring.	452.37	80	Solid powder
3.	Auramine O	 The structure shows a central carbon atom double-bonded to a chlorine atom (C=Cl) and single-bonded to two hydrogen atoms (C-H). This central carbon is also bonded to two para-substituted benzene rings. Each benzene ring has a dimethylamino group (-N(CH ₃) ₂) attached to it.	303.83	10	Solid powder

Table 2. Comparative study of cavigation (acoustic cavitation+coagulation), coagulation and acoustic cavitation

S. no.	Dye conc. (ppm)	pH	Coagulant	Coagulant dose (ppm)	Scheme	Percent dye removal		
						Cavigation	Coagulation	Cavitation
1	50	6.5 ^b	PAC SAB 18	15	2	74	37	0
2	50	6.4 ^b	PAC SAB 18	15	3	85	37	0
3	100	5 ^b	PAC SAB 18	20	3	63	31	0
4	50	5 ^a	PAC SAB 18	10	1	41	20	0
5	50	5 ^a	PAC SAB 18	10	2	58	20	0
6	50	5 ^a	PAC SAB 18	10	3	43	20	0
7	50	3 ^a	PAC SAB 18	2.5	2	48	68	5
8	100	3 ^a	PAC SAB 18	5	3	73	99	9
9	100	3.8 ^b	Iron (III) chloride	20	3	46	22	0
10	100	3.8 ^b	Iron (III) chloride	30	1	20	44	0
11	50	7 ^b	<i>Moringa oleifera</i>	330	2	61	34	0
12	50	6.9 ^b	<i>Moringa oleifera</i>	330	3	59	34	0
13	50	5.7 ^b	<i>Moringa oleifera</i>	650	1	12	51	0
14	100	4.9 ^b	<i>Moringa oleifera</i>	1600	3	57	94	0
15	100	4.8 ^b	<i>Moringa oleifera</i>	2300	3	70	99	0
16	50	3 ^a	<i>Moringa oleifera</i>	80	2	41	60	5
17	100	5 ^a	<i>Moringa oleifera</i>	800	2	68	51	7
18	50	5 ^b	<i>A. tetragonus</i>	300	3	99	66	0
19	50	5 ^b	<i>A. tetragonus</i>	860	1	97	75	0
19	50	5 ^b	<i>A. tetragonus</i>	860	3	95	75	0
20	100	5.2 ^b	<i>A. tetragonus</i>	300	1	66	50	0
21	100	5.2 ^b	<i>A. tetragonus</i>	300	2	66	50	0
22	100	5.2 ^b	<i>A. tetragonus</i>	300	3	75	50	0
23	50	5.9 ^b	<i>Cicer arietinum</i>	400	3	63	34	0

Note: ^aAdjusted pH, ^bNatural pH

References

1. P. R. Gogate, G. S. Bhosale, 71, 59,2013.
2. T. C. Hsu, C. S. Chiang, J. Environ. Sci. Health,7, 1921, 1997.
3. B. R. Babu, A. K. Parande, S. Raghu, T. Prem Kumar, B. R. Babu, T. P. Kumar, J. Cotton. Sci. 11,141, 2007.
4. F. Çiçek, D. Ozer, A. Ozer, A. Ozer, J. Hazard. Mater. 146 (1–2), 408, 2007.
5. Ranade, V. V.; Bhandari, V. M., Industrial Wastewater Treatment, Recycling, and Reuse; Elsevier, 2014.
6. K. P. Mishra, P. R. Gogate, Sep. Purif. Technol., 75 (3), 385, 2010.
7. T. H. Kim, C. Park, J. Yang, S. Kim, J. Hazard. Mater., 112 (1–2), 95, 2004.
8. A. K. Verma, R. R. Dash, P. J. Bhunia, Environ. Manage. 93 (1), 154, 2012.
9. A. Asfaram, M. Ghaedi, F. Yousefi, M. Dastkhooon, Ultrason. Sonochem. 33, 77, 2016.
10. P. B. Patil, P. Thanekar, V. M. Bhandari, Ind. Eng. Chem. Res., 2022. *Ind Eng Chem Res* **2022**. <https://doi.org/10.1021/acs.iecr.2c02519>
11. P. B. Patil, P. Thanekar, V. M. Bhandari, Chem Eng. Res. De., 187,623 ,2022.
12. D. V. Pinjari, A. B. Pandit, Ultrason. Sonochem. 17 (5), 845, 2010.
13. P. R. Gogate, R. K. Tayal, A. B. Pandit, Current science, 91, 35, 2006.
14. V. K. Saharan, A. B. Pandit, P. S. Satish Kumar, S. Anandan, Ind Eng Chem Res., 51 (4), 1981, 2012.
15. D. Dixit, P. Thanekar, V. M. Bhandari, Chem. Eng. Process. Proc. Intensification,172, 108799, 2022.
16. P. R. Gogate. Chem. Eng. Process. 47 (4), 515, 2008.
17. V. S. Moholkar, P. S. Kumar, A. B. Pandit, Ultrason. Sonochem., 6, 53, 1999.
18. M. Chethana, L. G. Sorokhaibam, V. M. Bhandari, S. Raja, V. V. Ranade, ACS Sustain Chem Eng 4 (5), 2495, 2016.
19. F. Anwar, S. Latif, M. Ashraf, A. H. Gilani, Phytother. Res 21, 17, 2007.
20. P. B. Patil, V. M. Bhandari, V. V. Ranade, Ultrason Sonochem 70, 105306, 2021.
21. P. B. Patil, V. M. Bhandari, J Environ Manage 311, 2022,
22. V. V. Ranade, A.A. Kulkarni, V. M. Bhandari, US 9,422,952 B2 2013, 2013.
23. M. H. Zonoozi, M. Reza, A. Moghaddam, M.Arami, Environ Eng Manag J., 71, 695, 2008.

24. O. Sahu, P. Chaudhari, *Journal of Applied Sciences and Environmental Management* 17 (2), 2013.
25. M. A. A. Razali, Z. Ahmad, A. Ariffin, *Advances in Chemical Engineering and Science* 02 (04), 490, 2012.
26. B. Shi, G. Li, D. Wang, C. Feng, H. Tang, *J Hazard Mater* 143 (1–2), 567, 2007.
27. Q. Wei, Y. Zhang, K. Zhang, J. I. Mwasiagi, X. Zhao, C. W. K. Chow, R. Tang, *Korean J Chem Eng* 39 (7), 1850, 2022.
28. T. H. Kim, C. Park, J. Yang, S. Kim, *J Hazard Mater*, 112 (1–2), 95, 2004.
29. S. Rajoriya, S. Bargole, V. K. Saharan *Ultrason Sonochem*, 34, 183, 2017.
30. V. K. Saharan, M. A. Rizwani, A. A. Malani, A. B. Pandit, *Ultrason Sonochem* ,20 (1), 345, 2013.
31. A. A. Pradhan, P. R. Gogate, *Chem. Eng. J.* 156 (1), 77, 2010.
32. P. R. Gogate, A. B. Pandit, *AIChE J.* 46 (8), 1641, 2000.
33. V. K. Saharan, M. P. Badve, A. B. Pandit, *Chem. Eng. J.*, 178, 100, 2011.
34. J. Beltran-Heredia, J. Sánchez-Martín, *J Hazard Mater* 164 (2–3), 713, 2009.
35. H. Patel, R. T. Vashi, *J. Saudi Chem. Soc.* 16 (2), 131, 2012.

⁴ Present address: Department of Civil Engineering, Vasavi College of Engineering, Hyderabad

⁵ Present address: Bernal Chair of Process Engineering, University of Limerick, Limerick, Ireland

Synthesis and Characterization of Pittal Bhasma

Babita Kale^{1*}, and Nilima Rajurkar²

1* P.E. Society's Modern College of Arts, Science and commerce college, Ganeshkhind,
Pune

2 Department of Chemistry, Savitribai Phule Pune University, Pune

Email: babita.kale95@gmail.com

Received: 24.1.23, Revised : 31.1.23, Accepted: 31.1.23

Abstract:

Ayurvedic Bhasmas play very important role in the treatment of various diseases. However, it should be in the pure form to avoid any adverse effects on human health. The present work describes the synthesis of copper and zinc based Pittal bhasma followed by its characterization using modern analytical techniques such as TEM, SEM, EDX, XRD, DLS and FTIR as well as some ayurvedic tests. Synthesis involves traditional method of shodhana, bhavana and marana . For the latter, traditional putas as well as modern electric muffle furnace were also used for heating purpose. The study reveals that Pittal Bhasma prepared by traditional method of heating has 60 % particles in the range of 300-750nm while that prepared by using electric muffle furnace has 65 % particles in 250-750nm range. In both cases the bimodal particle distribution is observed. The study concludes that bhasma can be useful medicine if it is prepared by standard method of preparation and analysis.

Key Words: Pittal Bhasma, Purification, Ayurveda, Traditional Medicine

1.Introduction:

Ayurvedic Bhasmas play very important role in the treatment of various diseases¹. Bhasmas are unique ayurvedic herbo-metallic preparations useful in various ailments. Starting raw material, various ingredients used during synthesis, trituration process and way of incineration process decides quality of bhasma. The incomplete incineration may result in impurities which can lead to the adverse effects and toxicity. If Bhasma is not prepared properly, it can cause multiple complications such as skin diseases, fever, delusion etc. Hence, Different classical textbooks of Rasashastra have mentioned various parameters for the Standardization of Bhasma², as a single method²⁻⁵ is not applicable for determining the accurate formation of a particular bhasma.

The various confirmatory parameters for prepared Bhasma are specified in the various Ayurvedic textbooks and literature⁵⁻⁹. Copper and zinc based Pittal Bhasma is used for the

treatment of various skin diseases^{3,4,9}. We had reported synthesis and characterization of different bhasmas from our laboratory, among which vanga bhasm and Abhrak bhasma were found to have formation of nanoparticles in it^{10,11}. The present work describes the synthesis of Pittal bhasma followed by its characterization using modern techniques such as TEM, SEM, EDX, XRD, DLS and FTIR as well as some ayurvedic tests.

2. Materials and Methods:

Pittal was purchased from the local Market and sheets were prepared in workshop of Chemistry Department, Savitribai Phule Pune University. Pittal Bhasma was synthesized as per the procedure described in ayurvedic literature [6]. It involves Shodhana process (purification of raw material) followed by Bhavana process (Levigation). At the end, Marana process (incineration) was carried out. Incineration was done with traditional putas as well as modern electric muffle furnace (EMF).

2.1 Purification:

Liquefaction and pouring methods were used for purification of raw material. In this process the metals are subjected for purification with various liquid media viz. sesame oil, butter milk, cow's urine, kanji, and decoction of horse gram. The Sheets of Pittal (brass) weighing 99.1 g were used for preparation of Bhasma. The metal plates (5×5 cm) were kept on flame and heated till the material becomes red hot. The red hot metal sheets were then quenched in 100 mL of sesame oil taken in earthen pot. Sesame oil was separated, and plates were dried and its weight was recorded. The above procedure was repeated for six more times. Similar purification was carried out using butter milk, cow urine, kanji, horse gram decoction respectively. For each step of purification fresh liquid media was used.

2.1. Special purification (Vishesh shodhana)

In special purification of brass metal, plate processed in previous step was heated till it became red hot and quenched in 100 mL mixture of Vitex nigundo leaves juice and 50 g powder of Curcuma longa Linn (haridra). The process was repeated 3 times. This procedure modifies the properties of the therapeutic material to enhance their potential.

2.2 Levigation:

The sample after Purification was subjected for levigation. The metal plates were converted into small pieces after purification. The pieces of brass from above step were ground with the leaves of *Calotropis gigantean* (*Rui*) plant till it was converted into fine powder.

2.3 Incineration:

In this method small pellets were prepared by using paste from levigation step. These pellets were then kept in closed vessel (sharav) and subjected for heating. The sample was slowly

heated in electric muffle furnace up to 1100⁰C and kept for 3h. The sample was also heated by traditional method. The process was repeated 7 times.

The final form of bhasma was yellowish in colour. It was then analyzed by ayurvedic tests and XRD, FTIR, SEM, EDAX, TEM and DLS techniques

3 Results and Discussion:

3.1 Ayurvedic tests of Pittal Bhasma:

The prepared bhasma was analyzed in view of ayurvedic tests, the results of which are recorded in Table 1

Observations recorded in Table 1 were found to match with those reported in ayurvedic literature.

The major changes observed during purification were that the sample melts after heating, while pouring into liquid media, the sample becomes hard and shiny. At the end of special purification, the sample was converted into small pieces which were more brittle.

The initial weight of raw Pittal was 50 g. The weight of finally obtained Pittal bhasma by traditional method of heating was 25 g and Electric muffle Furnace heating was 30.5 g.

3.1 XRD analysis at different stages of synthesis:

The synthesized bhasma was characterized using X- ray diffractometer SHIMADZU AA -7000 ,equipped with photo scintillation detector , angular range $2\theta = 10 -80^{\circ}$, rate of scanning $5^{\circ} / \text{min}$.The scanning angle was between $10-80^{\circ}$ C and the rate of scanning was $1^{\circ} / \text{min}$.

The XRD pattern at each stage of preparation of Pittal Bhasma is shown In Figures 1a and 1b The presence of sharp diffraction peak shows the highly crystalline nature of bhasma. The XRD spectra of starting material of Pittal Bhasma (Fig.1a) shows the major peaks at $2\theta = 35.5^{\circ}$, 35.6° 48.3° and in the sample shows diffraction peak mainly at $2\theta = 42.50^{\circ}$, 49.30° , 49.53° and 72.32° which indicates the planes 200,202 and 220, which is related to Cu and CuO. Spectra for the starting material after purification(Fig1b) shows similar peaks which are present in starting material except the peak at $2\theta = 72.32^{\circ}$.After purification the final product of Pittal Bhasma prepared by incineration with EMF heating and traditional method of heating (Fig.2a and 2b) shows clear phase change and crystalline nature of the sample. The major peaks are observed at $2\theta = 32.68^{\circ}$, 39.20° , 46.18° and 56.46° in the bhasma prepared by traditional method of heating (Fig.2a) which represents the planes 110,002, 202, 220.While the Pittal Bhasma prepared by electric muffle furnace heating (Fig.2b) shows major peaks at $2\theta = 27.88^{\circ}$, 29.98° , 35.32° , 38.70° , 48.66° , 62.38° which is related to planes 110, 002, 202, 200,

220. The peaks correspond to Cu_2O , Cu as well as Cu_4O_3 with reference to JCPDS file No. 05-0661 and 33-0480. The peaks are observed to be more intense in spectra for Pittal Bhasma incinerated with EMF heating than that of the spectra for the bhasma prepared by incineration with traditional method of heating.

The mean crystallite size calculated by Scherer equation (1) is recorded in Table 2

$$t = \frac{0.9\lambda}{\beta \cos\theta} \text{----- (1)}$$

Where, t = Crystallite size, λ = Wavelength, β = Full width at Half Maxima

An examination Table 2 shows that the mean crystallite size for the initial sample of Pittal Bhasma is 157.48 nm. This decreases after purification to 152.8 nm. Bhasma prepared by incineration with electric muffle furnace heating shows less crystallite size than that of the bhasma prepared by traditional method of heating.

3.2 FTIR analysis during Pittal Bhasma process:

The FTIR spectrum of sample shows peaks in 400- 4000 cm^{-1} region. The FTIR analysis was carried out on SIMADZU-7000. The major peaks obtained from FTIR spectra (Fig.3) for Pittal Bhasma is shown in Table 3.

As can be seen from Table 3 and Fig.3, for the Pittal Bhasma prepared by EMF heating shows major peaks at 519 cm^{-1} , 867 cm^{-1} , 1101 cm^{-1} and 2334 cm^{-1} . But the bhasma prepared by traditional method of heating shows peaks at 481 cm^{-1} , 2134 cm^{-1} , 2327 cm^{-1} . The spectra in low frequency region are mainly due to the metal oxide bond such as CuO , ZnO . The peak intensity is more in case of Pittal Bhasma incinerated with electric muffle furnace heating than the bhasma incinerated with traditional method of heating.

3.3 SEM Analysis during Pittal Bhasma Preparation process:

SEM of Pittal bhasma at various stages of synthesis are shown in Fig.4 and Fig. 5

The SEM analysis was carried out on FEI Nova-nano SEM-450. The scanning electron micrograms at various stages of preparation are shown in Figs.4 and Fig.5

An examination of Fig. 4a –4b reveals regular and uniform arrangement of cluster of granules in finally prepared bhasma, which was not observed in raw material (Fig.4a). It is clearly observed that the surface area was smooth after special purification (shodhan) treatment (Fig.4b) and organic constituents are adsorbed on the surface of the sample during

preparation. The particle size observed after special purification is 250nm - 1 μ m. Hence, it is clear that purification process reduces particle size. The bhasma prepared by traditional method of heating shows the uneven size of the bhasma particles (Fig.5a). The size of Pittal Bhasma prepared by EMF heating is less as compared to the bhasma prepared by incineration with traditional method of heating. This may be due to the uneven heating of sample in traditional method. The size of particles in Pittal Bhasma prepared using electric muffle furnace is between 50-100nm (Fig5b), while that of the bhasma prepared by traditional method of heating shows clusters of particles within 250nm -1 μ m (Fig.5a). It also shows some rod like structure.

3.5 EDX Analysis during Pittal Bhasma process:

Fig.6 to Fig. 9 show EDX spectra of Pittal Bhasma at different stages of preparation (using of Bruker XSHLASH-6 I30 electron microscope) and Table 4 to Table 7 includes elemental content obtained from EDX analysis of Pittal Bhasma at various stages of preparation

The EDX spectra of starting material of Pittal Bhasma (Fig.6 and Table 4) shows the Cu and Zn in major amount along with some trace elements such as S, Fe, C. After purification (Fig.7 and Table 5) it was observed that other elements are incorporated in bhasma Cu, O, S, C. The final product of Pittal Bhasma prepared by incineration with traditional method of heating (Fig.8 and Table 6) shows O, Si, Fe, Pb, Ca, Mg and P along with the Cu and Zn. The concentration of Cu is observed to be decreased, while the bhasma prepared by EMF heating (Fig.9 and Table 7) shows the presence of Cu, Zn, Al, Si, Mg, P, C, O and K. The source of elements other than Cu and Zn may be medicinal plants used during preparation of Pittal Bhasma. All these elements are obtained from the herb and useful to increase the efficacy of the bhasma. These seem to be additional supplement for curing the disease. Thus, the elemental analysis shows the nutrient elements present in the bhasma sample are due to the herbal material used in the preparation.

3.6 TEM analysis during Pittal Bhasma

TEM analysis of Pittal bhasma at various magnifications (using TecnaiG2U-twin200Kv Lab6FEI Netherlands) are shown in Fig. 10

The bright spots in SAED pattern support the highly crystalline nature of the Pittal Bhasma. The TEM image further shows spongy nature in bhasma. The inter planer distance in Pittal

Bhasma prepared by incineration with EMF heating (Fig.10b) is 0.268 nm while that of the bhasma prepared by traditional method of heating (Fig.10 a) is 0.299 nm. Thus, TEM analysis also supports that the bhasma prepared by EMF heating is better method than traditional method of heating.

3.7 DLS analysis During Pittal Bhasma preparation process:

The diffusion coefficient, effective diameter and polydispersivity of Pittal Bhasma are reported in Table.8

As can be seen from Table 8, the dynamic light scattering study of bhasma shows that the effective diameter for the bhasma prepared by EMF heating is less as compared to the bhasma prepared by traditional method of heating.

Conclusions:

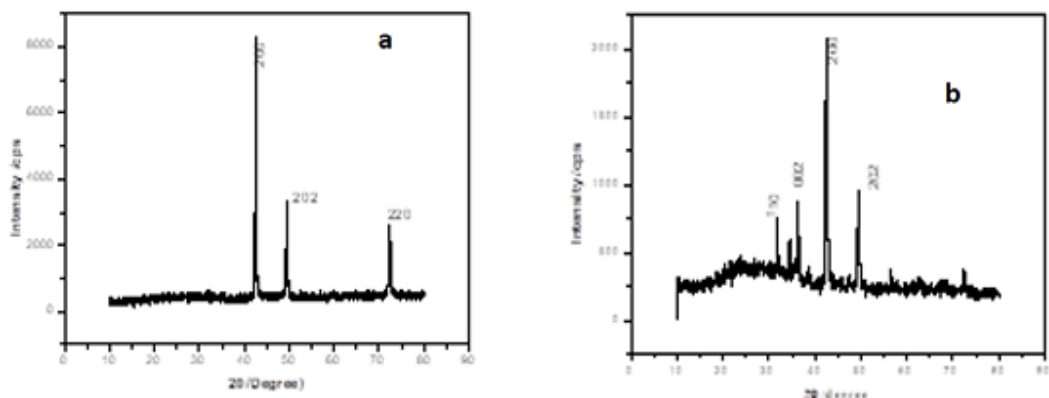
XRD of Pittal Bhasma shows the presence of CuO and granular appearance and polycrystalline nature. EDAX analysis of Pittal bhasma shows incorporation of number of nutrient elements.

SEM of Pittal Bhasma Shows particles with change in morphology. The Bhasma prepared by EMF heating are smaller in size than the Traditional Method of heating. FTIR for traditional method shows major peaks for C-H ,C=C ,Cu-O bond. Pittal Bhasma prepared by traditional method of heating has 60 % particles in the range of 300-750 nm while that prepared by using electric muffle furnace has 65 % particles in the range of 250-750 nm. In both cases the bimodal particle distribution is observed.

Acknowledgement:

Authors are thankful to Board of College and University Development (BCUD), Savitribai Phule Pune University for financial assistance and to Dr. Parag Adhypak and Dr. Shailesh Kantak for their cooperation.

Figures:



:

Fig. 1 XRD spectra of Pittal Bhasma a) before purification b) after purification

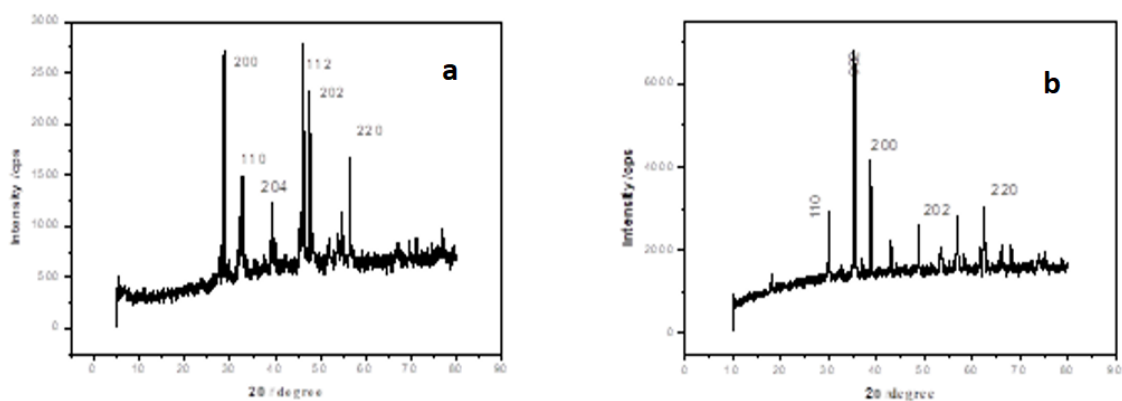


Fig. 2 XRD spectra of Pittal Bhasma prepared by a) Traditional method of heating b) EMF heating

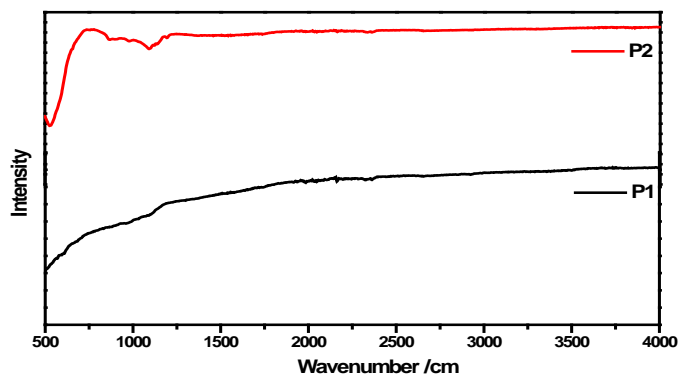


Fig.3 FTIR spectra of Pitta Bhasma

P1: Pittal Bhasma prepared by traditional method of heating

P2 :Pittal Bhasma prepared by EMF heating

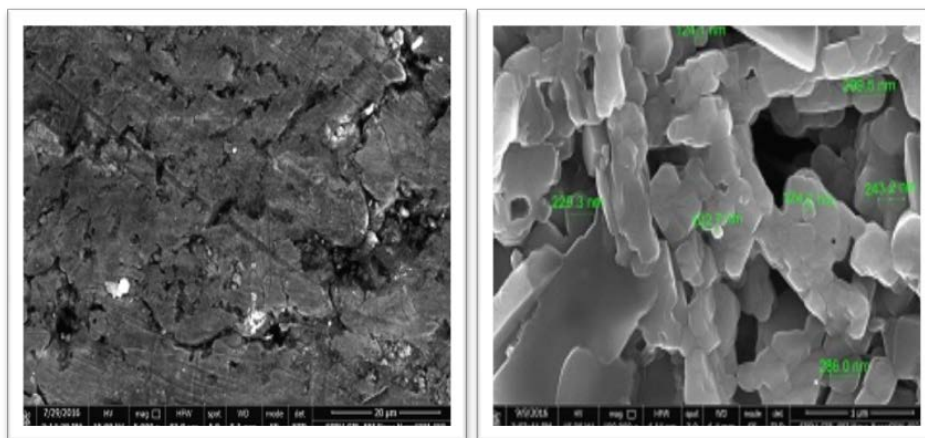


Fig. 4 SEM micrograph of a) starting material b) after Purification of Pittal Bhasma

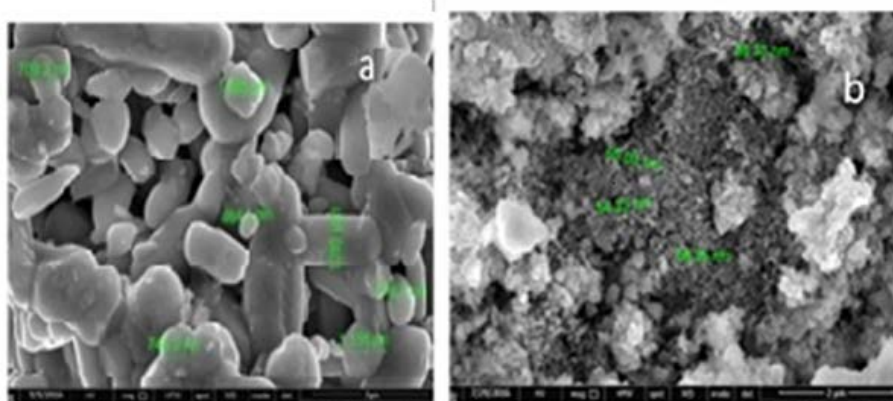


Fig.5 SEM Micrograph of Pittal Bhasma a) prepared by traditional method of heating b) prepared by EMF heating

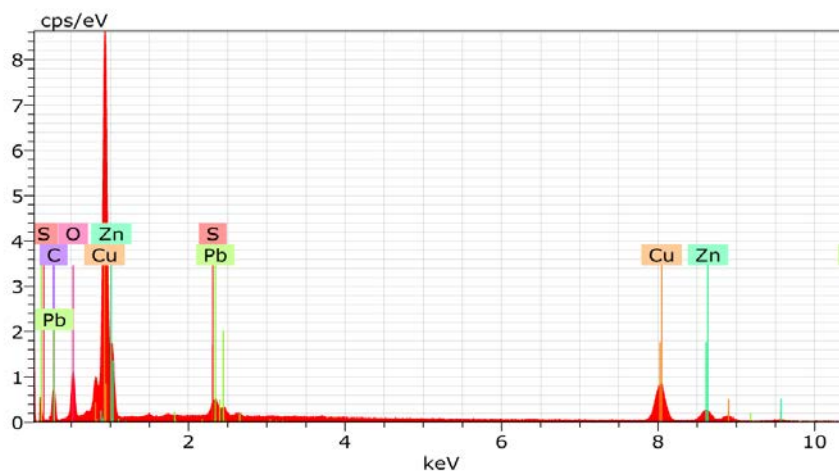


Fig.6 EDX spectra of starting material of Pittal Bhasma

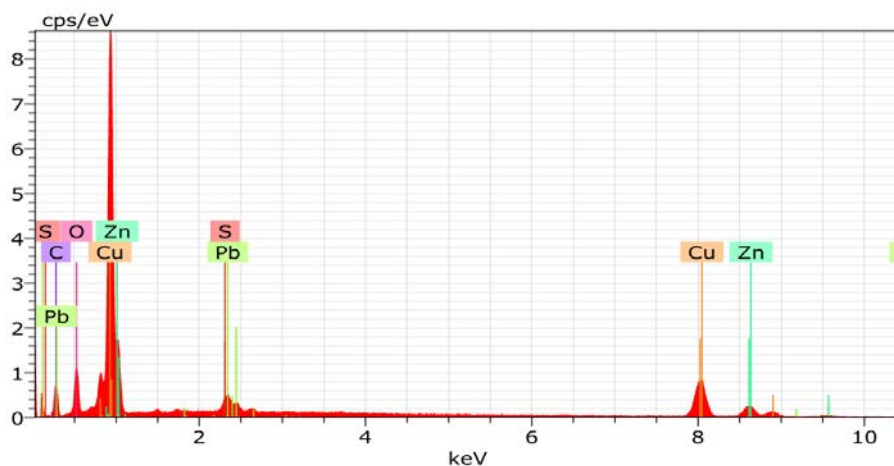


Fig. 7 EDX spectra of Pittal Bhasma after purification

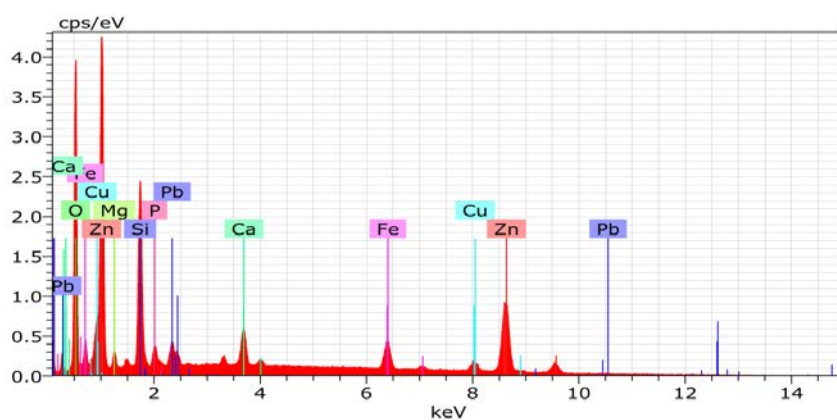


Fig.8 EDX spectra of Pittal Bhasma prepared by traditional method of heating

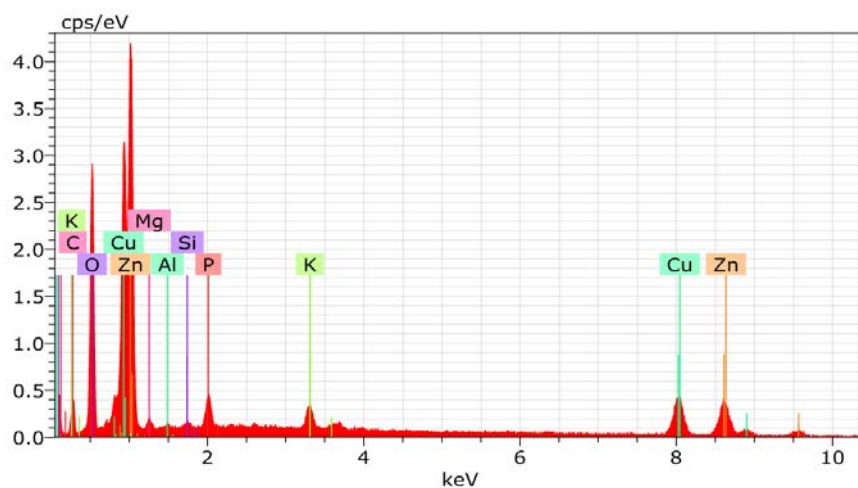


Fig.9 EDX spectra of Pittal Bhasma prepared by EMF heating

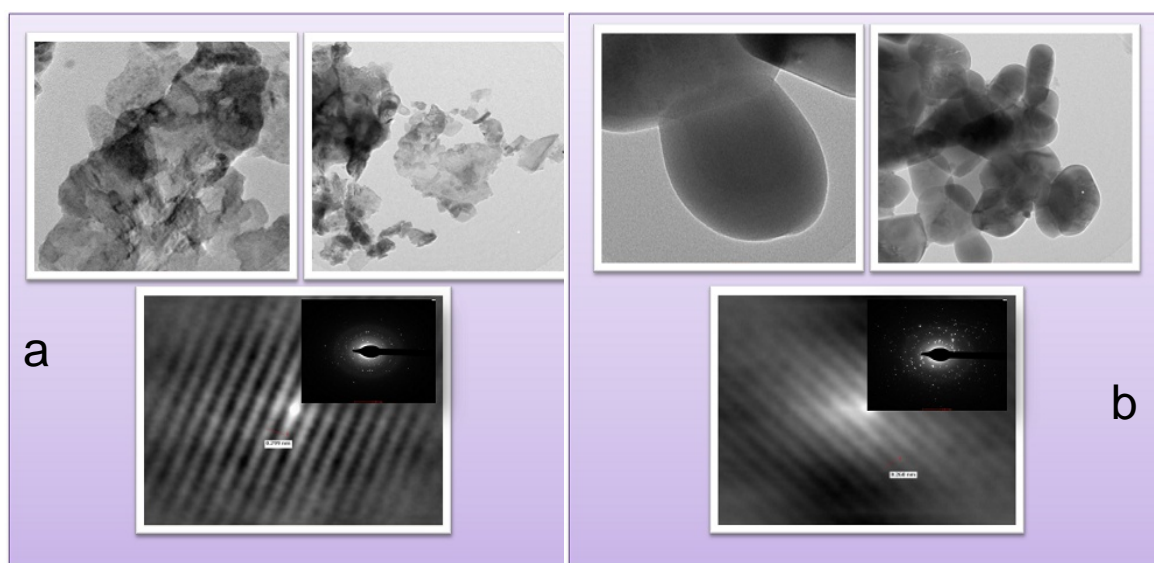


Fig. 10 TEM, HRTEM, SAED of Pittal Bhasma prepared by a) traditional method of heating b) EMF heating

Tables:

Table 1 Ayurvedic tests of Pittal Bhasma

TEST	P1	P2
Odor	Odorless	Odorless
Colour	Dark Brown	Dark brown
Nishchandravam	+ve	+ve
Rekhpurnavam	+ve	+ve
Varitratvam	+ve	+ve
Unnam	+ve	+ve

P1: Pittal Bhasma prepared by traditional method of heating

P2: Pittal Bhasma prepared by EMF heating

Table 2 Crystallite size during preparation of Pittal Bhasma

PittalBhasma	2θ (degree)	d value	Mean Crystallite size /nm
P1	42.50,49.30, 49.53,72.32	2.12,1.83,1.83, 1.30	157.48
P2	42.50,49.38	2.12, 1.84	152.80
P3	32.68,39.20,46.18,56.46	2.73,2.29, 1.96, 1.62	139.70
P4	27.88,29.98,35.32,38.70, 48.66,62.38	3.19,2.97,2.53,2.32, 1.86, 1.42	126.39

P1: Starting material of Pittal Bhasma

P2: Starting material of Pittal Bhasma after purification

P3: Pittal Bhasma Prepared by traditional method of heating

P4: Pittal Bhasma Prepared by EMF heating

Table: 3 FTIR analysis of Pittal Bhasma

Functional group	Absorption wavenumber /cm ⁻¹	
	P1	P2
Cu-O,Zn-O	431,461	519
C-O	-----	1101
O-H	2334	2334

P1: Pittal Bhasma prepared by traditional method of heating

P2 :Pittal Bhasma prepared by EMF heating

Table: 4 EDX analysis starting material of Pittal Bhasma

Element	Conc./%	Element	Conc./%
Zn	15.90	K	0.10
Cu	72.61	Fe	1.92
C	3.16	Mg	0.01
Na	0.52	S	16.02

Table 5 EDX analysis of Pittal Bhasma after purification

Element	Conc./%	Element	Conc./%
Zn	22.43	S	0.72
Cu	55.62	C	6.69
O	8.01	Pb	4.09

Table 6 EDX analysis of Pittal Bhasma prepared by traditional method of heating

Element	Conc./%	Element	Conc./%
Zn	15.17	Pb	0.50
Cu	35.17	Ca	2.69
O	15.01	Mg	1.33
Si	5.69	P	0.23
Fe	3.17		

Table 7 EDX spectra of Pittal Bhasma prepared by EMF heating

Element	Conc./%	Element	Conc./%
Zn	26.04	K	2.10
Cu	29.62	P	1.92
O	20.23	Mg	0.82
C	6.44	Si	0.23
Al	0.18		

Table 8 DLS analysis during Pittal Bhasma

Sr. No.	Sample No.	Diffussion coefficient /10 ⁻⁹ cm ² S ⁻¹	Effective diameter /nm	Polydispersivity
1	P1	8.02	611.21	0.279
2	P2	8.09	551.04	0.267

P1: Pittal Bhasma prepared by traditional method of heating

P2: Pittal Bhasma prepared by EMF heating

References:

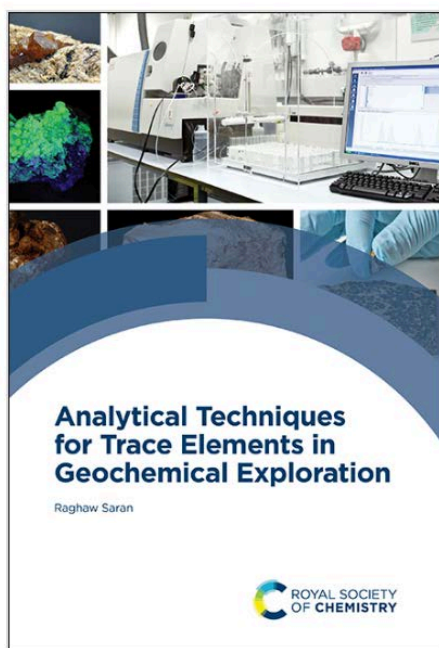
1. Sarkar PK and Chaudhary AK. Journal of Scientific & Industrial Research vol. page year 69, 901, 2010.
2. Rastarangini, Sharma S.. Delhi Edition 11th MotilalBanarasidas Publication, ,Delhi, India ; 362, 2000.
3. Sheenam R., Sharma A. Sharma U, Mitra S and Sharma K, International Ayurvedic Medical Journal ,2191, 2022 <https://doi.org/10.46607/iamj2510082022>
4. Pal D., Sahu CK, Haldar A., Journal of Advanced Pharmaceutical Technology and Research vol.5 , 1, 2014.
5. Giacomino A, Abollino O., Casanova C. La C., Gioia, E. Magi, M. Malandrino, Microchemical Journal, 120, 6, 2015.
6. Umarani RK and Paknikar KM. .Hindawi PublisingCorporation, Article ID 193156, Pgs.9, 2015. <http://dx.org/10.1155/2015/193156>
7. Sharma A, Shailajan S. Enviromental science an Indian Journal , 4(4), 135, 2009.
8. Chugh A., Journal of Intellectual Property Rights 16, 509, 2011.
9. Nagarajan S., Kalairasi S., Krishnaswamy S. , Premiah B, Sekarajan K, Krishnan UM , Seturaman S, Journal of Ethnopharmacology 151,1,2015.

10. Kale B. and Rajurkar N., J.Ayu. and Int. Med. 10 (2) ,111,2019.

11. Kantak S., Adhyapak P. and Rajurkar N. J.Ayu. and Int.. Med. 11 (2) ,236,2020.

Review of the Book: “Analytical Techniques for Trace Elements in Geochemical Exploration” by Dr. Raghaw Saran

Dr. D.K.Dubey
Former Director and Outstanding Scientist
DRDE, Gwalior
Email: dkdubey@rediffmail.com



Geochemical explorations are of paramount importance in optimally using the resources, thereby strengthening the economy. Trace element's analysis requires application of state-of-the-art techniques so as to detect and / or quantify them with utmost sensitivity and selectivity. The book *Analytical Techniques for Trace Elements in Geochemical Exploration* provides a comprehensive treatise of hitherto reported analytical techniques that could be used for geochemical analysis of multitude of samples.

The book is comprised of sixteen chapters, each one deals with a particular technique. Coverage of wide spectrum analytical techniques, ranging from UV-Vis spectrophotometry to ICP-MS with hyphenated techniques, meets the requirement of every laboratory according to their budget and projects. Description of sample preparation methods, wet chemistry and sample collection procedures are special features of this book which do not limit its scope to only instrumental techniques. Amongst various techniques described in the book, ICP-MS are of special mention as they offer highest sensitivity with attractive dynamic linearity range. Discussion on statistical treatment in the context of geochemical trace elements analysis makes this work worth reading for analysts. Provision of reference standards for each kind of sample and analytical technique would have also been very useful.

This book is a reader friendly text, covering all of the mainstream analytical techniques used by geochemical explorers, analysts and researchers. The book will also be of benefit to students embarking on research careers through PhD or other research degree.

Link for the book: <https://pubs.rsc.org/en/content/ebook/978-1-83916-572-6>

⁴ Present address: Department of Civil Engineering, Vasavi College of Engineering, Hyderabad

⁵ Present address: Bernal Chair of Process Engineering, University of Limerick, Limerick, Ireland